Indoor Air Quality: Impacts of Synthetic Ester Hydrolysis and Ventilation

Do Young Maeng

Submitted in partial fulfillment of the
requirements for the degree of
Doctor of Philosophy
under the Executive Committee
of the Graduate School of Arts and Sciences

COLUMBIA UNIVERSITY

2023

Abstract

Indoor Air Quality: Impacts of Synthetic Ester Hydrolysis and Ventilation

Do Young Maeng

Indoor air quality (IAQ) has a direct impact on our health, as more than half the air we inhale throughout our lifetimes is indoor air. With an increasing trend in dampness in modern buildings due to urban expansion into wetland environments and increased use of gypsum board in construction, hydrolysis in indoor surface films has been suggested to be an important chemical process in the indoor environment. Several synthetic esters (SEs) found in building materials, electronics, and consumer products may undergo hydrolysis to produce harmful volatile organic compounds (VOCs) to which building occupants may be exposed. In this dissertation, the impact of hydrolysis on indoor air quality is explored by experiments on alkaline hydrolysis kinetics and ventilation, followed by simulations of VOC production from hydrolysis.

Alkaline hydrolysis kinetics of four SEs, 2,2,4-trimethyl-1,3-pentanediol monoisobutyrate (TMPD-MIB), butylparaben (BP), bis(2-ethylhexyl) adipate (DEHA), and butyl benzyl phthalate (BBzP), in bulk solutions are investigated in chapter 2. With concentration decay profiles following pseudo first-order kinetics, the second order-rate constants were determined from measured pH values. The determined rate constants of the aforementioned SEs are compared with those of respective ester categories (e.g., parabens, phthalates), and the steric/polar effects of the ester substituents are discussed in detail. The results of this study contributed to the completion of the indoor chemistry box model GAMMA-CIE which was used for simulation studies in chapter 4.

Room-level ventilation measurements in educational spaces across different US regions (e.g., Northeastern, Southeastern, Western) are presented in chapter 3. In the wake of COVID-19 pandemic, ventilation data on a room-by-room basis were critical in planning a safe reopening in schools and universities. Three major approaches to ventilation measurements are outlined in this chapter: direct flow measurement, controlled release, and passive/in-situ monitoring. The application of these approaches is presented in case studies across various educational institutions, showcasing their advantages and disadvantages. The frequently observed range of 0.5-5.5 ACH in this study is taken into account in simulation conditions in chapter 4.

The predicted indoor generation of VOCs from alkaline hydrolysis of SEs occurring in surface aqueous films is discussed in chapter 4. Simulations were performed using GAMMA-CIE, which considers aqueous hydrolysis kinetics, interphase mass transport, and loss by ventilation. Three different scenarios were studied: (1) installation of PVC flooring on concrete; (2) coating of latex paint on concrete; and (3) uptake of airborne SEs by surface aqueous films. The simulation results suggested that: (1) the rate of hydrolysis of DEHA and DEHP from PVC flooring is not fast enough to generate high concentrations of 2-ethylhexanol observed during episodes of sick building syndrome (SBS); (2) fresh application of latex paint may cause acute exposure to 2,2,4-trimethyl-1,3-pentanediol (TMPD); and (3) hydrolysis of SEs diffused from indoor air is unlikely to produce significant amounts of alcohols associated with SBS.

Table of Contents

List of Figures

List of Tables

Acknowledgments

First and foremost, I would like to thank my advisor, Prof. Faye McNeill, for her guidance and support throughout my PhD journey. Your kind words and thoughtfulness are what led me here today. The work I have done and everything I have learned throughout my PhD are and will be unforgettable.

I would also like to thank the group members in the McNeill lab—Han (and her husband, Ming, as well), Will, Alison, and Woods. You all have been such a big influence during my early days of PhD, not only giving me advice in operating instruments and communicating my research to but also listening to my frustrations and complaints about day-to-day problems.

The initial stages of the COVID-19 pandemic were difficult for me, like it was for a lot of people; stranded alone in this big city with no close friends or family was unlike any other experience I have had. I owe a great debt of gratitude to my big brother, Sungin, for helping me emotionally throughout such hard times, and I am grateful that the pandemic actually provided an opportunity to rekindle our friendship. The late-night, podcast-esque conversations were quite interesting, to say the least—most of them were just silly and funny, but some of them really made me think about life.

I want to express my sincere appreciation to all the friends who made my time here very special. To Karthik, Emma, and Neal, thank you for all the fun, crazy moments, the only regret I have is not showing up as often as I wanted to. To Daniel, Jay, and Taeseok, thank you for the late night karaoke sessions that taught me how to sing somewhat correctly. To Peter, Hanyong, and Lexa, thank you for pulling me out of my studio to explore the city together. To Tyler, thanks for being such a close friend since high school and sharing together the struggles of being

a graduate student. And special thanks to Karthik and Peter for being the best workout buddies, I will dearly miss the lifting sessions at Dodge.

Lastly, thank you, Mom and Dad, for your unconditional love and support, this work would not have been possible without you.

Chapter 1: Introduction

1.1 The Importance and Challenges of Indoor Air Quality (IAQ)

In modern times, we spend most of their time indoors. The US Environmental Protection Agency (EPA) reported that Americans spend 93% of their time in indoor environments (e.g., residential spaces, offices, and schools).[1] Consequently, exposure to contaminants in indoor air directly impact our health and may cause various health problems.[2–5]

Asbestos and radon found in construction materials were particularly notorious in the mid-to-late 1900s because of their close association with a higher risk of lung cancer.[6,7] Pentachlorophenol found in paint and wooden materials also posed a health threat during the same period, as it was linked with an increased risk of nasal carcinoma and soft tissue sarcoma.[8] While the indoor levels of these contaminants have decreased in the late 1900s with various regulations set in place by the US EPA, concentrations of other pollutants such as volatile and semi-volatile organic compounds (VOCs and SVOCs) found in consumer products and building materials have increased substantially since then due to their widespread usage as plasticizers and additives.[9] Multiple studies have demonstrated that VOC and SVOC emissions from various indoor materials (e.g., paint, flooring, carpets, cleaning products) are closely linked with a phenomenon known as sick building syndrome (SBS), in which building occupants develop symptoms of irritation in the eyes, nose, or throat, headache, fatigue, and chest tightness.[2,10,11]

Biological contaminants such as bacteria, fungi, and viruses are also present in indoor air and may have negative health implications for exposed building occupants.[12] Bacteria (e.g., *Staphylococcus*, *Corynebacterium*, *Bacillus*) and fungi (e.g., *Penicillium*, *Cladosporium*, *Alternaria*) commonly encountered indoors originate from outdoor air, but their airborne concentrations may be higher in damp indoor environments which promote their growth.[13] SBS

and various respiratory diseases such as sinusitis, acute bronchitis, nocturnal cough, and asthma have been positively associated with exposure to high concentrations of indoor airborne microbes.[14,15] Maintaining optimal indoor air quality (IAQ) has been critical in preventing the spread of viral and bacterial infections with more serious health implications as well, namely SARS-CoV-2, measles morbillivirus, chickenpox virus, influenza virus, and *Mycobacterium tuberculosis*.[16,17]

It is evident that indoor air quality (IAQ) is important for our health and well-being. There has been a global effort to minimize indoor air pollution exposure, but limitations in our understanding of indoor chemistry and technicalities of ventilation systems act as obstacles in improving IAQ. The following sections provide an overview on each of these topics, both of which are closely related to the contents of this dissertation.

1.2 Indoor Chemistry

The field of indoor chemistry, relevant to residential spaces and buildings, is relatively new. The majority of the research in this field has emerged only within the past 30 years; research in indoor chemistry has primarily focused on the conservation of historical artifacts before 1991.[18] Indoor chemistry has gathered some attention since then, but it has not been studied as extensively as atmospheric chemistry, with only 565 scientific papers on indoor chemistry by the end of 2019 in comparison to ~12000 papers on atmospheric chemistry published between 1990 and 2010.[18,19] Several types of reactions (e.g., oxidation, photolysis) occur in both indoor and outdoor air, but the chemical species of interest are considerably different in an indoor setting because of its distinct emissions sources: building materials, paint, cooking, smoking, photocopiers/laser printers, cleaning agents, air refresheners, and so on.[20]

1.2.1 Indoor Gas-Phase Chemistry

A significant portion of research on indoor gas-phase chemistry has been on oxidation reactions of VOCs driven by ozone (O_3) or hydroxyl (OH) radical.[20] OH radical is one of the most important—if not the most important—oxidant in the atmosphere, produced by complex photochemistry involving O_3 or nitrous acid (HONO).[21] Contrary to atmospheric conditions, the UV photon fluxes indoors are believed to be less than 3% of those in the atmosphere,[22,23] so indoor OH radical production is predominantly from reactions of O_3 and alkenes, with O_3 arguably considered as the most important oxidant species instead in indoor environment.[24] O_3-initiated oxidation reactions of terpene compounds (e.g., D-limonene, α-terpineol, geraniol, and α-pinene found in cleaning products) have been investigated, focusing on its subsequent production of OH radical and secondary organic aerosol (SOA) formation.[25–28] It has been speculated that nitrate (NO_3) radical could play an important role, but several studies have concluded that its indoor concentrations were negligible and had minimal impact on the VOC oxidation process.[29,30]

1.2.2 Indoor Surface Chemistry

Surfaces play an active role in indoor chemistry, acting as a source of both primary (emitted directly) and secondary (generated by chemical transformations) emissions.[18,19] Of particular interest is the interaction of ozone with indoor surfaces, notably the deposition rate of ozone and the subsequent production of VOCs (e.g., aldehydes, acids) from heterogeneous oxidation on surfaces such as carpets and drywall.[31–34] Surface ozone oxidation of squalene, a

major component in skin lipids, occurring on human skin, hair, and soiled clothing has also received attention as an important source of secondary VOC emissions over recent years.[35–37]

The formation of organic and aqueous films from the uptake of VOCs, SVOCs, and water is another important topic which has emerged from recent studies. Indoor surface films can be a medium in which various reactions take place, and they may also affect the adsorption and desorption processes between indoor air and surfaces. Studies on the chemical and physical characterization of these films suggested typical film thickness in the nano- to micro-scale range and significant presence of chemicals (e.g., bis(2-ethylhexyl) phthalate, acetyltributylcitrate) found in building materials and consumer products.[38–40] Chemical processes such as O_3-driven oxidation, acid-base chemistry, and hydrolysis (in aqueous films) are believed to take place in indoor films, but not much is currently known about their reactivity.[38] Hydrolysis occurring on surfaces has been suggested as the major degradation pathway of DEHA and DEHP in PVC flooring, responsible for the production of 2-ethylhexanol which is notorious for its close association with SBS.[41] In this dissertation, hydrolysis of SVOCs in aqueous surface films and its impact on indoor air quality are discussed in detail.

1.3 Ventilation

Ventilation has been an effective tool for to prevent buildup of indoor air contaminants since the 18th century.[42] Several studies have suggested that increased ventilation rate is positively associated with increased work performance, higher levels of occupant satisfaction, and decreased SBS occurence.[43–45] Higher ventilation rates are also particularly important for reducing the transmission of airborne diseases in indoor settings, and they have been critical in

minimizing infection risks during the COVID-19 pandemic alongside masking and distancing.[46,47]

Establishing effective ventilation strategies, however, comes with several challenges. A major concern with mechanical heating, ventilation, and air-conditioning (HVAC) systems is their energy consumption; it is reported that HVAC systems account for 60 to 70% of total energy use in non-industrial buildings.[48] In scenarios such as the COVID-19 pandemic which demands minimum recirculation and maximum fresh/outdoor air intake, the energy cost would be even worse.[16] Ambiguity in problematic contaminants of concern impedes effective development of regulations and standards on ventilation. The focus has been first on carbon dioxide and then on a set of less than a dozen pollutants set by the WHO in 2010,[49] but it is likely that IAQ problems (e.g., SBS) may arise from a mixture of numerous pollutants, each at relatively low concentration.[50] Furthermore, variability in pollutant source strengths across regions encourages the involvement of other IAQ control strategies, such as air treatment and source control.[42]

Chapter 2: Kinetics of Alkaline Hydrolysis of Synthetic Organic Esters[1]

2.1 Introduction

Synthetic organic esters (SEs) are ubiquitous indoor pollutants used as additives in numerous consumer products and building materials. Phthalates, adipates, and isobutyrates are used as plasticizers which enhance the flexibility of the materials such as electronic cables, adhesives, PVC flooring, and latex paint.[51,52] Parabens provide microbial resistance as preservatives, and are therefore commonly found in cosmetics and food packaging.[53] Although SEs enter the indoor environment in the condensed phase (e.g. physically bound in plastic materials), they leach out and partition to the gas phase and/or dissolve in nanoscale aqueous films.[39,54,55] Such aqueous films, formed in damp conditions, can be acidic from the uptake of gases, or basic when in contact with alkaline surfaces such as concrete.[19] Esters are vulnerable to reaction with water molecules (hydrolysis) in the gas or aqueous phase, or on surfaces.[39,56] Due to relatively slow gas-phase hydrolysis rates, and the fact that ester hydrolysis may be either acid or base-catalyzed, hydrolysis on surfaces and in aqueous films is likely the most important pathway for hydrolytic degradation of SEs indoors.

Direct exposure to certain phthalates and parabens is known to be harmful for human health, with effects including reproductive toxicity, endocrine disruption, and allergy sensitization.[57,58] The degradation products of these species in the indoor environment also pose additional health concerns. Products of SE hydrolysis include alcohols, organic acids (or carboxylate salt, under alkaline conditions), or in the case of di- and tri- esters, mono- and di-

[1] This chapter has been published as: Maeng DY, McNeill VF. Kinetics of alkaline hydrolysis of synthetic organic esters. Int J Chem Kinet. 2022 Mar 22;54(3):218–22.

esters, respectively. Elevated gas-phase concentrations of volatile organic compounds (VOCs) from various indoor sources, including the alcohol degradation products of ester hydrolysis, are associated with sick building syndrome (SBS)—a condition where building occupants experience acute health effects and discomfort associated with their time indoors.[59] For example, exposure to 2-ethyl-1-hexanol, an alcohol generated during the hydrolytic degradation of bis(2-ethylhexyl) phthalate (DEHP) and bis(2-ethylhexyl) adipate (DEHA), has been connected to SBS and asthma-like symptoms, especially in buildings with signs of dampness or high humidity.[60,61]

Despite the concerning implications for indoor air quality, the kinetics of SE hydrolysis remain largely unknown. Thus, the objective of this study was to determine the alkaline hydrolysis kinetics of four synthetic esters commonly found in the indoor environment: 2,2,4-trimethyl-1,3-pentanediol monoisobutyrate (TMPD-MIB, also known as Texanol®), butylparaben (BP), bis(2-ethylhexyl) adipate (DEHA), and butyl benzyl phthalate (BBzP).

2.2 Materials and Methods

2.2.1 Chemicals

All chemicals were used as received. The reactant esters were 2,2,4-trimethyl-1,3-pentanediol monoisobutyrate (TMPD-MIB, 99% purity, Sigma Aldrich), butylparaben (BP, 99% purity, Thermo Fisher Scientific), bis(2-ethylhexyl) adipate (DEHA, 99% purity, Sigma Aldrich), and butyl benzyl phthalate (BBzP, 98% purity, Sigma Aldrich). Water (HPLC grade, Sigma Aldrich) and sodium hydroxide (NaOH, extra pure, 50 wt% solution in water, Thermo Fisher Scientific) were used to prepare the solvent mixtures, with the addition of isopropyl alcohol (Optima LC/MS grade, Thermo Fisher Scientific) for DEHA and BBzP hydrolyses. Acetic acid (glacial, Optima, Thermo Fisher Scientific) was used to neutralize the aliquots after

their extraction. The UPLC mobile phase solvents (listed in the Supporting Information) were of Optima LC/MS grade and purchased from Thermo Fisher Scientific.

2.2.2 UPLC-MS Analysis

TMPD-MIB, BP, DEHA, and BBzP were quantified using an ACQUITY Ultra-Performance Liquid Chromatography system (Waters Corporation, UPLC H-Class PLUS) in tandem with a quadrupole time-of-flight mass spectrometer (Waters Corporation, Xevo G2-XS QToF MS). All esters were separated on an ACQUITY UPLC CSH C18 Column (1.7 μm, 2.1 × 50 mm) (Waters Corporation). Signal interference from contamination was a noteworthy concern during the analysis because of the pervasiveness of the analyte esters in indoor environments. To mitigate this issue, an Isolator Column (Waters Corporation) was installed in the flow path prior to the injection port in UPLC to offset the background response from the sample analyte response. The QToF MS was operated with an electrospray ionization (ESI) source in positive mode for TMPD-MIB, DEHA, and BBzP analyses and in negative mode for BP analysis. Additional details regarding UPLC-QToF-MS operation and calibration are provided in the Supporting Information.

2.2.3 Kinetic Procedure

Second-order alkaline hydrolysis rate constants were determined by observing the hydrolytic degradation of TMPD-MIB, BP, DEHA, and BBzP over time. The product distributions of the hydrolysis reactions are provided in the Supporting Information.

The employed kinetic method outlined below is based on previous investigations on the alkaline hydrolysis of phthalate esters.[62] The experiments were performed in triplicate for each of the esters studied.

A bulk aqueous solution of 0.002~0.1 M sodium hydroxide (NaOH) was mixed with a dilute aqueous solution of each ester using a vortex mixer, and the reacting solution was contained in a sealed, sterile polypropylene tube at room temperature monitored with a temperature meter (Vaisala, HM40) throughout the reaction. The pH of the reaction solutions, measured using a pH meter (Thermo Scientific, Orion 4-Star pH/DO Benchtop Meter), varied from 11.27 to 13.01 as listed in Table 2.1 below. For DEHA and BBzP, which have relatively low water solubility ($<10^{-5}$ M), the solutions were prepared with 1% isopropyl alcohol in volume in order to facilitate dissolution. 1 mL aliquots were drawn from each reaction solution at predetermined time intervals and immediately quenched with diluted aqueous acetic acid for UPLC-MS analysis.

The alkaline hydrolysis of esters is known to follow second-order kinetics—first-order with respect to each of the reactants, the ester and OH^-.[63] Because OH^- was in large excess, the studied reactions were assumed to follow pseudo first-order kinetics. Therefore, the pseudo first-order rate constants were determined as the slopes of least squares regression lines of the natural logarithm of concentration ratio versus time. They were then divided by the OH^- concentrations to calculate the second-order rate constants of the reactions. Kinetic expressions and reaction mechanism are further explained in the Supporting Information.

2.3 Results and Discussion

Plots of natural logarithm of normalized-concentration versus time for all esters are shown in Figure 2.1. Weighted linear least squares curves were fitted to each data set, from which the pseudo first-order rate constants were found as the slopes of the curves. Strong linearity across all plots indicated that the pseudo first-order assumption was valid for the studied kinetics. Second-order rate constants of the reactions, listed in Table 2.1, were determined as described in the previous section.

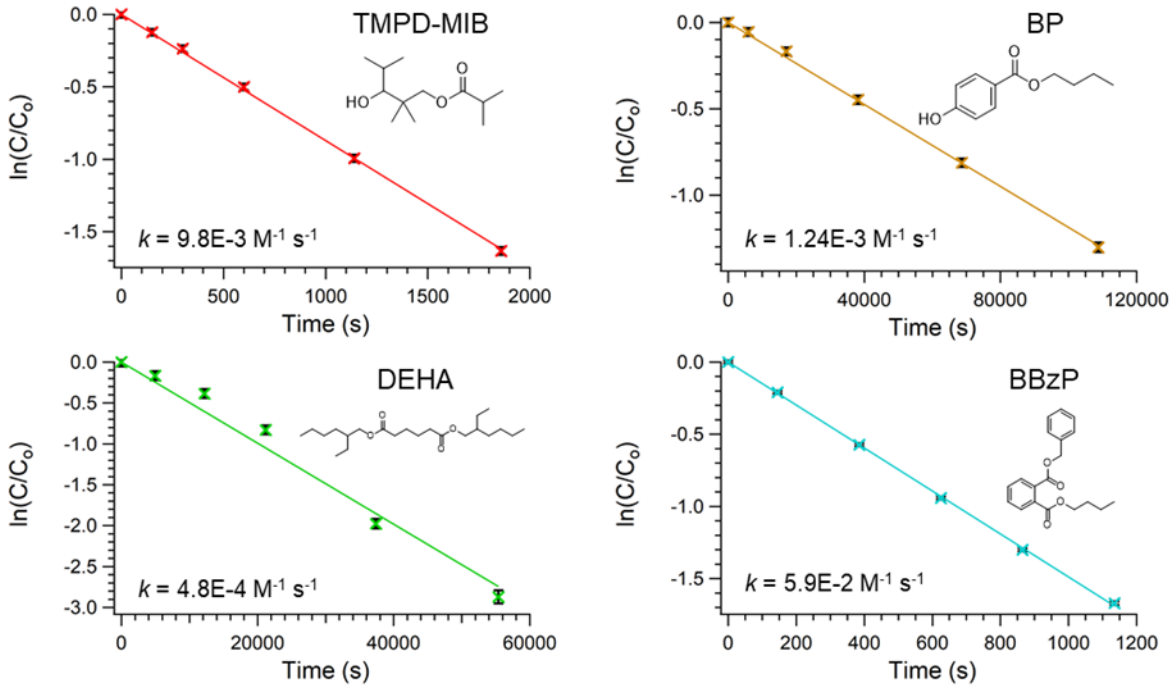

Figure 2.1: Hydrolytic degradation of TMPD-MIB (red), BP (yellow), DEHA (green), and BBzP (blue) over time in alkaline (pH 13) aqueous solution at room temperature. Error bars represent standard deviations based on triplicate measurements.

Table 2.1: Alkaline Hydrolysis Second-Order Rate Constants of Synthetic Esters

Ester	k $[M^{-1} s^{-1}]$	Temperature [°C]	pH	Reference
Isobutyrate				
2,2,4-Trimethyl-1,3-pentanediol monoisobutyrate (TMPD-MIB)	$(9.8 \pm 1.3) \times 10^{-3}$	20.2 ± 0.2	12.95 ± 0.06	this study
Paraben				
Methylparaben	$(8.7 \pm 0.3) \times 10^{-4}$	30 ± 0.1	13[a]	63
Ethylparaben	$(4.2 \pm 0.2) \times 10^{-4}$	30 ± 0.1	13[a]	63
Propylparaben	$(3.0 \pm 0.1) \times 10^{-4}$	30 ± 0.1	13[a]	63
Butylparaben (BP)	$(1.24 \pm 0.17) \times 10^{-4}$	20.9 ± 0.7	12.98 ± 0.06	this study
Adipate				
Bis(2-ethylhexyl) adipate (DEHA)	$(4.8 \pm 0.6) \times 10^{-4}$	21.0 ± 1.3	13.01 ± 0.06	this study
Phthalate				
Butyl benzyl phthalate (BBzP)	$(5.9 \pm 0.8) \times 10^{-2}$	21.2 ± 0.2	12.40 ± 0.06	this study
	$(2.8 \pm 0.4) \times 10^{-2}$	19.3 ± 0.2	11.27 ± 0.06	this study
Dimethyl phthalate	$(6.9 \pm 0.3) \times 10^{-2}$	30.00 ± 0.05	10 to 12[a]	61
Diethyl phthalate	$(2.5 \pm 0.2) \times 10^{-2}$	30.00 ± 0.05	10 to 12[a]	61
Di-n-butyl phthalate	$(1.0 \pm 0.05) \times 10^{-2}$	30.00 ± 0.05	10 to 12[a]	61

[a]Estimated from the reported NaOH concentrations[62,64]

It should be noted that, for diesters such as DEHA and BBzP, the tabulated rate constants are associated with the overall degradation rate of each species. In the case of DEHA, which has two identical ester moieties, both reaction sites are equivalent in terms of their contribution to the rate of hydrolysis. In the case of BBzP, however, its ester moieties have different chemical structures, resulting in two distinct pathways for its hydrolysis reaction. The benzyl ester is likely

much more vulnerable to hydrolysis than the butyl ester for reasons described in detail below, but further study is needed to determine the kinetics associated with each ester moiety within the compound.

Neglecting minor differences in reaction temperature, the alkaline hydrolysis rate constant of BBzP was the greatest, followed by those of TMPD-MIB, DEHA, and lastly BP. The differences in hydrolysis reactivity are explained by comparing the substituents of the esters. The substituents can either hinder or facilitate the rate-determining nucleophilic attack of OH^- on the carbonyl carbon of the ester by exerting polar and steric effects. The phenyl substituent of BBzP is more electron-withdrawing than the alkyl substituents of TMPD-MIB and DEHA, increasing the electrophilicity of the reaction site and consequently promoting the reaction. In contrast, the phenol substituent of BP is electron-donating instead and significantly slows the rate of hydrolysis. Alkyl chain substituents are found in both TMPD-MIB and DEHA, but those in TMPD-MIB are shorter and therefore exert a weaker steric effect than those in DEHA, resulting in TMPD-MIB being more reactive than DEHA.

Alkaline hydrolysis kinetics of other parabens and phthalates—ester families encompassing BP and BBzP, respectively—have been investigated in the past.[62,64] BP and BBzP alkaline hydrolysis kinetics results are compared to those of other members of their respective families in Table 2.1. Taking into account the aforementioned polar and steric effects of substituents, the kinetic results of BP and BBzP reasonably fit the trend among the literature values of their respective families. The reaction rate constant of BP is lower than those of other paraben species with smaller alkyl chains. On the contrary, the reaction rate constant of BBzP is significantly greater than other phthalates with alkyl chain substituents because of the electron-withdrawing phenyl group in BBzP.

BBzP alkaline hydrolysis was studied at two pH values, 12.40 and 11.27, with observed second-order rate constants of $5.9(\pm0.8)\times10^{-2}$ and $2.8(\pm0.4)\times10^{-2}$ M^{-1} s^{-1}, respectively. The second-order rate constant is expected to be constant with respect to the activities of the reactants, but may be dependent on the temperature and ionic strength of the reacting solution. Based on previous reports on the activation energies of parabens and phthalates ranging approximately between 44 and 60 kJ mol^{-1},[64–66] the temperature difference of 2 °C between the two studies is not likely large enough to significantly impact the measured rate constants. Other studies of alkaline ester hydrolysis have also reported increasing k^{II} with increasing pH and ionic strength.[16] Ion-dipole reaction kinetics are believed to be affected by changes in ionic strength,[63] and this effect could be pronounced for BBzP due to the high polarizability of its aromatic leaving group. Further investigation in future studies of the impacts of pH and ionic strength on ester hydrolysis kinetics, for esters with different substituents, is needed.

There is significant uncertainty about the pH of the indoor aqueous films, in association with the acidity and basicity of the surface and the uptake of acidic gases,[19,67] but the highly alkaline conditions of this study could represent instances in which the aqueous film is in direct contact with a screed or fresh concrete.[61,68] Assuming highly alkaline conditions (pH 13) at room temperature (20-22 °C), SEs would be short-lived in the aqueous phase, as illustrated by their calculated hydrolysis half-lives in Table 2.2. The half-life calculations are described in detail in the Supporting Information. Considering the possibility of accelerated hydrolysis kinetics in such nano- or microscale aqueous films,[19,69] the generation of volatile and semi-volatile compounds from SE hydrolysis could degrade indoor air quality and cause health problems for building occupants in damp indoor environments with insufficient ventilation and alkaline surfaces.

Table 2.2: Half-Lives of Synthetic Esters at pH 13 and Room Temperature

Ester	Half-life [hr]
2,2,4-Trimethyl-1,3-pentanediol monoisobutyrate (TMPD-MIB)	0.20
Butylparaben (BP)	15.5
Bis(2-ethylhexyl) adipate (DEHA)	4.0
Butyl benzyl phthalate (BBzP)	0.033

Besides pH, the hydrolytic degradation of esters and the subsequent production of volatile organic compounds (VOCs) is dependent on other important physicochemical processes, such as ester migration from surfaces (leaching) and air-water partitioning of esters and their hydrolysis products. More data on these processes, along with information on surface film properties, are needed before substantial claims can be made on the impact of SE hydrolysis on indoor air. Further study on these topics, as well as modeling which couples the gas and aqueous phase chemistry with the multiphase mass transfer, is necessary to understand the relationship between building-related illnesses and the hydrolysis of synthetic esters.

2.4 Supporting Information

Reaction Scheme

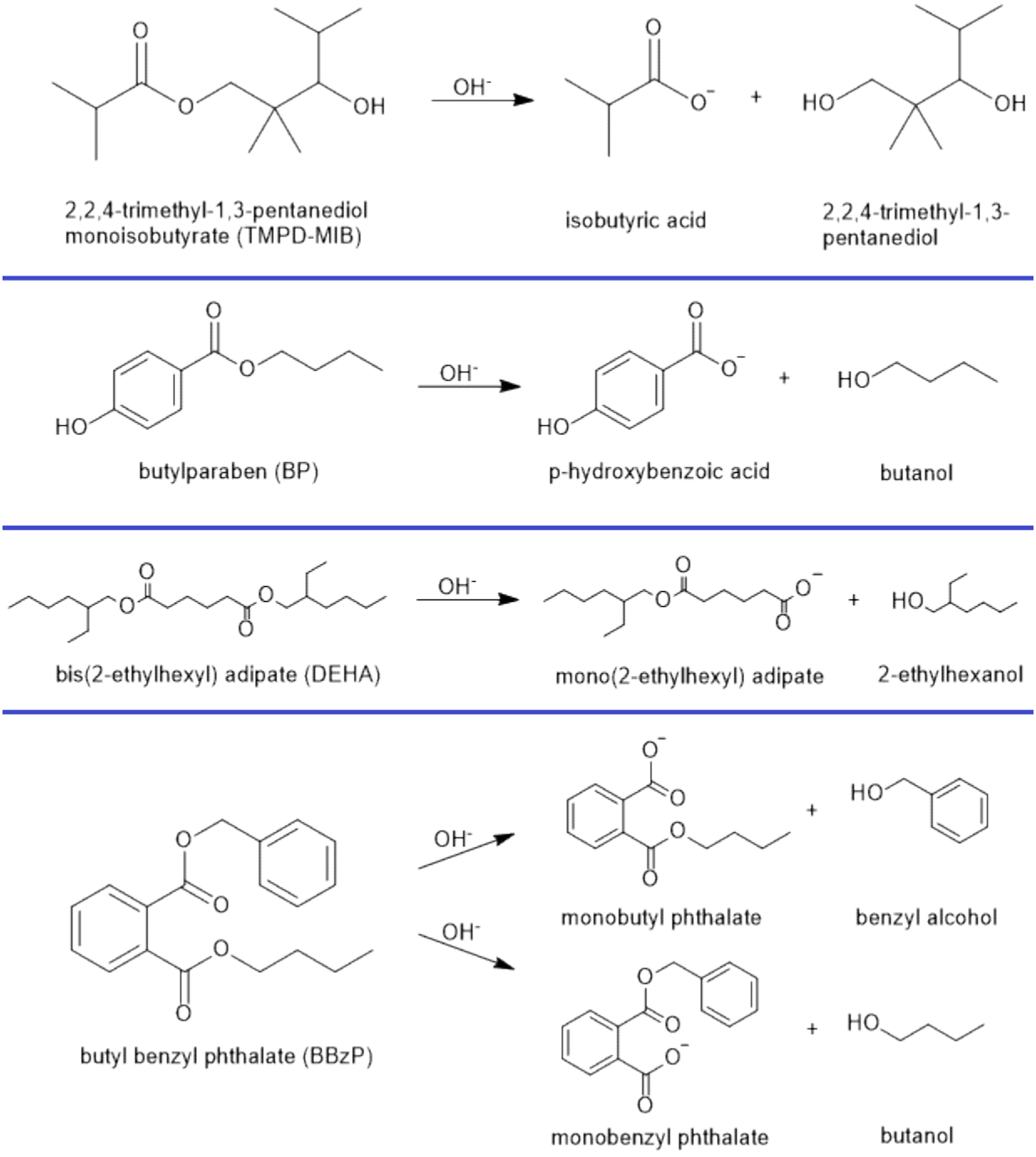

Figure 2.2: Hydrolyses of TMPD-MIB, BP, DEHA, and BBzP. As illustrated in the figure, the hydrolysis reaction yields an alcohol and either an acid or a lower-order ester.

Kinetic Expression and Mechanism of Alkaline Hydrolysis of Organic Esters

Overall, hydrolysis of organic esters can occur by three different pathways—acidic, neutral, and alkaline. Therefore, the rate expression is as follows:[63]

$$\frac{d[\text{ester}]}{dt} = (k_{neutral} + k_{acid}[\text{H}^+] + k_{alk}[\text{OH}^-])[\text{ester}] \qquad (2.1)$$

where [ester] is the ester concentration, t is time, $k_{neutral}$ is the neutral hydrolysis rate constant, k_{acid} is the acid hydrolysis rate constant, $[H^+]$ is the hydrogen ion concentration, k_{alk} is the alkaline hydrolysis rate constant, and $[OH^-]$ is the hydroxide ion concentration. At highly basic pH, the rate at which neutral and acid hydrolyses occur is negligible, and the equation above can then be simplified into:

$$\frac{d[\text{ester}]}{dt} = k'[\text{ester}] = k_{alk}[\text{OH}^-][\text{ester}] \qquad (2.2)$$

where k' is the observed pseudo first-order rate constant, equivalent to the product of k_{alk} and $[OH^-]$.

Alkaline hydrolysis mechanism ($B_{AC}2$) is depicted below.[63]

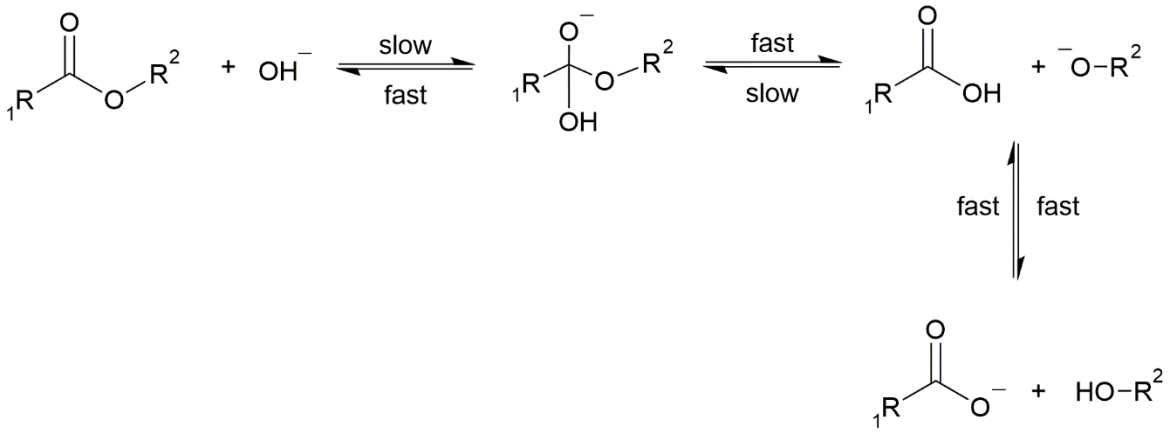

Figure 2.3: $B_{AC}2$ mechanism. The hydroxide ion adds to the carbonyl carbon of the ester, resulting in acyl-oxygen cleavage.

Details of the UPLC-QToF-MS Operation and Calibration

All esters were separated on an ACQUITY UPLC CSH C18 Column (1.7 μm, 2.1 × 50 mm) (Waters Corporation) maintained at 40 °C. Sample injection volumes of TMPD-MIB, BP, DEHA, and BBzP were 0.3, 2, 0.7, and 0.4 uL respectively. The mobile phase solvents were water with 0.2% v/v formic acid (solvent A) and methanol:isopropyl alcohol 80:20% v/v solution (solvent B). The mobile phase flow rate was set to 0.35 mL/min. For TMPD-MIB and BP analyses, the gradient profile was as follows: at 0 min, 60% A, 40% B; at 0.5 min, 60% A, 40% B; at 4.5 min, 1% A, 99% B; at 5 min, 1% A, 99% B; at 5.1 min, 60% A, 40% B; at 8.1 min, 60% A, 40% B, curve 6 for all sections. For DEHA and BBzP analyses, the gradient profile was as follows: at 0 min, 50% A, 50% B; at 0.5 min, 50% A, 50% B; at 3.5 min, 0% A, 100% B; at 5.5 min, 0% A, 100% B; at 5.6 min, 50% A, 50% B; at 8.6 min, 50% A, 50% B, curve 6 for all sections.

The QToF MS was operated with an electrospray ionization (ESI) source in positive mode for TMPD-MIB, DEHA, and BBzP analyses and in negative mode for BP analysis. Additional information on QTof MS operating conditions is listed in Table 2.3.

Table 2.3: Xevo G2-Xs QToF MS Operating Conditions

Parameter	**TMPD-MIB**	**BP**	**DEHA & BBzP**
Capillary Voltage	0.5 kV	2.5 kV	3 kV
Sampling Cone Voltage	30 V	30 V	30 V
Source Temperature	120 °C	120 °C	120 °C

Desolvation Temperature	350 °C	350 °C	350 °C
Cone Gas Flow	10 L/hr	10 L/hr	10 L/hr
Desolvation Gas Flow	650 L/hr	700 L/hr	650 L/hr
Collision Energy	6 V	6 V	6 V

Extracted-ion chromatogram (EIC) peaks were integrated with the MassLynx ApexTrack Peak Integration software. Extracted m/z, mass tolerance window, and retention time of each analyte are tabulated in Table 2.4.

Table 2.4. Extracted m/z, Mass Tolerance Window, and Retention Time of Analytes

Name	**m/z**	**Mass Window (Da)**	**Ret. Time (min)**
TMPD-MIB	239.162	0.02	3.74
BP	193.087	0.02	3.42
DEHA	393.298	0.02	5.10
BBzP	335.125	0.02	3.76

Five-point calibration curves were plotted for all esters as shown in Figure 2.4 using standard samples of known ester concentrations. The detected mass for each species listed in Table 2.4 is that of the sodium adduct for each analyte excluding BP. Thus, the standard samples were spiked with appropriate amounts of sodium acetate to match the sodium concentrations of aliquots from kinetic experiments. Linear correlation between instrument response and standard concentration

observed in all calibration curves suggested that the instrument response was reliable for the working concentration range in hydrolysis experiments.

.

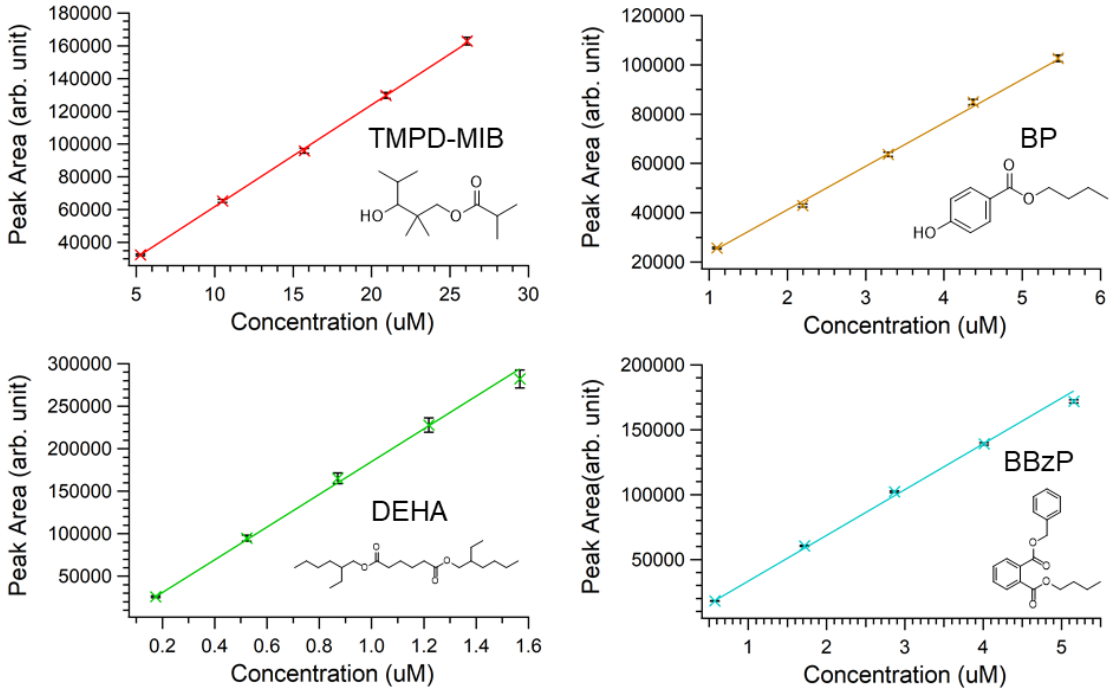

Figure 2.4: Calibration curves of TMPD-MIB (red), BP (yellow), DEHA (green), and BBzP (blue). Error bars represent standard deviations.

Half-Life

The half-life of each ester species at pH 13 was calculated using the following equation for pseudo first-order reactions:

$$t_{1/2} = \frac{\ln 2}{k'} \qquad (2.3)$$

where $t_{1/2}$ is the half-life of the species and k' is the pseudo first-order rate constant. The pseudo first-order rate constants at pH 13 were calculated by multiplying the second-order rate constants in Table 2.1 by the assumed OH concentration of 0.1 M.

Chapter 3: Room-level Ventilation in Schools and Universities[2]

3.1 Introduction

Adequate ventilation with air free of harmful air pollutants is essential to maintaining a healthy indoor environment. In modern buildings, particularly in the U.S., this is usually accomplished by providing indoor spaces with a combination of outside and recirculated, conditioned, and filtered indoor air via a mechanical heating, ventilating, and air conditioning (HVAC) system. Although critical discussions of ventilation are usually focused on buildings with mechanical HVAC, in many parts of the U.S. it is common for schools and university buildings to have only natural ventilation, which means ventilating by opening windows and doors. Natural ventilation is typically encountered in older buildings in the Northeast or in more temperate climates in the West. The ventilation design standard of the American Society of Heating, Refrigerating and Air Conditioning Engineers (ASHRAE) for education-related buildings ranges from 4.3 liters per second per person (L s^{-1} $person^{-1}$) of outdoor air for a lecture classroom to 8.6 L s^{-1} $person^{-1}$ for a science laboratory.[70] Many schools and universities in the U.S. do not meet this minimum standard.[71] Inadequate ventilation may result from: malfunctioning (or improperly configured or scheduled) air handling equipment, excessive air recirculation, inadequate natural ventilation (in buildings without mechanical HVAC), or simply by design to save on energy costs.

[2] This chapter has been published as: McNeill VF, Corsi R, Huffman JA, King C, Klein R, Lamore M, Maeng DY, Miller SL, Ng NL, Olsiewski P, Godri Pollitt KJ, Segalman R, Sessions A, Squires T, Westgate S. Room-level ventilation in schools and universities. Atmos Environ X. 2022;13:100152.
The author's contribution was ventilation data acquisition & analysis of North East University (1/2) and writing. Data acquisition & analysis and discussion of Coastal California K-12 Schools, Southern California University, Southern California Secondary School, Mountain West University, South East University, and North East University (2/2) were provided by collaborators listed above.

Outbreaks of COVID-19, influenza, and other infectious diseases have been connected to inhalation of virus-laden respiratory aerosol in inadequately ventilated indoor spaces.[71–74] Ventilation has well-documented benefits for reducing airborne infectious disease transmission, as well as other negative health and education outcomes.[71,75,76] Masking, improved ventilation, reduced occupancy, physical distancing, and other efforts to mitigate the spread of COVID-19 in the U.S. during the 2020-2021 flu season also led to dramatic reductions in other airborne illnesses such as influenza.[77]

In the wake of the COVID-19 pandemic shutdowns, safe reopening of schools and universities for in-person instruction, and sustainable maintenance of safe conditions, has become an international priority. Since inhalation of respiratory aerosols containing infectious material is a key route of transmission for SARS-CoV-2 and other airborne pathogens,[74] gathering of students and educators in school facilities with insufficient ventilation poses a public health risk. Since aerosol transmission is significant at both short- and room-scale distance, ventilation and filtration, along with distancing and mask wearing, are important components of layered risk reduction.[71] A correlation between improvements in ventilation and air filtration in schools and lower rates of COVID-19 incidence has been shown (Gettings et al. 2021).[78]

In addition to building-level guidelines, e.g. that HVAC filters should be upgraded, outdoor air dampers should be opened entirely when weather permits, and demand control ventilation should be disabled,[79] increased attention is being placed on room-level ventilation and air cleaning. The Harvard Schools for Health group[80] and others[71,81] recommend classrooms meet a minimum of 3 outdoor-air supplied air changes per hour at standard occupancy and room sizes, and that this should be augmented with air cleaning (i.e., filtration or ozone-free upper-

room germicidal ultraviolet light) for a total of 4-6 air changes per hour of outdoor plus filtered air. These recommendations are consistent with the minimum ventilation rates recommended by ASHRAE.[70] In spaces with known ventilation issues, steps may be taken to increase the fraction of outdoor air that is supplied, improve the filtration efficiency of the recirculated air, or provide filtration on a room level. However, there is an overall lack of room-level ventilation data in educational spaces in the U.S. that would allow such planning. There are a number of reasons for this data gap, including that, while recommended guidelines exist for room-level ventilation,[70] in many locations strict requirements only exist for special room types such as wet-chemical laboratories and auditoriums, or for buildings with special certification.[82] Room-level ventilation can be difficult to quantify as it can fluctuate with weather, season, room occupancy, etc.[83–85] Moreover, conventional ventilation metrics and codes were designed to address different risks than those posed by infectious diseases. In particular, standard ventilation codes ensure enough fresh air is supplied to flush the exhalation and other bio-effluents of a specified number of occupants, generally assumed to be identical in their emissions and respiratory intake. Mitigating the spread of infectious disease, however, introduces an additional demand -- to flush a room's air quickly enough to reduce the risk of occupants inhaling airborne pathogens generated by even one infected individual.

The direct flow measurement techniques used by building managers and engineers to characterize ventilation rates in mechanically ventilated buildings cannot be applied to naturally ventilated spaces. Other approaches for characterizing ventilation may require technical expertise for execution or data interpretation, or specialized instrumentation, which reduces accessibility. As educators, administrators, and building managers plan for safe operations in the wake of COVID-19, there is a need for practical approaches for characterizing ventilation on the room

level, as well as support for small-scale, short-term decision making, e.g., with respect to opening windows and doors and running fans, air conditioners, or supplemental air cleaning.

Here, we describe efforts taken by this group of scientists and educators using different approaches to characterize ventilation in educational spaces in different U.S. locations in collaboration with facilities managers, administrators, and other decision makers. We discuss our findings, best practices, and lessons learned.

3.2 Methodology

In this section, we describe practical approaches for characterizing ventilation on a room level in universities and schools, highlighting their advantages and disadvantages. The approaches discussed are summarized in Table 3.1. Broadly, these can be classified as direct flow measurements, controlled-release studies, and passive in situ monitoring. Note that ventilation rates, especially in naturally ventilated spaces, are highly dependent on factors including but not limited to environmental conditions (indoor-outdoor temperature difference, wind speed, etc.) and occupancy.

We have used the approaches summarized in Table 3.1, alone and in combination, to characterize ventilation on a room level in classrooms and other educational spaces. They require instrumentation of varying levels of sophistication, ranging from low-cost (anemometer/velocity probe, nondispersive infrared (NDIR) CO2 sensors, low cost PM2.5 sensors) to research-grade. Some instrumentation may serve multiple purposes, for example, NDIR CO2 sensors can be used for controlled-release experiments as well as passive monitoring. Operation of the instruments and execution of the measurements requires varying levels of training. The use of lower-cost sensors allows measurement in several rooms simultaneously, or use of several

monitors in a single room to assess spatial variability in tracer concentrations (mixing). Passive monitoring with user-friendly sensors will be more accessible to nonspecialists than other techniques such as balometry and controlled release experiments, and may be used as part of a long-term strategy for indoor air quality management.

Table 3.1: Table Summary of Approaches for Characterizing Ventilation on a Room Level

Approach	Technique	Advantages	Disadvantages
Direct Flow	**Balometer or anemometer**	• Accepted method, accessible to building managers • Measures total flow of recirculated + outdoor air	• Inconclusive measurements in spaces with no mechanical ventilation • Not possible to separate outdoor and recirculated air exchange rates with this measurement alone
Controlled Release	**CH_4 or C_2H_6**	• Indicates outdoor air exchange rate, gives results for spaces with no mechanical ventilation • Low natural background • High sensitivity • Few indoor sources, occupancy does not interfere with measurements	• Generally requires research instrumentation • Flammable gas
	CO_2	• Gives results for spaces with no mechanical ventilation • Low-cost, reliable sensors readily available • Non-flammable, readily available gas	• Requires empty room since CO_2 emission from the occupants interfere with measurements • Potential for interference from recirculated CO_2
	noninfectious aerosol particles	• Dispersion experiments provide insight into airflow patterns, movement of aerosol within a space	• Technically challenging to generate and detect aerosols • Loss of particles to surfaces, filtration, and resuspension must be accounted for
Passive	**CO_2**	• Collect data during normal facility operation, occupancy • No expertise required • Directly shows of the impact of human exhalation on indoor air	• Uncontrolled conditions complicate interpretation of the results • Other CO_2 sources (vehicles, cooking, recirculated air) may cause interference
	$PM_{2.5}$	• Provides valuable indoor air quality data during normal facility operation • Characterize impact of indoor air pollution sources	• Uncontrolled conditions complicate interpretation of the results • Respiratory particles are greatly outnumbered by 'background' PM • Loss of particles to surfaces, filtration, and resuspension must be accounted for

The ventilation metrics discussed here are summarized in Table 3.2. Ventilation rate is generally expressed as air volume per unit time (and sometimes per occupant). Mitigating the spread of airborne disease requires different metrics, which are generally less familiar to practitioners. Since the goal is to minimize the steady-state concentration of pathogens exhaled

by an infected individual within a room's air, relevant metrics capture how frequently the room's air is flushed, regardless of the number of occupants.

Table 3.2: Ventilation Parameters and Their Definitions.

Parameter	**Units**	**Definition**
Ventilation rate	L s^{-1} or L s^{-1} $person^{-1}$	Volumetric rate of delivery or Volumetric rate of air delivery, per occupant
Air changes per hour (ACH)	h^{-1}	Rate at which room air is replaced by recirculated and outdoor air and equals volumetric ventilation rate normalized to room volume
Tracer air changes per hour (ACH_T)	h^{-1}	ACH as determined by measuring the decay of a tracer species
Balometer air changes per hour (ACH_B)	h^{-1}	ACH as determined via balometry measurements
τ	h	Air change timescale

3.2.1 Direct Flow Measurements

Direct measurements of air flow in ducts are the most basic and commonly accepted method for measuring ventilation on a room scale.[86] As a first pass, or when resources are low, a simple check using tissue paper may be used to determine if air flow exists and identify malfunctioning air handling equipment. In more sophisticated measurements, a balometer (essentially a portable hood that measures volumetric flow rate from supply grilles) or velocity probe is used to measure flow into and out of the room through supply and return grilles. For more information, see ASHRAE (2017). Air changes per hour (ACH, h^{-1}), or the rate at which room air is replaced, can be calculated from balometer measurements by dividing the incoming volumetric air flow rate by the room volume. This is also commonly referred to as the air exchange rate. ACH calculated using direct flow measurement data will include both recirculated

and outdoor air. An obvious major disadvantage of the direct-flow approach is that it cannot be used for spaces without mechanical ventilation, nor can it be used to test the impact of opening doors and windows. For naturally ventilated spaces, another approach is needed.

3.2.2 Controlled Release

Another family of approaches for characterizing ventilation in indoor spaces involves releasing a fixed quantity of an inert tracer substance and observing its decay with time.[84,87,88] A major advantage of controlled-release measurements is that this approach provides ventilation data for naturally ventilated spaces as well as mechanically ventilated ones. These experiments provide an ability to quantitatively test ventilation scenarios to support policy decisions. Controlled-release experiments measure the total ventilation, which could include some infiltration or exfiltration as well as airflow through design openings (windows). Tracer substances employed may include gases such as CO_2, CH_4, C_2H_6, volatile organic compounds (VOCs), SF_6, or particulate matter (PM). Note that, for some gas tracers, particularly VOCs, reactive or deposition loss is possible. In PM tracer studies, particle deposition or filtration must be accounted for. Resuspension of deposited particles is also possible and should be considered in the data analysis. If humans or their activities emit the tracer substance (e.g., in the case of CO_2 or PM) indoors, or if the tracer may be considered harmful to health at the levels used for the test, the room must be unoccupied during the measurement. Occupancy and furnishings may also affect air flow, e.g. by enhancing mixing or obstructing air flow. Fans should be used to disperse the tracer species throughout the space, and mixing should be verified with measurements in different locations throughout the space. Under the assumption of well-mixed

conditions and no sources of emission, the mass balance for a substance in a given space is described as follows:

$$\frac{dC}{dt} = -\frac{1}{\tau}(C - C_{background}) \quad (3.1)$$

where C is the concentration of the tracer substance in the room, t is time, τ is the air change timescale, and $C_{background}$ is the background concentration of the tracer substance in the room when ventilation is operated at a specified condition but no tracer substance has been released. By introducing a corrected concentration variable, $\hat{C} = C - C_{background}$, Eq. (3.1) simplifies into:

$$\frac{d\hat{C}}{dt} = -\frac{1}{\tau}\hat{C} \quad (3.2)$$

Thus, τ can be determined as the inverse slope of the linear regression line of natural logarithm of $\hat{C}$ versus time. Note that if sources of the tracer compound are present, $C_{background}$ may vary with time, resulting in nonlinearity of this relationship. Once exponential decay is confirmed, analysis can be simplified by calculating τ as the e-folding time, or the time for the peak concentration to be reduced by a factor of e. We define $\mathrm{ACH_T}$ (ACH as inferred from tracer decay observations) as follows:

$$\mathrm{ACH_T} = \frac{1}{\tau} \quad (3.3)$$

Figure 3.1 shows typical data from a controlled-release CO2 experiment exhibiting exponential decay, consistent with equation (3.2).

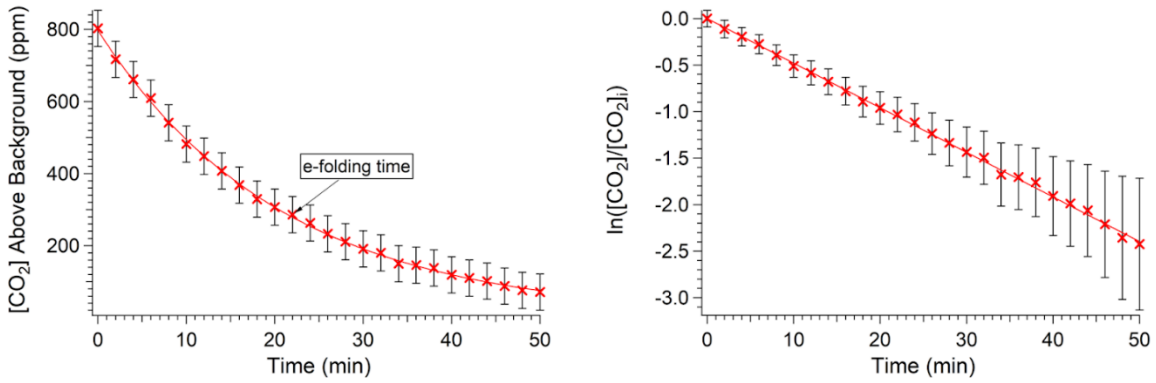

Figure 3.1: Data from a controlled-release CO_2 experiment at North East University A. The decay is exponential as shown in the corrected concentration profile (C-$C_{background}$) on the left. ACH_T is calculated either from the e-folding time or via a linear fit to the log-linear plot. See the Results section for more details.

ACH_T may differ from ACH determined via flow measurements. In naturally ventilated or mechanically ventilated spaces with no recirculation or other air exchange between rooms, $C_{background}$ is the outdoor concentration of the tracer and ACH_T can be interpreted as the rate at which room air is replaced with outdoor air. This is also true for mechanically ventilated spaces with recirculation as long as there are no sources of the tracer elsewhere in the building. The potential exists for interference in CO_2 decay measurements in a densely occupied building with air recirculation or other sources of mixing between rooms. CO_2 transported from occupied rooms would result in an elevated CO_2 baseline reading and potentially interfere with measured decay rates. (Note that, at the time of writing, the background outdoor CO_2 concentration in North America is ~415 ppm).[89] Similarly, small natural gas leaks can cause interference when CH_4 or C_2H_6 is used as the tracer and a sensitive detector is used. Simultaneous measurement of the tracer in the recirculated air is recommended in those cases. ACH_T measurements can be complemented with direct flow measurements for a more complete picture. For PM decay studies in such a scenario, if HVAC filtration effectively removes PM from recirculated air,

ACH_T is the sum of the outdoor and filtered air change rates, and $C_{background}$ would be lower than the outdoor PM concentration.

The choice of tracer substance depends on a number of factors, including the availability of the substance and a suitable detector for the measurement, and the technical complexity of the measurement. Despite the potential for interference described above, CO_2 gas is a widely used tracer for controlled-release experiments. The gas itself is non-flammable and non-toxic at low levels. It is available in gas cylinders from specialty gas or food service suppliers, or in the form of dry ice or canisters for limited studies or demonstrations. Low-cost (~USD $100-200) NDIR CO_2 sensors are readily available and can be repurposed for in situ monitoring after the experiment. CH_4 and C_2H_6 studies have several advantages over CO_2 in that (i) these gases are not emitted by humans so the presence of occupants in the room or elsewhere in the building does not interfere with the test (ii) these gases have a comparatively low natural background concentration (1 ppm for CH_4), allowing high sensitivity in large rooms. However, one disadvantage is that higher-cost (~USD $48,000) research-grade instrumentation is required for sensitive, low noise, high-frequency measurements of CH_4 and C_2H_6. Lower-cost and lower-sensitivity NDIR methane sensors do exist and could potentially be a more affordable alternative, but we have not tested them. SF_6 has similar advantages to CH_4 and C_2H_6, but it has fallen out of use in recent years as it has become recognized as a potent greenhouse gas. N_2O and several halocarbon gases have also been previously used.[84,88]

Controlled-release experiments using dispersion of non-infectious particles may provide insight into airflow patterns and movement of aerosol within a space. This information is especially relevant in the context of COVID-19-related ventilation concerns. Many tracer particle types are possible, including soot from a combustion source, organic aerosols, e.g. from a fog

machine, inorganic salt aerosols such as NaCl, or engineered particles with special properties such as fluorescence.[90] The technical challenges of generating and detecting well-characterized aerosols make this more of a research exercise. There may also be challenges in securing permission for measurements and communicating the data, due to misunderstandings about infectious vs. noninfectious aerosols and safety concerns about inhalation. Information can be inferred about particle dynamics in the space if different PM sizes are measured. We found that building activities which result in periodic aerosol release (i.e., disinfectant fogging) present an opportunity for a 'natural experiment' if appropriate detectors are in place. Low-cost PM sensors may be appropriate for these measurements although there is some concern about the data quality for many of the instruments on the market and attention must be paid to their calibration.[91]

In addition to the considerations listed above, when analyzing the decay of tracer particles, one must account for the particle dynamics that remove PM from air that are not related to ventilation, such as surface deposition, as well as, possibly, resuspension. Therefore, tracer particle decay rates represent total aerosol removal from the room rather than purely room ventilation or ACH. Further research needs to be done investigating size dependence of aerosol decay as well as how aerosol decay directly compares to decay of other tracer gases and room ACH. However, the decay rates found by analyzing in situ $PM_{2.5}$ levels, analogous to the total time that aerosols are suspended in the air, may more directly represent the potential time of exposure to particle contaminants under 2.5 microns (including resuspended SARS-CoV-2-containing aerosols) than would a tracer gas-calculated ACH.

3.2.3 In Situ Monitoring

A third approach for characterizing ventilation in indoor spaces is the placement of sensors for one or more trace species in a space, for passive monitoring during normal facility operation.[92–94] Tracers which are emitted by humans (e.g. CO_2, aerosol, volatile organic compounds) and therefore will fluctuate with occupancy are especially appropriate. This approach is attractive in that it requires relatively little technical expertise and does not disrupt operations. Collecting data during normal occupancy provides a direct measure of the impact of human exhalation on indoor air. Passive CO_2 data can also be useful as a real-time proxy of occupancy that shows daily usage schedules, and may reveal unexpected trends in room usage. In the best case, the real-time data can be linked into publicly visible outputs to support decision making. Long-term in situ monitoring of CO_2 can be accomplished with the same low-cost sensors used for controlled-release experiments, reducing capital investment.

In situ monitoring during events such as in-person classes, which can lead to a buildup of CO_2, and fogging events which occur when a room is disinfected with a cleaning aerosol spray, allow for calculation of the room ACH_T. This approach is demonstrated in Figure 3.2 using data from the two classrooms at the South East University. CO_2 decay after an in-person class is shown in panel A. Note that occupancy in the building was low during the period of these measurements so no interference from CO_2 in other rooms is observed. ACH_T was estimated using Equations 3.1 and 3.2, analyzing the in situ buildup in CO_2 levels during room occupancy and the resulting exponential CO_2 decay after the occupants left the room. $PM_{2.5}$ data for a fogging episode in another classroom is shown in panel B. $PM_{2.5}$ levels in the room varied no more than 1-5 $\mu g/m^3$ during class time, indicating that the concentration of aerosols produced by fogging (an order of magnitude higher) should not be greatly affected by potential particle

resuspension or accumulation during the monitored decay. ACH_T was calculated from in situ PM data following the same exponential decay model. For additional details see the Results section.

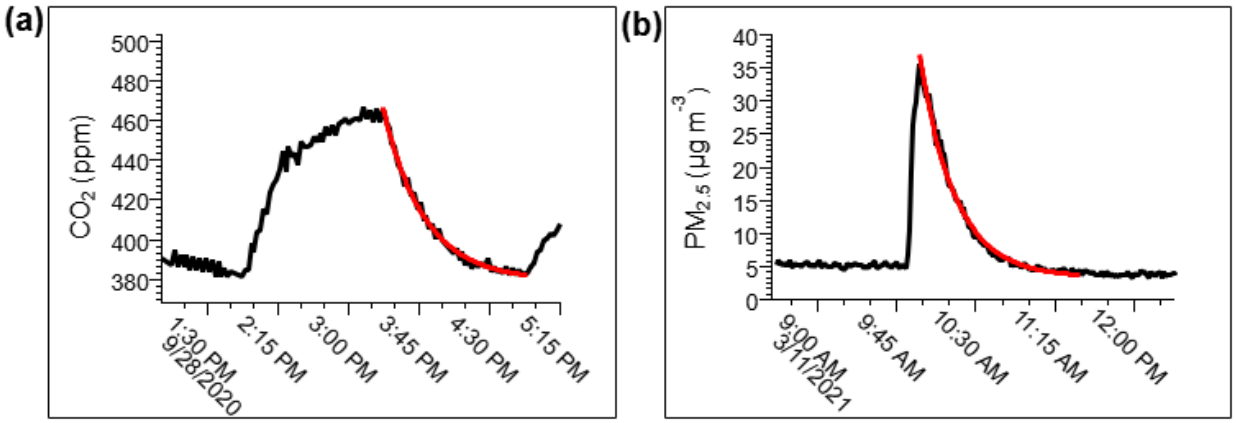

Figure 3.2: Data from the South East University demonstrating the use of in situ data for calculation of ACH_T. (a) Room A CO_2 profile and exponential decay fit (in red) during class time. This room has mechanical ventilation (recirculating indoor air and outdoor air, with a MERV 13 filter between circulation cycles). ACH_T was calculated to be 2.3 h^{-1}. (b) Room B $PM_{2.5}$ profile and exponential decay fit (in red) during a fogging event. This classroom has mechanical ventilation and a portable air cleaner with a high-efficiency particulate air (HEPA) filter. ACH_T was calculated to be 2.8 h^{-1}.

The main limitation of the in situ approach is that uncontrolled conditions complicate interpretation of the results. Direct quantification of ventilation parameters is difficult with this method. Usually, the tendency of the tracer levels to stay within a range (e.g., 600-800 ppm CO_2) is taken as an indicator of sufficient or insufficient ventilation. Sometimes, transient events, such as a gathering of people in a space, may cause temporary buildup of the tracer, allowing observation of its decay and calculation of the air change timescale as described in the previous section. Interference may be caused by other sources of CO_2, such as cooking or vehicles in a garage or near an air intake. As in controlled release CO_2 experiments, interference from CO_2

recirculated or otherwise mixed from other spaces in the building may also be an issue. For this reason, ideally, CO_2 should be measured in the supply air as well as room air.

In situ monitoring of aerosols may lead to confusion in the COVID-19 context since respiratory particles are greatly outnumbered by 'background' PM indoors, as well other particles generated by human activities such as resuspended floor dust, skin flakes and clothing fibers. Therefore, number-based monitoring would not allow detection of a respiratory aerosol signature. Detection of virus-containing respiratory particles requires advanced sampling methods and instrumentation.[95] Selective monitoring of a subset of the indoor aerosol,[96] or analysis of the particle size distribution data may reveal subtle trends linked to human emissions, but will require further research.

3.3 Results

Here we describe ventilation studies conducted by this group using the methods described in the previous section. Controlled-release methods were used in a university and a secondary school in Southern California, two universities in the Northeast with facilities with a range of ages, and two K-12 school districts in Coastal California. Passive sampling was used in a university in the Southeast U.S. and one in the Mountain West. These institutions are referred to herein using pseudonyms.

3.3.1 North East University A

Controlled-release CO_2 experiments were performed between August-December 2020 in nine buildings across two of the University's campuses, located in a dense urban area within a three mile radius. Relatively newer buildings with mechanical ventilation (built 1961-1996) and

older buildings (built 1897-1911) were studied. The older buildings were originally constructed with steam heat and natural ventilation but were later fully or partially retrofitted with mechanical ventilation. In buildings with partial mechanical ventilation, certain parts of the building relied only on natural ventilation. Classrooms to be studied were initially prioritized based on an informal survey of faculty and student recollections of thermal comfort and perceived air quality. Once the method was established and trust was developed with campus facilities and administration, the scope of the measurements was expanded to include a broad survey of classrooms, conference rooms, and elevators.

The spaces were unoccupied during and immediately before each test. A baseline CO_2 reading was taken before initiation of each experiment. Experiments were performed by releasing compressed CO_2 (TechAir) into each room with fans for mixing until a level of 1000-1500 ppm was reached as measured using calibrated NDIR CO_2 sensors (Aranet4, Aranet) which were connected via Bluetooth to an Apple iPhone XR running Aranet software. The primary sensor was located close to the center of the space, while three auxiliary sensors were placed near the corners. Once the CO_2 reading reached the target level and the room air was well-mixed (i.e. auxiliary sensor readings within 250 ppm of primary sensor reading), the operator then exited the room and observed the decay of CO_2 to the baseline via the Aranet software. CO_2 levels in each case exhibited exponential decay consistent with equation (3.2) (cf. Figure 3.1, Methodology section).

The differences between the measured baseline level ($C_{\text{background}}$) and the outdoor background readings preceding the experiments were within the sensitivity of the sensor (<50 ppm) for all but one classroom. This is consistent with the fact that the measurements were performed at a time of very low occupancy in the buildings. For the one exception observed,

$C_{background}$ was 83 ppm higher than the outdoor CO_2 concentration. In this specific case, the experiment was conducted immediately following a controlled-release experiment in the adjacent classroom.

Results for classrooms are summarized in Figure 3.3. In the newer and retrofitted buildings, ventilation was generally satisfactory, with 2.7 $h^{-1} \leq ACH_T \leq 8.7$ h^{-1} for classrooms. Some problem areas with ACH_T substantially lower than 3 h^{-1} were identified in classrooms with natural ventilation in older buildings. The data were shared with campus facilities and administration, resulting in the installation of portable HEPA filter units in classrooms with $ACH_T < 3$ h^{-1} across campus.

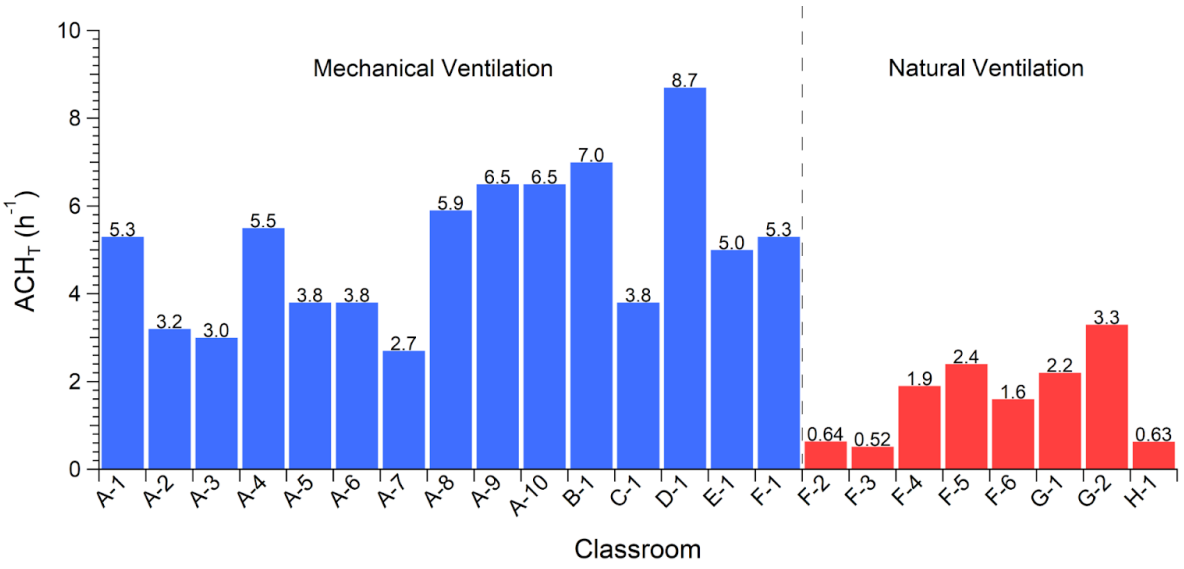

Figure 3.3: Summary of ACH_T as measured via CO_2 decay rate in controlled-release experiments in classrooms for a university in the Northeastern U.S. (North East University A) with a mix of mechanical and natural ventilation.

In parallel with the tracer measurement effort, an independent engineering firm conducted balometer measurements at the supply inlets of some of the mechanically ventilated

classrooms that we characterized. Measurements were not made on the same days, so differences in weather conditions (indoor-outdoor temperature difference, wind speed, heating/cooling load, etc.) and HVAC operation on those days may be a source of discrepancy.[93] Comparison between results of the controlled-release measurements and balometer measurements is shown in Figure 3.4. The buildings had been set for maximum air intake before these measurements were made, and there was relatively low occupancy due to remote study and COVID-19 related occupancy restrictions at the time of the measurements. Ventilation was satisfactory for all of the rooms in this measurement set, by both measures (ACH_T and $ACH_B \geq 3\ h^{-1}$). The two sets of measurements exhibited general agreement for most of the compared classrooms. However, there were significant disparities, up to 6.2 h^{-1} among the remaining 25% of the classrooms, where the balometer results were substantially greater than the controlled-release results. The low baseline CO_2 concentrations that we observed, consistent with the low building occupancy, allowed us to rule out recirculated CO_2 as a major contributor to the observed differences. Some discrepancies may be attributable to the fact that the balometer measurements and controlled-release studies in each classroom were made 2-4 weeks apart during the summer-autumn transition, so cooling and heating conditions varied. HVAC settings were also changed during this time period. In one case, a relatively high ACH_B as compared to ACH_T alerted the facilities manager that outdoor air intake to the building had not yet been increased, and adjustments were made. Besides the classroom measurements, tracer measurements were also conducted in ten conference rooms and four elevators in four different mechanically ventilated buildings. Two out of the ten conference rooms had inadequate ventilation ($ACH_T < 3\ h^{-1}$) and were subsequently equipped with HEPA filter units by facilities. All of the four stationary elevators were well-ventilated ($ACH_T > 5\ h^{-1}$), even reaching values as high as 21 h^{-1}.

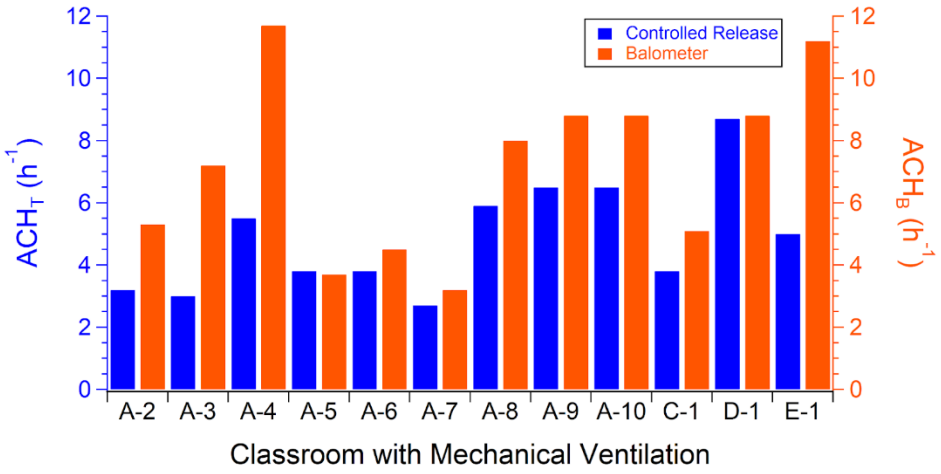

Figure 3.4: Comparison Between the Controlled Release CO_2 Decay Rate and Balometer Air Change Measurements for North East University A.

3.3.2 Coastal California K-12 Schools

Controlled release of CO_2 experiments using the same methodology as described above for North East University A were performed in 50 classrooms across two K-12 school districts in Coastal California, which included preschool, elementary, junior high and senior high schools. These neighboring districts are in a temperate zone where the majority of classrooms were designed with natural ventilation. Many of these classrooms therefore had large windows and most had exterior hallways so classroom doors open directly to the outside, enabling cross-flow. Researchers trained facilities personnel to conduct CO_2 decay measurements using Aranet4 NDIR CO_2 sensors. Facilities personnel then performed experiments and sent CO_2 data to the researchers for analysis. Measurements were performed during January-March 2021. Within each school, the architecture consisted of many similar classroom arrangements and architectures. Therefore, in each school, only a selection of representative classrooms was measured. In each of those classrooms, CO_2 monitors were placed at three separate locations

with respect to the windows and doors. ACH_T was measured first in the "sealed" room with doors and windows closed and HVAC turned off (if available). Once CO_2 returned to background levels, the controlled-release experiment was then repeated under a variety of other conditions: 1) windows open, 2) windows and doors open (usually on different walls leading to cross flow), 3) with the ventilation system on (when available), and 4) with a fan facing out of a doorway or open window. Experiment (4) was only performed in rooms that were suspected by facilities personnel to have ventilation issues. The results are summarized in Figure 3.5. Measurements were taken only on relatively calm days without unusually high wind speed, though a few schools located on coastal bluffs are generally breezy. This led to a dataset of approximately 460 measurements across 50 classrooms.

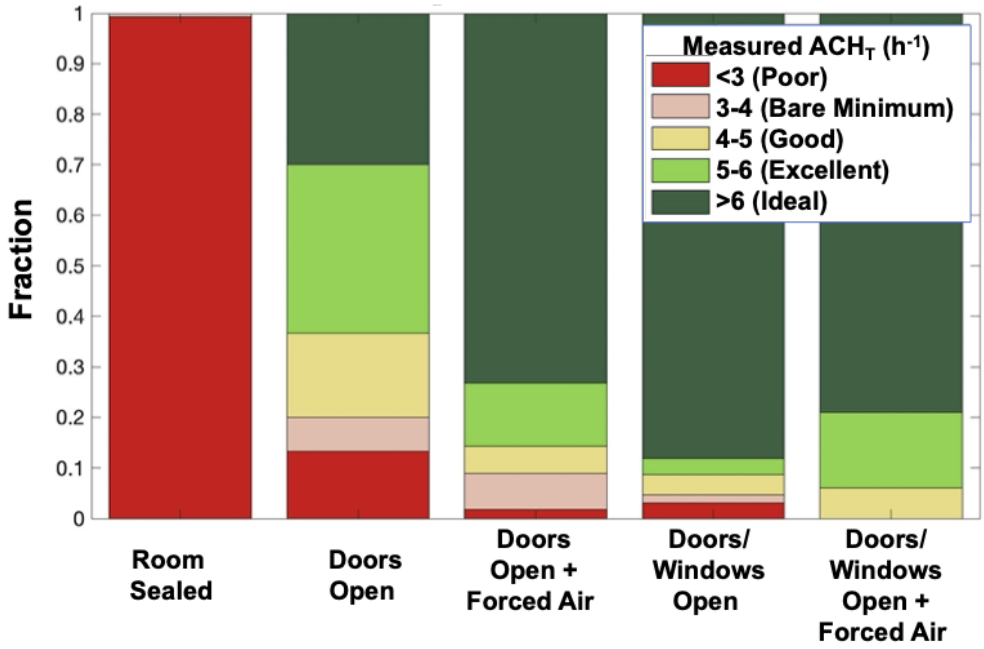

Figure 3.5: The results of CO_2 decay measurements in Coastal California K-12 Schools under different room conditions. ACH_T is binned and color-coded following the ventilation categories of Jones et al. (2020). Dataset represents approximately 460 measurements in 50 classrooms (3 sensors per room, 3-4 measurement conditions per room).

As observed in North East University A, CO2 levels showed simple exponential decay in the majority of rooms and conditions, and were accurately fit as described in the Methodology section. Representative curves are shown in Figure 3.6. As seen in Figure 3.5, none of the classrooms studied had $ACH_T > 3\ h^{-1}$ with closed windows and doors. Unsurprisingly, opening one or two exterior doors increased the overall ventilation rate dramatically; opening windows in addition to exterior doors led to $ACH > 5\ h^{-1}$ in >90% of classrooms measured. Panels (c) and (d) on Figure 6 highlight the additional insight and information that was made possible by using multiple sensors to simultaneously measure CO_2 levels in different locations within each room. In most cases (panels a-b), there is no difference in ACH_T measured at different locations within the room. However, some other rooms showed a positional lag, where CO_2 levels in some locations stayed constant for several minutes after the room was opened, before beginning to decay. Figure 3.6(c) shows data from a room that showed very little CO_2 decay when the doors and windows were sealed. Once two doors were opened, the front, middle, and back of the room still showed no decay for the first 4, 8, and 11 minutes. The onset of decay traveled from one open door towards the other over approximately ten minutes, more reminiscent of a plug flow than the continuously-stirred, well-mixed assumption that leads to eq (3.2). In this room and others, opening windows or adding mechanical ventilation typically reduced or eliminated this lag. Another example, shown in Figure 3.6(d), shows differences in air turnover rates measured within a classroom containing a small alcove set off from the main classroom area. CO_2 decay within the alcove lagged sensors in the main classroom by a few minutes with the door and windows open. While the main room had a high air turnover frequency ($\sim 17\ h^{-1}$), the alcove was lower ($\sim 10\ h^{-1}$). Placing a fan at the door, directed outwards, eliminated the lag in the alcove. Curiously, the added fan actually lowered the general room ACH ($17\ h^{-1}$ to $13\ h^{-1}$, alcove from

10 h^{-1} to 9 h^{-1}), suggesting that the door served as a natural inlet for airflow, which the fan's orientation opposed. Despite these spatial heterogeneities, air turnover was well above target in all locations measured. In a less well-ventilated space, problem zones such as the alcove could be addressed via use of portable air cleaners.

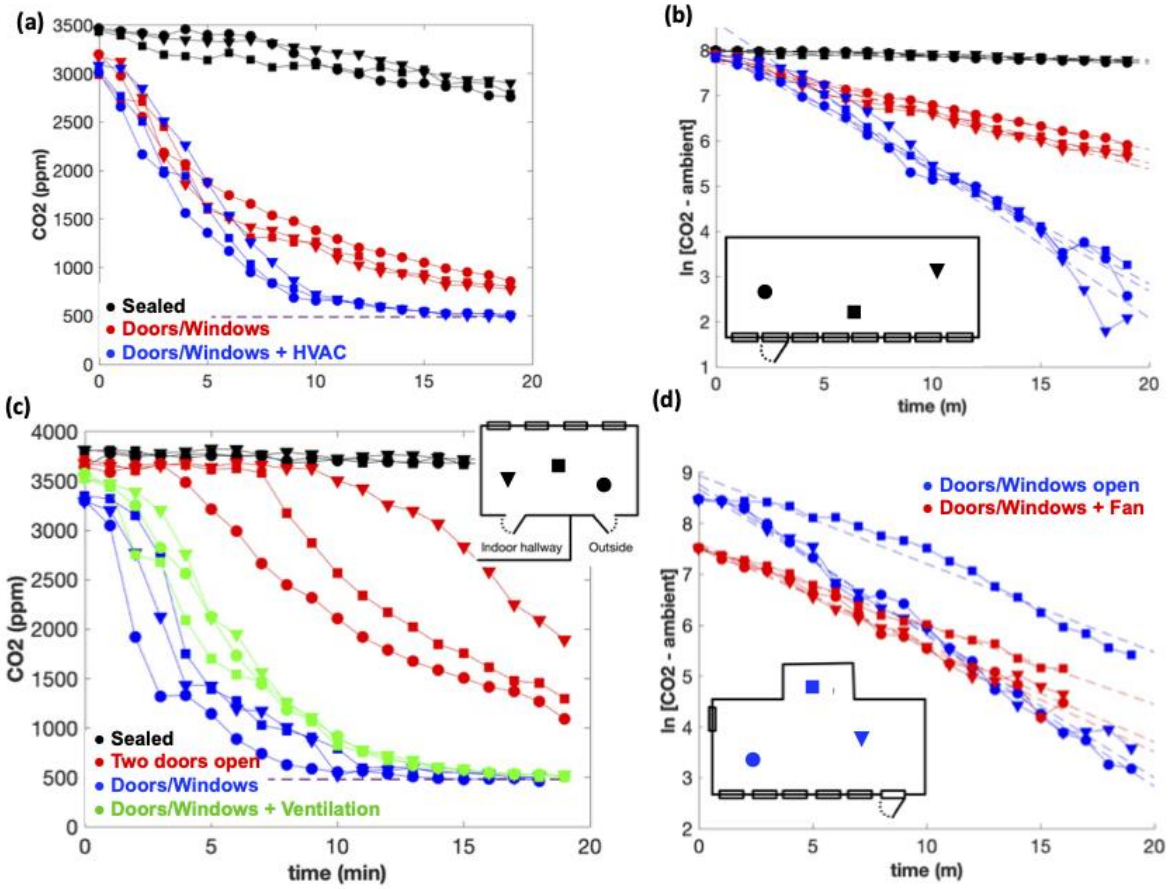

Figure 3.6: (a) CO2 decay measured in three different locations of a Coastal California classroom, under three conditions: closed doors and windows (black), open doors and windows (red) and open doors and windows plus HVAC (blue). The dashed line indicates ambient CO2 level, measured separately. (b) Log-linear plot of data from panel (a); ACH determined from slopes obtained from linear regression fits (dashed). No difference appears between different locations within the room. (c) Room with non-exponential decay and positional lag. (d) Classroom with an 'alcove'.

3.3.3 Southern California University

Controlled release of methane (CH_4), combined with a portable, scientific-grade methane and ethane detector (Picarro GasScouter, a mid-IR cavity-ringdown spectrometer) was employed to measure fresh-air ventilation rates in 21 buildings across the campus from July 2020 through April 2021. Tested buildings were mostly large, monolithic, multistory buildings whose construction spans the past 100 years, and comprise a mixture of laboratory, classroom, meeting, and office spaces. All buildings are mechanically ventilated, and most of the buildings have operable windows. The high data quality (rapid sample rate, low noise) of this sensor allows shorter experiments as well as more confident interpretation of subtle features in decay curves. These advantages are balanced by the substantial cost of the instrumentation; in our case it was also being used for other research studies. Methane (1% in N_2 to exclude the possibility of ignition) was added to a room using a 700 cfm shop fan to boost the ambient concentration to 10-20 ppm, then decay was monitored to below 30% of peak concentration, typically for 10-40 minutes. Using this approach, one person is able to test 8-12 rooms per day, with repeat measurements. We have measured rooms up to 1500 ft^2, with the primary limitation being the ability to keep room air well mixed.

Test results for two research labs are shown in Figure 3.7, plotted as a function of elapsed time with a logarithmic concentration axis. When exponential tracer decay is plotted in this log-linear space, transient changes in ventilation rate can be visually identified as breaks in the slope. The results for Lab 1 are typical for a room with isolated HVAC supply and no recirculated air. Lab 2 exhibited an unexpectedly rapid drop in tracer at the beginning of the test, which we can interpret as resulting from dilution of the tracer into an adjacent space that shares ventilation with Lab 2. Occupants of the two rooms would not be effectively isolated from each other. This

demonstrates the utility of high-performance measurements in finding unexpected (and perhaps undocumented) aberrations in HVAC system construction or operation.

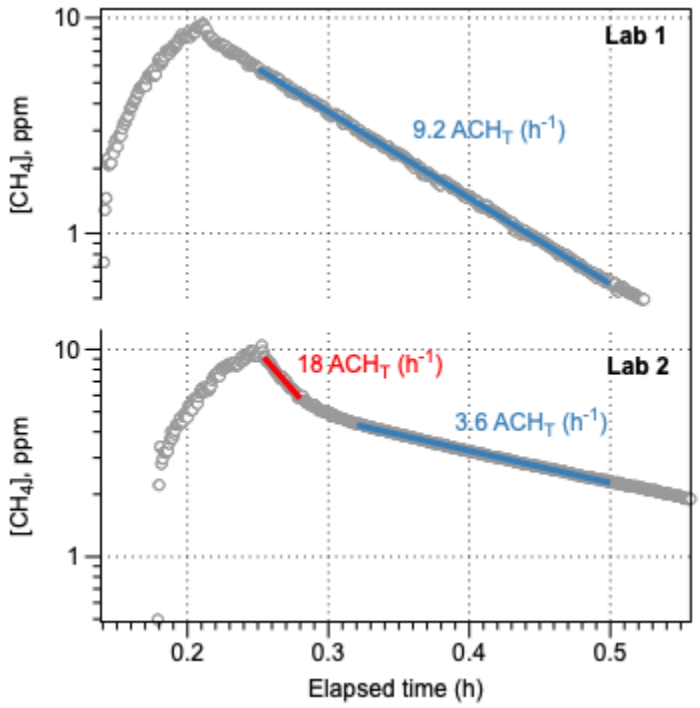

Figure 3.7: Ventilation test results using CH_4 tracer and a Picarro GasScouter sensor for two different labs at Southern California University. Lab 1 is typical for spaces with isolated ventilation, but in Lab 2 we observed rapid dilution of the tracer (red line) into an adjacent room before stabilizing into a normal decay. Note that each test lasted <30 minutes total.

After a period of initial method development and optimization, the methane test equipment has been deployed by the University's Facilities & Operations staff, and is being used in support of reoccupation planning. Figure 3.8 summarizes the data collected thus far. Fresh-air exchange rates varied from room to room, and building to building, over a very large range. Low values were typically encountered in offices and restrooms, and the highest values (>10 h^{-1} ACH_T) almost all represent laboratory spaces. These ranges highlight the inherent difficulty of measuring a few spaces and extrapolating to others in the building. Note that many higher

education laboratories are operated with 100% outside air ventilation. Also visible is a decline in the average air-exchange rates from the oldest buildings through those built in the 1980's, a result of historically increasing prioritization of energy efficiency, recirculation, and air-tight building construction.

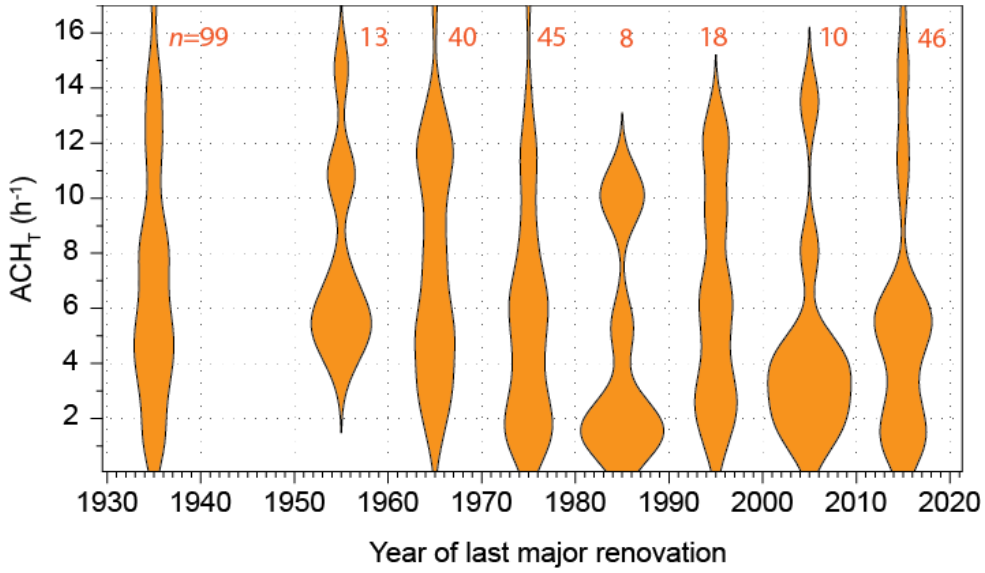

Figure 3.8: Violin plot of ACH_T calculated from CH_4 tracer measurements in 279 rooms from 21 buildings across the Southern California University campus, binned by decade of last HVAC system replacement. Each vertical symbol represents the probability distribution function (PDF) of ACH values among rooms from buildings of that age class. Number of rooms in each age class is given at the top in red.

3.3.4 Southern California Secondary School

The same methane tracer and Picarro GasScouter technique described in the previous section was also employed at a nearby secondary school during October 2020. The school comprises a campus of multiple buildings constructed over the past century, with a range of construction types from cottages and small (4-6 room) single-story buildings to larger, multistory monolithic buildings with >30 rooms. Given the moderate climate, similar to the California

Coastal schools, many of the older buildings were originally built without forced-air heating or air conditioning, and were instead designed with large banks of windows on opposing walls to maximize natural ventilation. The tested rooms included classrooms, offices, and other specific-use spaces (dining, choir, theater) across a representative cross-section of buildings. Since leaving windows open all winter is a realistic option for this school, our initial interest was to compare ventilation rates with windows sealed and HVAC systems continually running, versus with windows open. Consistent with the Coastal California School study, comparison of 11 classrooms and offices demonstrated the clear benefit of opening windows, with ventilation in every space at least doubling, and increasing 3-fold or more in many rooms (Figure 3.9). This led quickly to a decision that all windows would remain open when the school was occupied, regardless of outside temperature. In our experience, this ability to test scenarios and provide immediate, quantitative data to support policy decisions is one of the key benefits of the trace-gas testing methodology.

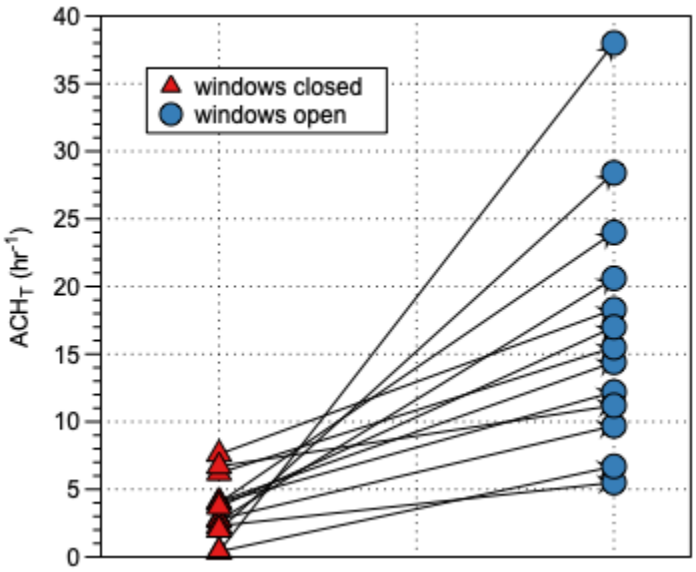

Figure 3.9: Comparison of measured outside-air ventilation rates for 11 classrooms and offices in the Southern California Secondary School with windows closed, HVAC on (filled symbols) versus with windows open (open symbols).

With the decision to keep windows open, all subsequent testing was done as such. Results are summarized in Figure 3.10, which bins buildings by age of construction. This comparison emphasizes the contrast between older, smaller buildings with many windows, versus newer, larger buildings that rely on mechanical ventilation. Nevertheless, even the newest buildings all achieved ≥ 4 h^{-1} ACH_T. In the older buildings, rooms with windows open achieved a stunning 21.3 h^{-1} ACH_T on average, levels that are more than 3 times the WHO guidelines even for healthcare settings (6 ACH). These encouraging results provide a counterpoint to our findings in North East University A and B, that older buildings in cold climates, which were designed for heat retention, often have poor (<2 ACH) natural ventilation.

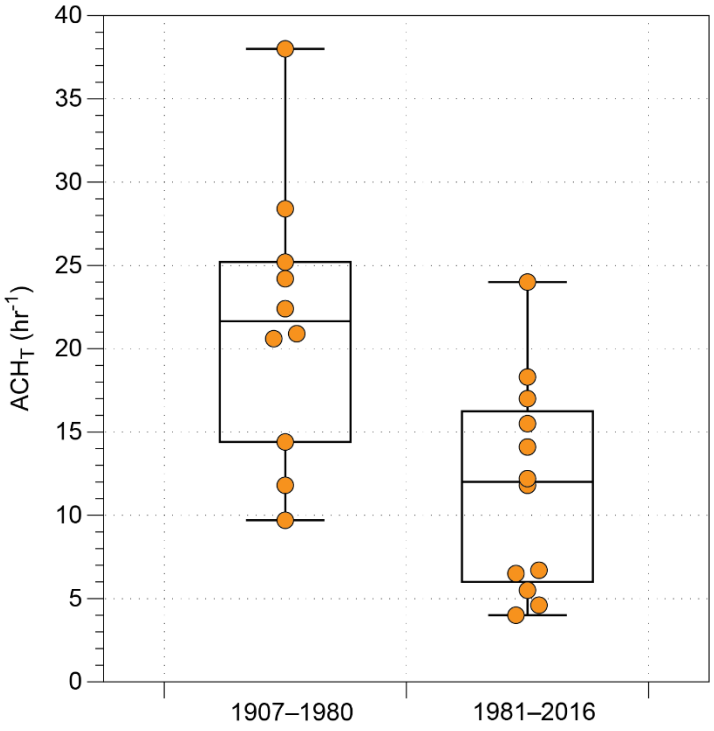

Figure 3.10: Summary of ventilation test results for 22 classrooms and offices of the Southern California Secondary School, binned by year of construction. All spaces were tested with windows open using the CH_4 controlled-release method.

3.3.5 Mountain West University

Twelve NDIR CO_2 sensors (Aranet4, Aranet) were installed in mechanically ventilated rooms in buildings across the campus from September 2020 through April 2021 for passive in situ monitoring, with the goals of gaining insight into room usage and ventilation. Building construction dates spanned from 1985 (lecture classrooms) to 1999 (gym complex) and 2002 (music building). Information was shared with the campus facility managers to allow for optimization of ventilation. The rooms included four large ensemble music classrooms, two individual music practice rooms, two standard lecture classrooms, one science laboratory classroom, and three rooms in the campus gym facility. In all cases, ventilation is provided via forced air through centrally regulated HVAC units.

The sensors recorded CO_2 levels every 2 minutes. Data was averaged during typical main usage hours (08:00 – 22:00 for music classrooms and practice rooms; 09:00 – 15:00 for lecture classrooms; 15:00 – 21:00 for the gym), over non-holiday weekday (Monday-Friday) periods during the academic term between September and April. Figure 3.11a shows that during typical hours of operation, most rooms with sensors showed CO_2 levels <500 ppm for 70-80% of measurements. The average of the three gym sensors showed higher average readings, though these measurements show that 95% of measurements were still <800 ppm. These CO_2 levels are within a range that would indicate satisfactory ventilation during full occupancy of the space, but we note that there was reduced occupancy during the time of these measurements due to COVID-19-related restrictions.

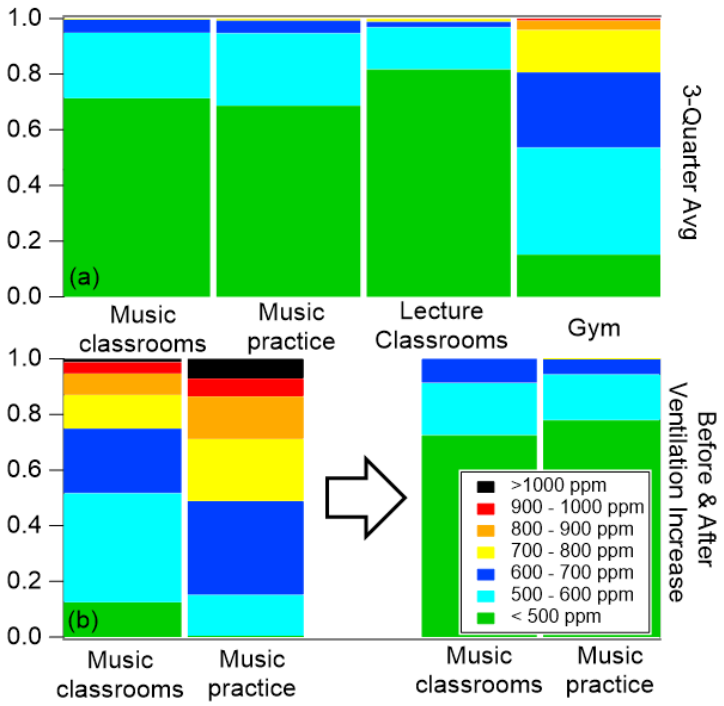

Figure 3.11: Passive CO_2 measurements showing relative fraction of time observed in each concentration range from the Mountain West University. (a) Data reported for four different types of classrooms, averaged over in-use periods during three academic terms of observation. (b) Nighttime data for music classrooms and practice rooms for Fall academic term comparing before (left columns) and after (right columns) building ventilation was optimized to run at night and on weekends. See the text for additional details of the averaging periods.

As an example of actionable information that was obtained, overnight (10:00 PM - 2:00 AM) CO_2 buildup was observed in classrooms and practice rooms in the music building when the rooms were used informally as practice spaces after hours (Figure 3.11b). The ventilation operation for that building was initially set up based on anticipated classroom usage to run only from 5:30 AM until 6:00 PM and was off at nights and on weekends. Figure 3.12a shows data from one music classroom over a two-week period as an example of the high CO_2 concentrations, overnight buildup in CO_2, and slow decay rates frequently observed. After the data was shared with the facilities managers, the HVAC schedule was updated to include ventilation after hours. This is important if the space is being occupied after hours. CO_2 levels at

night fell dramatically to where only <10% of measurements were >600 ppm (Fig 12b), and variability in CO_2 concentration decreased. A time-series of CO_2 concentration following schedule optimization shows the average CO_2 concentration dropped from 741 ± 105 ppm to 517 ± 43 ppm.

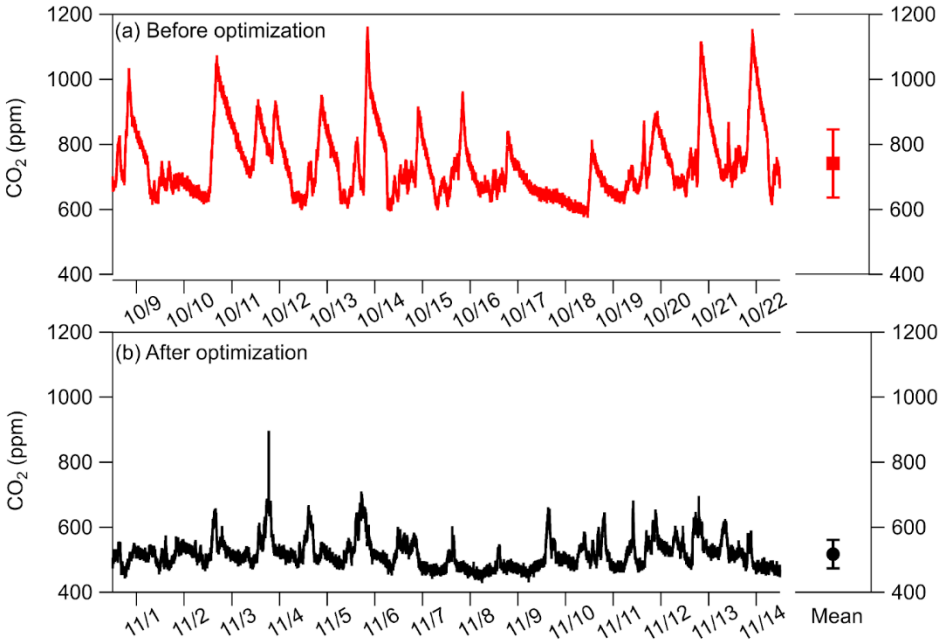

Figure 3.12: CO_2 concentrations shown for a single ensemble music classroom at the Mountain West University before (a) and after (b) ventilation schedule optimized to run also at nights and on weekends. Mean value shown for two-week window displayed in each case, where bars show standard deviation of measurements.

As the above example illustrates, the usage of passive CO_2 devices provides a relatively simple, inexpensive, and low-maintenance way to monitor ventilation or changes in space usage, that allows facility managers to make critical updates to ventilation schedules based on real usage data. Observations in the gym complex provided (Figure 3.16 in the Supporting Information) a complementary example to the music building scenario, in which passive CO_2

monitoring revealed trends in space usage and confirmed the suitability of the ventilation schedule for that facility. See Supporting Information for more details.

A single PM sensor (QuantAQ MODULAIR-PM) was also continuously operated to passively monitor particulate concentrations in one private music practice room where a CO_2 device was also installed for passive monitoring. Over a six-month measurement period of November – April, CO_2 and PM1 concentrations were compared on an hourly basis and are shown in Supplemental Figure 3.17. The time series of CO_2 and PM_1 values (Fig. 3.17a) show only mild and inconsistent similarity, and a direct correlation plot (Fig. 3.17b) shows an extremely low R^2 value of <0.1. Correlations with $PM_{2.5}$ and PM_{10} are similarly poor, but are not shown. As expected, these two pollutants are not related as there are many other sources of particulate matter indoors that do not also emit CO_2. In some cases, CO_2 concentrations are high and PM is relatively lower, and in other cases the opposite is true. These data illustrate that in situ PM monitoring alone, or in combination with CO_2 monitoring, cannot easily provide information about the risk of transmission of airborne pathogens in an indoor space, due to the low contribution of respiratory-generated particles or aerosol-borne pathogens to the overall aerosol burden.

3.3.6 South East University

Professional grade low-cost sensors (QuantAQ MODULAIR-PM and MODULAIR) with the capability to detect carbon dioxide (CO_2) and particulate matter (PM) were deployed to monitor these species and characterize ventilation rate in various classrooms and indoor spaces at a university in the urban Southeast U.S. from August 2020 through March 2021. The MODULAIR-PM sensor measures PM through a combination of an optical particle counter

(OPC) and nephelometer. Similar to Mountain West University, poor correlation was observed between simultaneous in situ CO_2 and PM measurements. Buildings studied were built from 1920-2020 and have mechanical or natural ventilation systems. Portable HEPA filter-based air cleaners were added as a mitigation to rooms with older mechanical ventilation systems (prior to 1960s). As discussed in the Methodology section, we took advantage of in-person classes and fogging events that occurred when a room was disinfected with a cleaning aerosol spray to calculate ACH_T. In-person classes led to a buildup of CO_2 in the room, while fogging released PM. It was ensured that fogging was conducted when no one was in the classroom, and that the personnel performing the fogging were wearing appropriate personal protective gear. In our calculations, it is assumed that the room is well mixed, the only sources of CO_2 during classroom occupancy are the occupants, and the only source of PM during the fogging event is the fogging spray. When using PM data to estimate ventilation rate, it is assumed that the effects of aerosol deposition and gravitational settling on aerosol decay rate are negligible. Thus, the calculated ventilation rate based on PM decay analysis may be an overestimation.

Data from two selected classrooms were presented in Figure 3.2 of the Methodology section as examples of the technique. Room A is a large lecture hall that is equipped with an HVAC system recirculating indoor air and new outdoor air. The mixture of recirculated and outdoor air is filtered by a MERV 13 filter. Room B is a smaller 20-person classroom that is equipped with an older HVAC system and has a mix of recirculated and outdoor air that is filtered by a MERV 8 filter. Room B also has an added portable air cleaner with a HEPA filter. In these two rooms, background indoor CO_2 levels ranged from 350 to 450 ppm, and CO_2 levels during in-person classes averaged from 430 to 600 ppm, occasionally reaching 1000 ppm. Background $PM_{2.5}$ levels ranged from 1 to 10 μg m^{-3} in general, with occasional levels up to 20

μg m^{-3}, while fogging events resulted in $PM_{2.5}$ levels of 40-80 μg m^{-3}. The primary filtration of air in Room B is due to the portable air cleaner, which can provide an ACH of up to 4 h^{-1} at the maximum setting. Using the decay of $PM_{2.5}$, the ACH for was estimated to be 2.8 h^{-1}. This indicates that the unit was likely not running at the maximum setting during the fogging event.

Figure 3.13 shows a summary of ACH_T calculated from CO_2 decay data in six different classrooms in six buildings across campus over a 2 week period in March 2021. Data are also shown for ACH calculated from the HVAC air supply rates that were available. It is important to note that the ACH values estimated from HVAC flow rates are based on total air flow to the room, which is a mixture of outdoor air ("clean" air) and air recirculated from other rooms (that may contain higher levels of CO_2 from occupancy.) Although during the sampling period there were low building occupancy levels due to COVID-19 restrictions, the ACH estimated from HVAC supply flow could be an overestimate of clean air changes. ACH calculated using the air supply was similar to the measured ACH_T in each case, suggesting that there is no significant interference from recirculated CO_2. Overall, the absolute ACH values found across all buildings were on a similar order of magnitude, regardless of building age or type of ventilation (mechanical vs natural). The one exception is the room in building 5, which saw significantly lower ACH values. This observation was in agreement with building 5 having one of the older HVAC systems on campus, and for this reason was equipped with an additional portable HEPA filter air cleaner prior to the beginning of the semester. Unlike the observation by North East University A, the ACH_T for the naturally ventilated classroom was on the higher end of the range of mechanically ventilated room ACH_T values, despite being much older than the other buildings investigated. Similar to what Southern California Secondary School noted, this can be attributed to the fact that building 6 is a small classroom with multiple windows. In contrast, buildings 1-5

have no windows, appear more tightly sealed, and run with mechanical ventilation systems. This is common in both the Southeast U.S. (due to high humidity and heat) and in large university buildings in order to combat high energy expenditures.

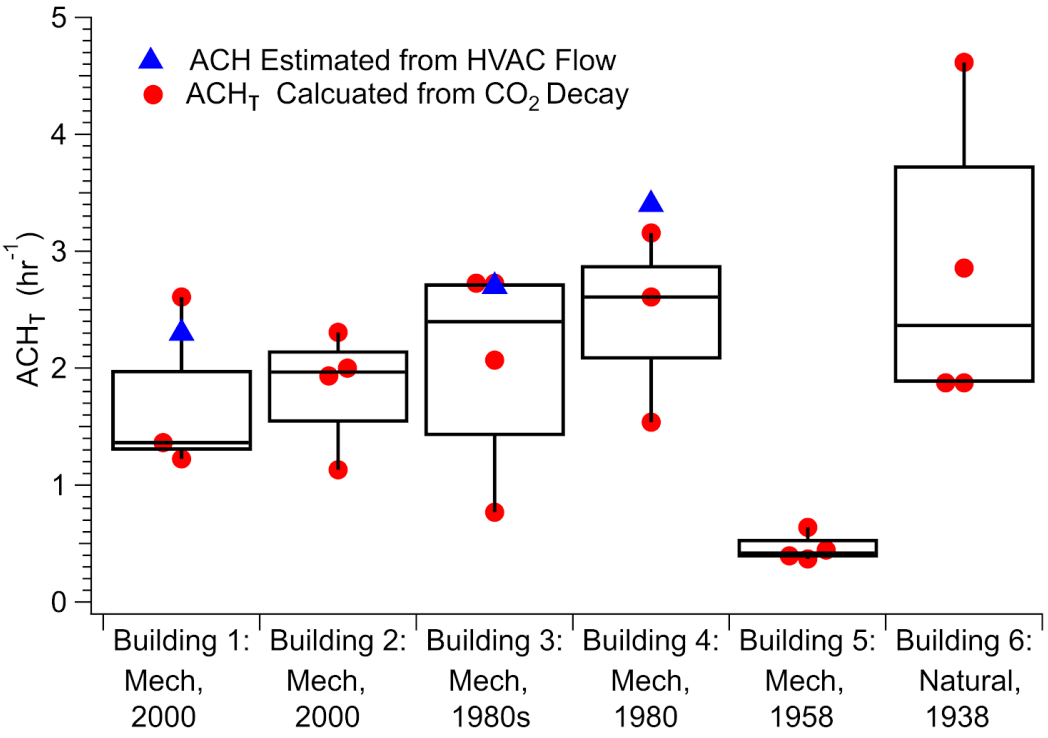

Figure 3.13: Samples collected from 6 rooms in 6 different buildings with either mechanical (Mech) or natural ventilation over the same 2 week period. Red dots are calculated from in situ CO2 data during different classes in the same room. Blue triangles are from recorded HVAC air supply rates.

In addition to structure and ventilation design, the rooms studied in buildings 1-5 are centrally located in the building layout. These factors, combined with the fact that buildings 3-5 have older ventilation systems, could partly explain why observed ACH values were lower than those reported by some of the other universities. It should also be noted that during the sample period, ventilation rates were not at their maximum levels. The rooms in buildings 1 and 2 have CO_2 demand-controlled ventilation, meaning that once CO_2 levels reach a certain value (often

800-1000 ppm) the HVAC system will automatically increase air flow rates. During the time period that these samples were collected, classroom occupancy was limited due to COVID-19 precautions and CO_2 levels did not exceed 750 ppm in either room. It is possible that higher CO_2 levels would result in higher ACH_T values.

3.3.7 North East University B

Similar to North East University A, North East University B is situated in an urban area, and comprises buildings with a range of ages and ventilation types. To address the challenges of increasing ventilation and filtration in campus spaces without mechanical ventilation or limited supply, we explored the impact of two portable air cleaner devices on air change rate, and the spatial variation in PM concentrations in a naturally ventilated space, via controlled release of particulate matter. The two air cleaner devices were: (a) a commercially available HEPA recirculating air cleaner (Model HPA 304, Honeywell, Charlotte, NC) as well as (b) an in-house designed and fabricated unit known as the Air Filtering Ventilation Unit (AFVU), which brings in some outdoor air, tempers with a return, and includes MERV 14 filtration, effectively simulating a typical mechanical ventilation system (Figure 3.18, see Supporting Information for more details).

A library space on campus with no mechanical ventilation, was used for testing as it was representative of other classroom spaces and common rooms on campus. Additional details of the testing space are given in the Supplemental Information. The room was pre-cleaned by HEPA filtered vacuuming and damp wiping of hard surfaces, and a sticky mat was placed at the room entryway. Radiator blower fans were turned “off” during testing. In addition, all windows, fireplaces, passive air transfer grilles, built-in wall bookcases, radiator covers, and floor rugs

were covered with polyethylene sheeting and taped shut. As testing was conducted in January 2021 with lower humidity levels (19-22%), all polyethylene sheets used in the space were electrically grounded by bonding with aluminum metal tape and copper wire to metal outlet covers to help reduce static electricity. The commercial air cleaner was operated in two modes (80 CFM and 320 CFM) and was positioned in the center of the room, 0.6 m away from one of the 4 sampling locations (S1, Figure 3.19). Details of the AFVU placement and operation can be found in the Supporting Information.

Test PM was generated using fog generators (Model C Breeze, Degree Controls, Inc., Milford, NH) with long-duration fog liquid. Paraffin candles ("Glimma", Ikea Systems, BV, Sweden) were also used to generate test PM. PM levels (0.02-1.0 μm) were monitored in real-time using a P-Trak monitor (Model 8525, TSI, Shoreview, MN). Four P-Trak monitors were positioned at different locations across the testing space and operated in parallel. Temperature and humidity (Model EVM, 3M, Oconomowoc, WI) was also continuously monitored at the approximate room center.

In the first set of experiments, we used the controlled release of PM to evaluate the air change rate provided by each of the portable air cleaner devices. This procedure was modified from one developed by the Association of Home Appliance Manufacturers (AHAM) for testing portable air cleaning devices inside a sealed laboratory chamber, but here we use a real-life space with less controlled conditions and a different PM source. In this set of experiments we released PM from two foggers, which were oriented facing the center of the room, positioned 1 m from opposite walls, and 1 m above the ground (Figure 3.14). The generated PM was dispersed in the room using two box fans (Model 9723, AirKing, Inc., West Chester, PA) for 1 minute. These box fans werepositioned under the fogger devices. The foggers were then shut off, room air

mixing continued for one additional minute with the box fans, and particle concentrations monitored for 10 minutes, at which time four recirculating HEPA-filtered blowers (Model Defendair HEPA 500, Sylvane, Inc., Roswell, GA) were turned on to clean room air in preparation for the next test. Natural particle removal (decay) rates were measured this way under static room conditions without any ventilation or air cleaning equipment running. The effectiveness of the AFVU and the commercially available HEPA air cleaner were assessed individually by turning each unit on once the fog release and air mixing were completed, and the rate of aerosol removal was compared to the natural decay rate. PM decay was assessed at each of the four sampling locations; the mean and associated standard deviation are shown Figure 3.14. The AFVU and the commercially available portable air cleaner both enhanced ACH_T compared to natural ventilation in the test space (1.9 per hour). Operation of the commercial filtration unit at the low fan speed (80 CFM) provided 3.6 ACH_T. Increasing the flow of this unit to 320 CFM achieved a similar ACH_T as the AFVU 4.4 per hour.

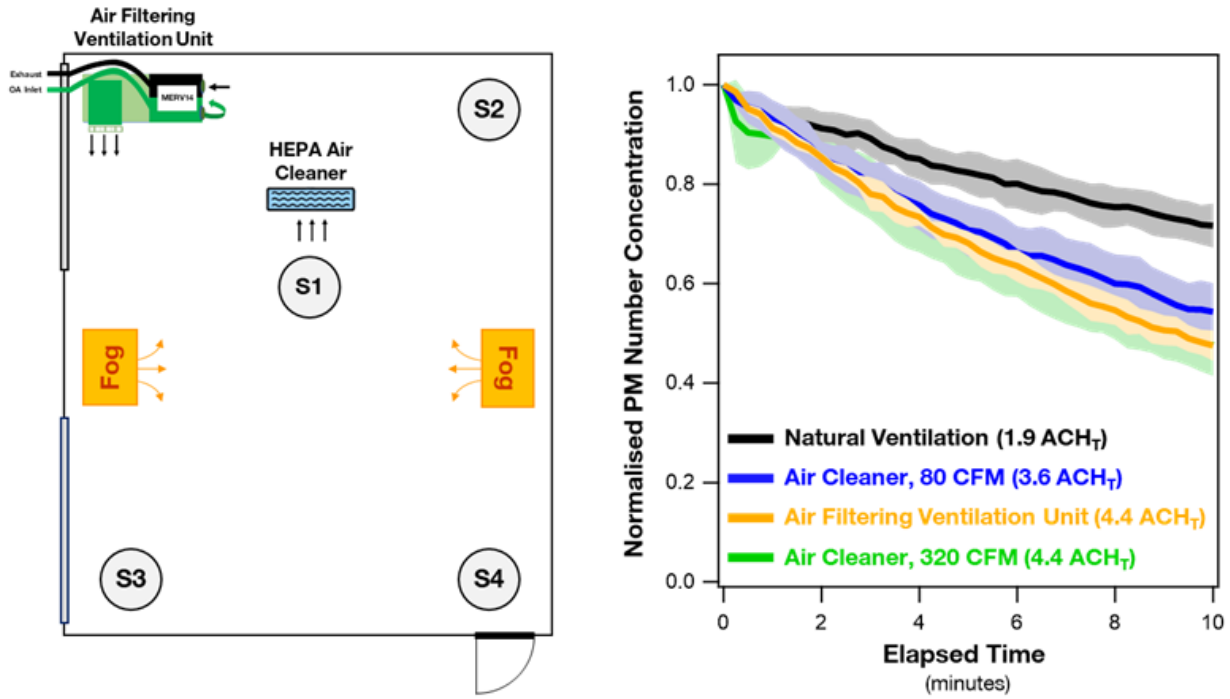

Figure 3.14: Comparison of PM tracer decay using different filtration/ventilation approaches in a naturally ventilated library test space in North East University B. Left: The plan view indicates the location of two fog generators, the PM sampling locations (S1-S4), and the two supplemental filtration/ventilation devices that were individually evaluated: an air filtering ventilation unit and a commercially-available air cleaner. Right: Ventilation test results for various scenarios are shown with the measured ACHT.

We also evaluated the spatial distribution of aerosol across the test space using the two supplemental filtration/ventilation approaches (see Supporting Information). When a continuous PM source was provided via burning candles in the center of the test space, use of the commercial HEPA recirculating filter resulted in more spatial heterogeneity than the AFVU, with high stable PM concentrations found over the entire test period at sampling locations S1 and S3 (Figure 3.19 in Supporting Information). This was attributable to the poor mixing of vertical discharge under dynamic continuous PM generation for the ventilation conditions of the room and lower airflow rate compared to the AFVU. Details may be found in the Supporting Information.

Overall, the mid-sized recirculating HEPA-filtered air cleaner improved ACH_T in the naturally ventilated library. The highest fan speed of the commercial device achieved an equivalent total ACH as the AFVU that provides 20% outdoor air. The AFVU, however, provided improved PM removal rates across the test space compared to the commercial unit when tested against continuously generated PM that might occur in an occupied room. We concluded based on these studies that deployment of the two tested portable air cleaners in spaces without mechanical ventilation on campus could be used to improve indoor air quality, aligning spaces with applicable ventilation guidelines and support increases in room occupancy rates.

3.4 Discussion

Figure 3.15 shows a summary of the ACH measurements made at the different institutions in this study.

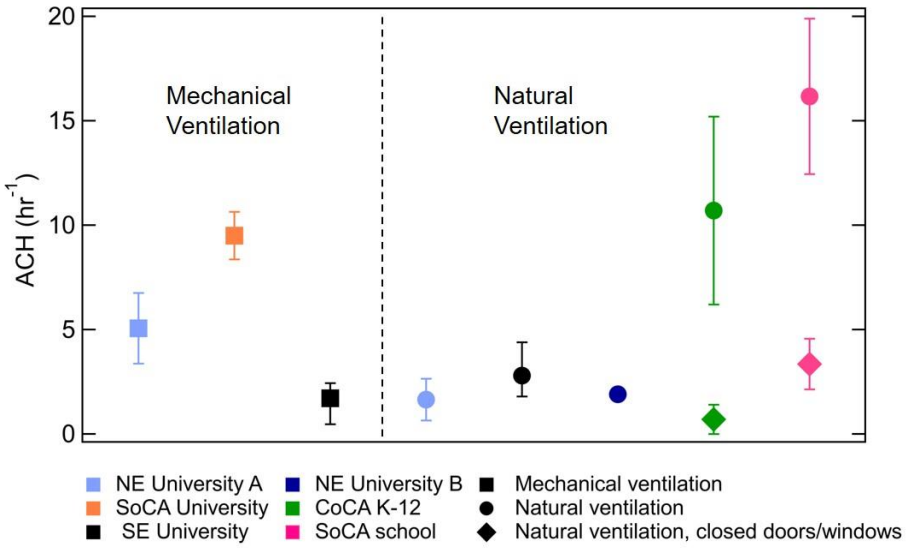

Figure 3.15: Summary of ventilation measurements reported here. NE: North East, SE: South East, CoCA: Coastal California, SoCA: Southern California.

The naturally ventilated buildings on the West Coast studied here were designed for cross-ventilation and had relatively high ACH, particularly when windows and exterior doors were opened, consistent with previous findings.[97] In each case, cross-ventilation with open windows and/or doors led to higher ventilation rates than sealing the room and using HVAC. For the buildings studied in Southern California, older construction corresponded to better ventilation.

Older buildings in the Northeast U.S. without mechanical ventilation, designed to keep heat in during cold winters, often have insufficient air exchange. Many buildings in the Northeast were designed in the wake of the 1918 influenza pandemic for windows to be open year-round, even while a steam radiator was in operation during winter.[98] This practice has fallen out of favor over the past century as energy efficiency became a priority. Given the relatively low cost of portable filter-based air cleaners, their installation in buildings of this type may be justified even when ventilation data are not available for these spaces, or measurements are not practical.

We note that, for both naturally and mechanically ventilated systems, ventilation parameters and airflow patterns vary with occupancy and ambient weather conditions or season. Measurements should ideally be made for a variety of conditions to get a more comprehensive picture of ventilation for a particular space.

The controlled-release experiments described here were effective for characterizing ventilation in a mixture of building types encountered in U.S. universities and K-12 schools in a repeatable manner. While all the approaches discussed here yielded valuable insights, those employing low cost, reliable, easy-to-use sensors are best suited to general use. Other approaches employed costly equipment or required specialized technical expertise to perform the experiments or interpret the data.

At North East University B, controlled-release PM experiments allowed estimation of air change rates and revealed spatial variation in flow patterns in naturally ventilated rooms. Those results, along with the observations of delayed clearance in sections of some irregularly shaped classrooms in the Coastal California K-12 School District (Figure 6), highlight that a room-level evaluation of ventilation may mask heterogeneity in flow fields and potentially problematic microenvironments within an otherwise well-ventilated room. The effectiveness of this approach relies on the use of very fine particles that have minimal additional removal process such as deposition to surfaces. In situ monitoring of absolute PM concentrations is fundamentally limited as an indicator of aerosol pathogen risk, however, because the concentration of PM associated with respiratory emissions of infected individuals will generally be small compared to background aerosol.

CO_2 controlled-release experiments, such as were performed at North East University A and Coastal California K-12 School District, are most effective for naturally ventilated buildings or during periods of low occupancy in mechanically ventilated buildings, due to the risk of interference from recirculated CO_2. For the studies presented here, which were conducted in Summer-Fall 2020 and early 2021, low occupancy was the norm due to COVID-19 related occupancy restrictions, but similar conditions may be encountered after hours or during holidays.

In situ monitoring is an accessible approach for observing air quality trends while a space is being actively used, allowing quick response once problems are identified, in the form of schedule changes or engineering interventions. Setup and maintenance of low cost sensors for CO_2 or PM requires relatively little technical expertise.

Ddd

3.5 Conclusion

Ventilation and filtration are key components of a layered approach towards risk reduction for the transmission of airborne infectious diseases. Such an approach also includes vaccines, masking, physical distancing and other controls on occupancy, and testing. Adequate ventilation and air cleaning is also critical for maintaining healthy indoor air quality.

We have presented a number of practical approaches for gathering room-level ventilation data for educational spaces, and anecdotal examples of their application in a range of building and room types, and climates across the U.S. In particular, approaches using reliable low-cost air quality sensors show promise for use by nonspecialists. Room-level ventilation data allows consideration of indoor air quality and transmission of respiratory disease in decision making with regards to occupancy and ventilation strategies. As we have demonstrated, it can also be critical in identifying areas for mitigation (i.e. with filtration devices) and providing clues into building occupancy patterns which must be accounted for in the ventilation strategy.

Ventilation data can also be useful for communicating and building trust with faculty, staff, students, and the rest of the community. Knowing that ventilation is satisfactory, problem areas have been identified, and mitigation measures have been put into place can ease anxieties and build confidence about return to campus or increased occupancy, and improve confidence in the future indoor air quality. Broad participation in the process of data collection, made possible by the use of more accessible approaches such as in situ CO_2 monitoring with low cost sensors, can provide an additional sense of agency.[99]

3.6 Supporting Information

Mountain West University

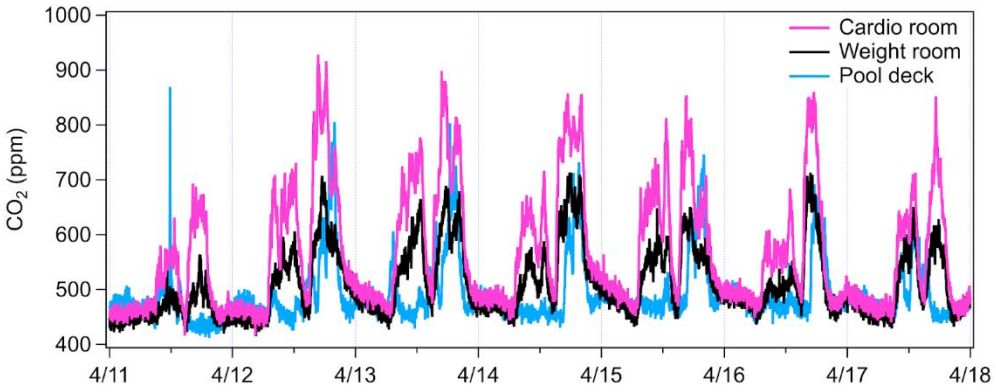

Figure 3.16: CO_2 concentrations for a one-week period in three areas of the Mountain West University campus gym.

Figure 3.16 shows the time series of CO_2 concentration in three areas of the campus gym. The average concentrations match observations shown in Figure 3.12a. Having access to CO_2 information at high resolution, especially if in real-time, however, shows trends in usage that are not observable from broader averages. Figure 3.16 shows a very repeatable daily cycle matching differences in room usage. The cardio and weight rooms are used more heavily, with daily peaks in the late morning and early evening. A drop in CO_2 concentrations can be seen at 1:00 PM when the gym closes for an hour. Having access to passive CO_2 data like this can be an efficient, non-invasive way not only to record gym usage, but to verify that occupancy is well-matched to HVAC strategies. In this example, the data shows that concentrations rarely exceed 800 ppm in the cardio room, and never significantly above 700 ppm in either the weight room or on the pool deck. These results suggest a ventilation strategy generally well-matched to the usage of rooms.

Simultaneous passive CO_2 and PM_1 monitoring results from one private music practice room are shown in Figure 3.17. As described in the main text, the correlation between PM and CO_2 in this space was poor.

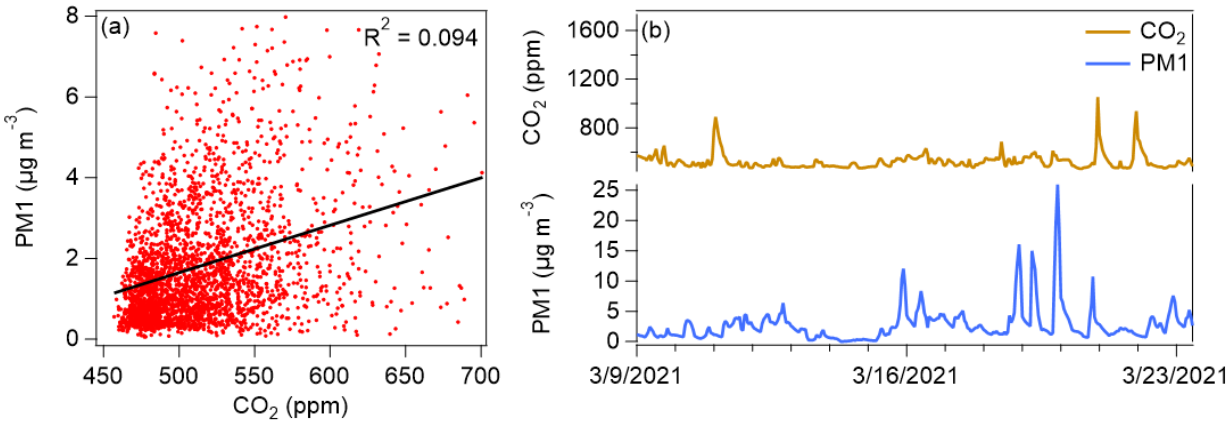

Figure 3.17: Comparison of PM1 and CO_2 concentrations in a private music practice room of the Mountain West University. Data shown as 1-hour averages from November 1 - April 23. Time series (b) shown for a 2-week period as an example of lack of correlation.

North East University B

The testing space was ~600 ft^2 with an 11-foot ceiling (6,600 ft^3). The room had single pane glass windows on both long walls of the room and furnishings included wood tables, lamps, and chairs. The room had no mechanical ventilation but had a passive air transfer grille and wall radiators with recirculating blowers below the window bays. Significant efforts were taken to create as clean, enclosed, and air-tight a space as possible to minimize influences from air infiltration/exfiltration and resuspension of dust from books, furnishings, and flooring.

The AFVU unit consisted of flexible supply and exhaust ductwork, an energy recovery element, main blower fan, MERV 14-rated filter, and a ducted supply air register (Figure 3.18).

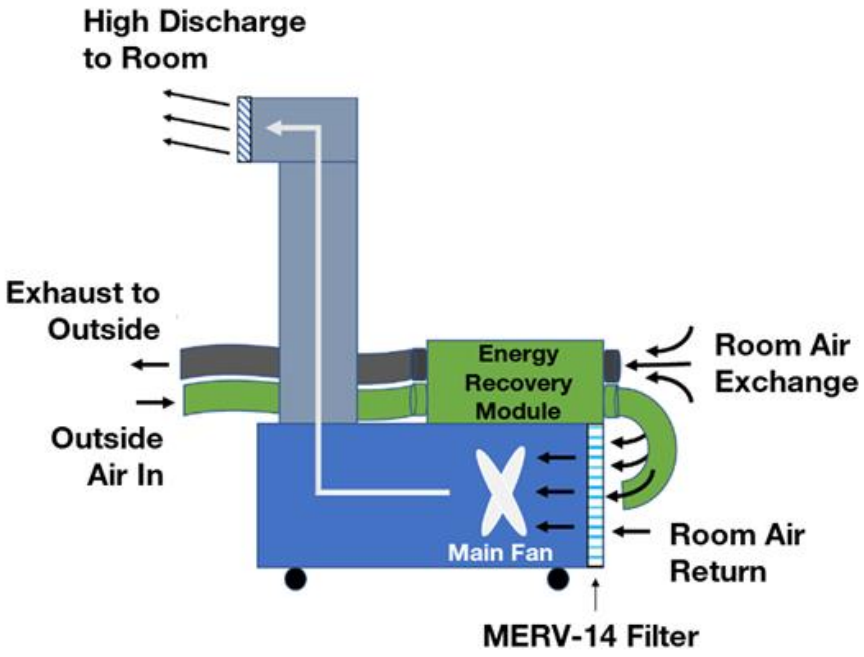

Figure 3.18: Schematic diagram of the air filtration ventilation unit designed for use in naturally ventilated spaces for North East University B.

The device was operated as an air handling unit, delivering air to the space and exhausting a portion of room air back outdoors. As configured for testing, the AFVU provided 125 CFM of outdoor air and 645 to 670 CFM of total supply air, comparable to or higher than applicable ASHRAE ventilation standards[70] (ASHRAE 2019) and typical of mechanical ventilation systems on campus. This unit was placed in the corner of the test space with an elevated discharge (8 ft above the floor) through an upward angled grille – this configuration was demonstrated to be optimal for PM removal efficiency based on testing in the library space (data not shown). The AFVU was purposefully designed to operate on standard 120 V power for widespread deployment, with a fan motor rheostat to provide a range of total delivered airflows. Since the AFVU operates at equal volumetric airflows of outdoor supply and exhaust air, its deployment was not expected to impact room pressurization.

To simulate continuous PM generation as would occur in an occupied classroom, two new candles were placed on a table in the center of the room and were burned for 15 minutes. PM number concentration was measured at the four sampling locations (S1-S4, Figure 3.19). This test was performed twice; once while operating only the AFVU and again with only the HEPA recirculating air cleaner operated at 320 CFM. The variation in PM levels across the test space are shown in Figure 3.19. The AFVU and commercial cleaners produced noticeably different results with continuously burning candles. With the AFVU running, PM concentrations reached a maximum of ~30,000 particles/cm^3, then decreased by about 33% in 15 minutes. When the AFVU was turned off, PM concentrations increased at all sampling locations while the candles were burned. In contrast, when the commercial air cleaner was running, PM levels remained high at two of the four sampling locations (S1 and S3).

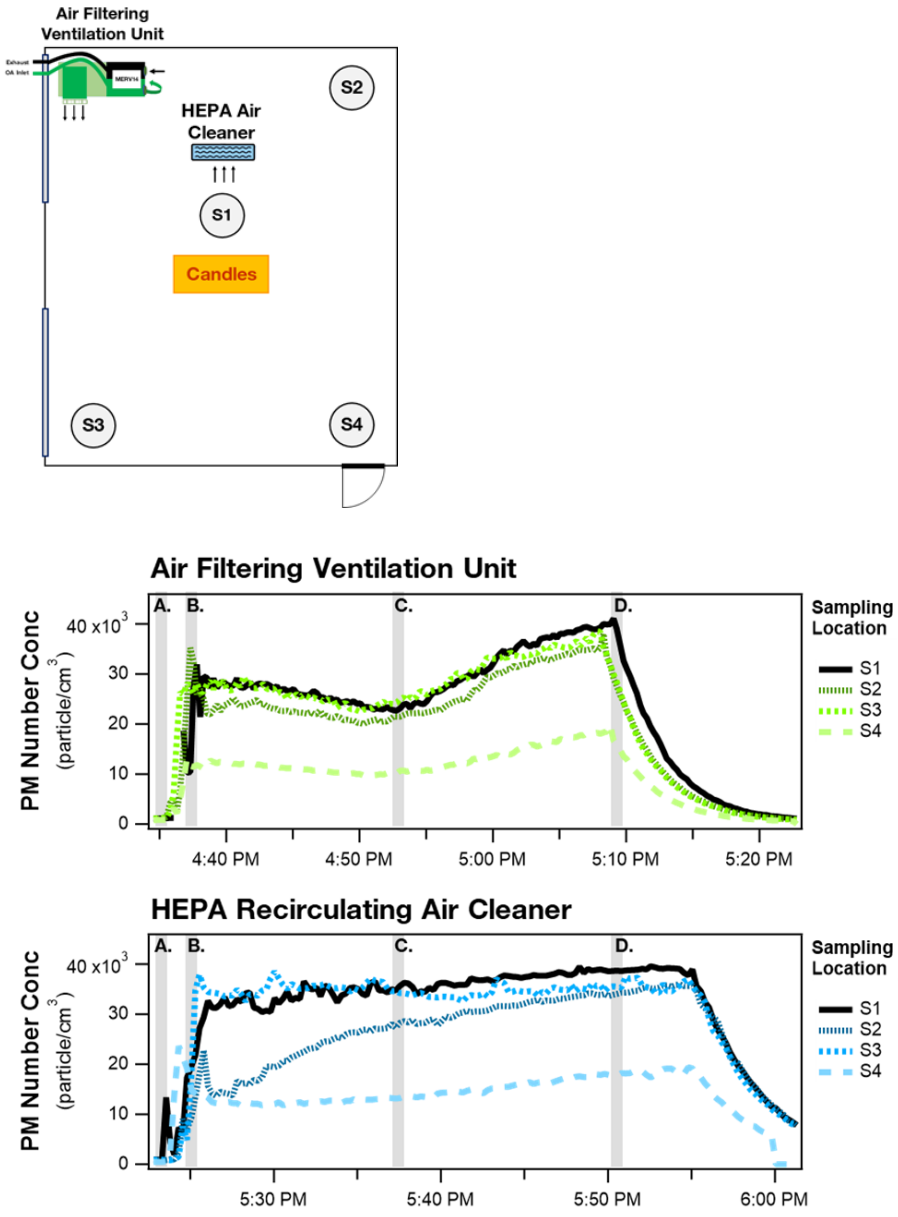

Figure 3.19: Evaluation of the spatial distribution of PM in a naturally ventilated library test space in North East University B using different filtration/ventilation approaches. *Top*: The plan view indicates the location of candles used for continuous PM generation, the PM sampling locations (S1-S4), and the two supplemental filtration/ventilation devices that were individually evaluated: an air filtering ventilation unit and a commercially available air cleaner. *Bottom*: PM number concentration measured at the four sampling locations across the test space for each filtration/ventilation approach. Time point A indicates when candle burning was started, time point B shows when the AFVU or HEPA-recirculating air cleaner was turned on, time C notes the time when these devices were turned off, and time D indicates the time candles were extinguished and the recirculating HEPA-filtered blowers started operation.

Chapter 4: Numerical Simulations of Synthetic Ester Hydrolysis in the Indoor Environment[3]

4.1 Introduction

Hydrolysis has been identified as a potentially important indoor chemistry process, responsible for secondary emissions of several notable indoor pollutants.[20] In the context of indoor environment, it was first speculated as a source of volatile organic compounds (VOCs) in studies observing the effect of relative humidity on VOC emission from building products in the 1990s.[100,101] Since then, the discussion on hydrolysis in indoor air has gained attention due to its association with 2-ethylhexanol, the hydrolysis product of bis(2-ethylhexyl) phthalate (DEHP) and bis(2-ethylhexyl) adipate (DEHA). Incidents of asthma-like symptoms, referred to as "sick building syndrome" (SBS), have been reported following occupant exposure to 2-ethylhexanol, believed to be generated via hydrolysis of DEHP and DEHA found in polyvinylchloride (PVC) flooring.[60,61,102,103] While hydrolysis of synthetic esters (SEs)—such as DEHP and DEHA—is relatively slow even under alkaline conditions which may be present on concrete,[62,64,104] the ubiquitous nature of SEs in the indoor environment raises concerns about the possible contribution of these pathways to poor indoor air quality during both acute SBS episodes and more ordinary conditions. Recent studies have also observed the presence of hydrolysis products of SEs in sampled household dust in the United States and East Asia, further suggesting the relevance of hydrolysis in typical indoor conditions.[105,106] Despite the increasing evidence that hydrolysis may be a source of volatile organic compounds (VOCs) indoors, the temporal

[3] This chapter has been published as: Maeng DY, McNeill VF. Numerical Simulations of Synthetic Ester Hydrolysis in the Indoor Environment. Environ Sci Technol. 2023 Jun 27;57(25):9234–42.

evolution of VOCs from SE hydrolysis has not been investigated in relation to hydrolysis chemical kinetics and interphase mass transfer.

In order to investigate the possible effects of SE hydrolysis on indoor air quality, we adapted the multiphase atmospheric chemistry box model, GAMMA,[107] to numerically simulate SE hydrolysis occurring in surface aqueous films in the indoor environment, including mass transfer from the surface, through the boundary layer, into the room air (breathing zone). We call this new model GAMMA-Chemistry of the Indoor Environment (GAMMA-CIE). We tested three scenarios in which hydrolysis has been hypothesized to impact indoor air quality: (1) installation of PVC flooring on damp concrete, resulting in hydrolysis of bis(2-ethylhexyl) adipate (DEHA) and bis(2-ethylhexyl) phthalate (DEHP);[41,61] (2) application of latex paint on concrete, resulting in hydrolysis of 2,2,4-trimethyl-1,3-pentanediol monoisobutyrate (TMPD-MIB);[52,108] and (3) gas-phase SE uptake by surface aqueous film in contact with concrete, resulting in hydrolysis of common phthalate esters (PEs) and phosphorus flame retardants (PFRs).[38,54,109] The generation of gas-phase 2-ethylhexanol (2-EH), 2,2,4-trimethyl-1,3-pentanediol (TMPD), and other semi-volatile and volatile organic compounds (SVOCs and VOCs) from the aforementioned hydrolysis reactions was simulated and compared to literature data. In order to investigate the possible effects of SE hydrolysis on indoor air quality, we adapted the multiphase atmospheric chemistry box model, GAMMA,[107] to numerically simulate SE hydrolysis occurring in surface aqueous films in the indoor environment, including mass transfer from the surface, through the boundary layer, into the room air (breathing zone). We call this new model GAMMA-Chemistry of the Indoor Environment (GAMMA-CIE). We tested three scenarios in which hydrolysis has been hypothesized to impact indoor air quality: (1) installation of PVC flooring on damp concrete, resulting in hydrolysis of bis(2-ethylhexyl)

adipate (DEHA) and bis(2-ethylhexyl) phthalate (DEHP);[41,61] (2) application of latex paint on concrete, resulting in hydrolysis of 2,2,4-trimethyl-1,3-pentanediol monoisobutyrate (TMPD-MIB);[52,108] and (3) gas-phase SE uptake by surface aqueous film in contact with concrete, resulting in hydrolysis of common phthalate esters (PEs) and phosphorus flame retardants (PFRs).[38,54,109] The generation of gas-phase 2-ethylhexanol (2-EH), 2,2,4-trimethyl-1,3-pentanediol (TMPD), and other semi-volatile and volatile organic compounds (SVOCs and VOCs) from the aforementioned hydrolysis reactions was simulated and compared to literature data.

4.2 Methods

4.2.1 GAMMA-CIE

Following McNeill et al. (2012), GAMMA-CIE consists of 784 coupled differential equations describing the temporal evolution of parent SE compounds undergoing hydrolysis reactions and the formation of reaction products in the aqueous phase, mass transfer between gas phase and aqueous phase, and gas-phase oxidation.[107] GAMMA-CIE runs on a personal computer in the MATLAB environment using the `ode15s` stiff solver.

In GAMMA, the aqueous phase consists of spherical aqueous aerosol or cloud droplets suspended in air. In GAMMA-CIE, the aqueous phase consists of a flat aqueous film in direct contact with an indoor surface instead. As such, the mass transfer scheme following Schwartz (1986) was modified to account for diffusion through the gas-phase boundary layer and mixing into the room air by adopting the multi-layer approach described by Shiraiwa et al. (2010) and Morrison et al. (2019).[110–112] Figure 4.1 illustrates the general schematic of GAMMA-CIE below.

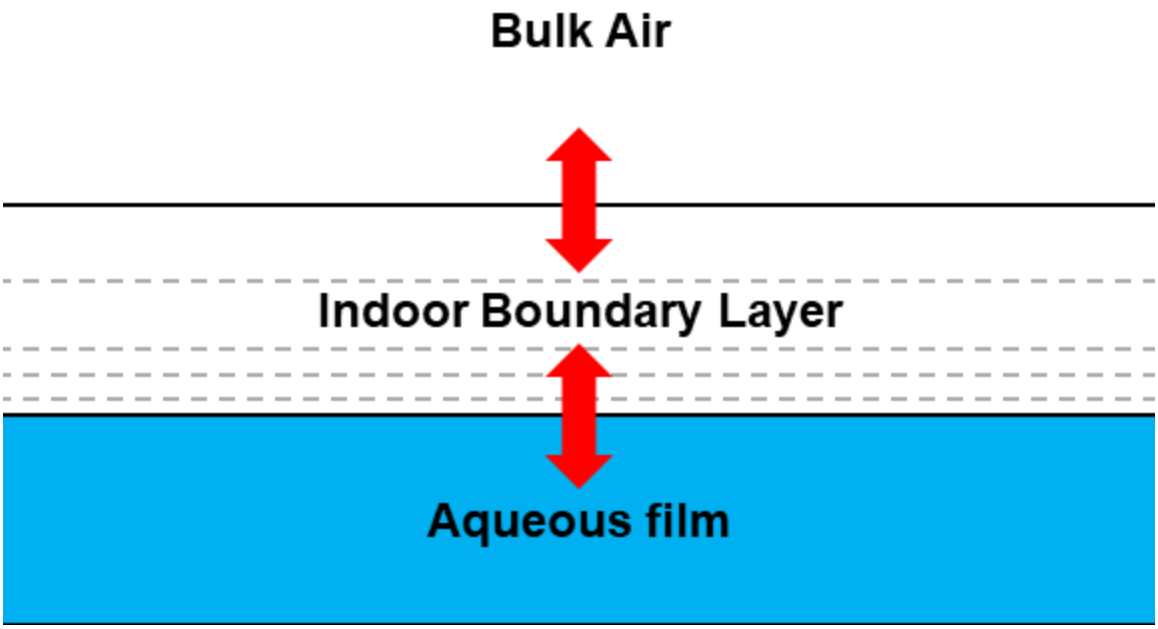

Figure 4.1: GAMMA-CIE model schematic. As described in Equations 1 through 4, the model considers reaction kinetics and mass transfer for each layer. Additionally, loss by ventilation is also taken into account for the bulk air layer.

The concentration of a species *i* in the bulk gas phase and the boundary layer, separated into *n* layers with the *n*th layer as the bottommost, is described by the set of equations below:

$$\frac{dP_{i,bulk}}{dt} = \left(P_{i,1} - P_{i,bulk}\right)\left(\frac{D_{g,i,bulk,1}}{d_{bulk,1}}\right)\left(\frac{A_{bulk}}{V_{bulk}}\right) + \sum_j r_{ij,gas} - ACH \cdot P_{i,bulk} \quad (4.1)$$

$$\frac{dP_{i,1}}{dt} = \left(P_{i,bulk} - P_{i,1}\right)\left(\frac{D_{g,i,bulk,1}}{d_{bulk,1}}\right)\left(\frac{A_1}{V_1}\right) + \left(P_{i,2} - P_{i,1}\right)\left(\frac{D_{g,i,1,2}}{d_{1,2}}\right)\left(\frac{A_1}{V_1}\right) + \sum_j r_{ij,gas} \quad (4.2)$$

$$\frac{dP_{i,k}}{dt} = \left(P_{i,k-1} - P_{i,k}\right)\left(\frac{D_{g,i,k-1,k}}{d_{k-1,k}}\right)\left(\frac{A_k}{V_k}\right) + \left(P_{i,k+1} - P_{i,k}\right)\left(\frac{D_{g,i,k,k+1}}{d_{1,2}}\right)\left(\frac{A_k}{V_k}\right) + \sum_j r_{ij,gas} \quad (4.3)$$

$$\frac{dP_{i,n}}{dt} = \left(P_{i,n-1} - P_{i,n}\right)\left(\frac{D_{g,i,n-1,n}}{d_{n-1,n}}\right)\left(\frac{A_n}{V_n}\right) + k_{mt,i}a_L\left(\frac{C_i}{H_i^*} - P_{i,n}\right) + \sum_j r_{ij,gas} \quad (4.4)$$

where layers $k = 2, 3, \ldots, n\text{-}1$, P_i is the partial pressure of species *i*, $D_{g,i}$ is the gas-phase diffusion coefficient of species *i*, *d* is the average travel distance (equivalent to the mean thickness of the

two participating layers), A_k and V_k are the surface area and volume of layer k, respectively, ACH is the air changes per hour (i.e., ventilation rate) in the given indoor space, $r_{ij,gas}$ is the rate of gas-phase reaction j that species i participates in, $k_{mt,i}$ is the gas-aqueous mass transfer coefficient for species i, a_L is the aqueous liquid fraction ($cm^3\ cm^{-3}$), C_i is the aqueous-phase concentration of species i, and H_i^* is the effective Henry's Law constant of species i. The gas-phase diffusion coefficient, $D_{g,i}$, factors in both molecular diffusion and eddy diffusion as shown by the equation below:[113]

$$D_{g,i} = D_{m,i} + D_{e,i} \tag{4.5}$$

where $D_{m,i}$ is the molecular diffusion coefficient of species i, and $D_{e,i}$ is the eddy diffusion coefficient at height y above the aqueous film given by

$$D_{e,i} = K_e y^2 \tag{4.6}$$

where K_e is the turbulence intensity, varying from 0.1 to 10 s^{-1}.[23] $D_{e,i}$ was evaluated at the height corresponding to the boundary between two participating layers.

The gas-aqueous mass transfer coefficient, $k_{mt,i}$, and aqueous liquid fraction, a_L, have been adjusted from Schwartz (1986) to accommodate for an indoor aqueous film instead of an aqueous aerosol particle in the atmosphere. $k_{mt,i}$ and a_L are now expressed as follows:[110]

$$k_{mt,i} = \frac{1}{\frac{\delta_n \delta_{film}}{D_{m,i}} + \frac{4\delta_{film}}{\omega_i \alpha_i}} \tag{4.7}$$

$$a_L = \frac{\delta_{film}}{\delta_{film} + \delta_n} \tag{4.8}$$

where δ_n is the bottommost gas-phase layer thickness, δ_{film} is the aqueous film thickness, ω_i is the thermal velocity of species i, and α_i is the accommodation coefficient of species i. Data on gas-aqueous accommodation coefficients for these species are not available, so they were all

assigned values of 0.02, which is representative of the uptake of semi-volatile organic compounds to aqueous surfaces.[114]

The aqueous-phase concentration of a species *i* is shown below:

$$\frac{dC_i}{dt} = \frac{k_{mt,i}}{\mathbf{R}T}\left(P_{i,n} - \frac{C_i}{H_i^*}\right) + \sum_k r_{ik,aq} \quad (4.9)$$

where **R** is the gas constant and *T* is temperature. Further details on the model parameters, gas- and aqueous-phase reactions, boundary layer characterization, effective Henry's Law constant calculation, and mass transfer coefficient derivation can be found in the Supporting Information.

4.2.2 Gas-Phase Chemistry

Consumption of gas-phase SEs and their hydrolysis products by hydroxyl radical (OH) oxidation is considered in the model. Oxidation kinetics data were only available for certain phthalate and alcohol species.[115,116] For species with missing kinetics data, rate constants were estimated using structure-activity relationships (EPI Suite AOPWIN).[117] OH concentrations in indoor air are predicted to vary approximately between 1×10^5 and 4×10^5 molecules cm^{-3},[22] depending primarily on the rates of chemical production (e.g., terpene ozonolysis, nitrous acid photolysis) and consumption (e.g., OH reactions with organics).[112,118] For SVOCs and VOCs of interest in this study, their loss by OH oxidation was much slower than their removal by ventilation as noted by the timescales of these two processes in the Supporting Information, so OH concentration was treated as a constant at 4×10^5 molecules cm^{-3}. All OH oxidation reactions and their rate constants in GAMMA-CIE are listed in Table 4.7 (Supporting Information).

4.2.3 Aqueous-Phase Chemistry

Alkaline hydrolysis of esters (R'COOR) drives the production of acids and alcohols predicted in this study. The simplified reaction equation is illustrated below:[63]

$$R'COOR + OH^- \rightarrow R'COO^- + ROH \quad \text{(R4.1)}$$

where R'COO- is the deprotonated acid or lower-order ester, and ROH is the alcohol. The rate of this second-order reaction is pH dependent as described by the following:

$$r_{hydrolysis} = k[R'COOR][OH^-] \quad (4.10)$$

where *k* is the alkaline hydrolysis second-order rate constant. Multiple studies have investigated the hydrolysis kinetics of esters abundant in the indoor environment,[62,64,104,119] but for the hydrolysis of lower-order esters for which experimental data are not available, EPI Suite HYDROWIN estimations were used instead.[117] Species are grouped by their relevant hydrolysis cascade reactions in Table 4.1 for a general overview on the three aforementioned scenarios. Complete list of hydrolysis reactions can be found in Table 4.8 (Supporting Information).

Table 4.1: List of Parent SEs and Hydrolysis Products

Scenario #	Parent Ester	Hydrolysis Product Lower-Order Ester	Alcohol/Acid
1	Bis(2-ethylhexyl) adipate (DEHA)	Mono(2-ethylhexyl) adipate (MEHA)	2-Ethylhexanol (2-EH) Adipic acid (AA)
1	Bis(2-ethylhexyl) phthalate (DEHP)	Mono(2-ethylhexyl) phthalate (MEHP)	2-Ethylhexanol (2-EH) Phthalic acid (PA)
2	2,2,4-Trimethyl-1,3-pentanediol monoisobutyrate (TMPD-MIB)	*N/A*	2,2,4-Trimethyl-1,3-pentanediol (TMPD) Isobutyric acid (IBA)

3	Diethyl phthalate (DEP)	Monoethyl phthalate (MEP)	Ethanol (EtOH) Phthalic acid (PA)
3	Diisobutyl phthalate (DIBP)	Monoisobutyl phthalate (MIBP)	Isobutanol (*i*-BuOH) Phthalic acid (PA)
3	Dibutyl phthalate (DBP)	Monobutyl phthalate (MBP)	Butanol (BuOH) Phthalic acid (PA)
3	Benzyl butyl phthalate (BBzP)	Monobenzyl phthalate (MBzP) Monobutyl phthalate (MBP)	Benzyl alcohol (BnOH) Butanol (BuOH) Phthalic acid (PA)
3	Tris(2-chloroethyl) phosphate (TCEP)	Bis(2-chloroethyl) phosphate (BCEP)	2-chloroethanol (2-CE)
3	Tris (1-chloro-2-propyl) phosphate (TCIPP)	Bis(1-chloro-2-propyl) phosphate (BCIPP)	1-chloro-2-propanol (1C2P)

4.2.4 Test Conditions

For all case studies, the temperature was set to 25 °C to represent typical room temperature. The aqueous film was assumed to be a rectangular layer in contact with an alkaline surface (e.g., concrete), resulting in the migration of hydroxide ions from the surface to the aqueous film.[68] Therefore, the pH of the aqueous film was varied between 10 and 13—pH range observed on screed or young concrete surfaces[61,68,120]—and was held constant throughout each simulation (i.e., rate of consumption of hydroxide ion by hydrolysis was considered negligible compared to its rate of migration from concrete to the film). Ventilation rate was varied between 0.5 and 5.5 ACH to account for different locations, from naturally ventilated homes with relatively low ACH to mechanically ventilated buildings with relatively high ACH.[97,121,122]

Further details on the following test conditions specific to individual scenarios are provided in the Supporting Information.

Scenario 1: Hydrolysis of DEHA and DEHP

DEHA and DEHP were assumed to be present in excess in the surface material (e.g., PVC flooring), leading to an instantaneous migration of DEHA and DEHP from the surface into the aqueous film (i.e., DEHA and DEHP concentrations were treated as constants at the aqueous solubility limit). The reported water solubilities of DEHP varied by two orders of magnitude in literature,[123,124] so both low- and high-DEHP solubility conditions were considered in this study. There are uncertainties regarding the thickness of the aqueous film, which is affected by several factors such as the chemical composition of the film, hygroscopicity of the surface, and relative humidity (RH).[125] Schwartz-Narbonne & Donaldson (2019) measured water uptake varying in the range of 1–5 $\mu g/cm^2$ at RH > 60%, equivalent to 10-50 nm in thickness assuming a layer of even thickness with density of pure water.[126] To simulate the upper bound of hydrolysis activity, however, we assumed film thickness to be 1 μm which may be plausible in consideration of conditions favorable for water adsorption on indoor surfaces.[39] Sensitivity of gas-phase evolution to film thickness is reported in the Supporting Information. Bulk air dilution factor of 0.4 m^{-1} was used in consideration of standard indoor floor-to-volume ratio.[127] Simulated time of 12 h was sufficient for DEHA, DEHP, MEHA, MEHP, and 2-EH concentrations to reach steady state as shown in Figures 4.10 through 4.13 (Supporting Information).

Scenario 2: Hydrolysis of TMPD-MIB

The whole latex paint film was treated as an aqueous film in which a finite amount of the parent ester TMPD-MIB hydrolyzes over time. Thus, the film thickness was set to 100 μm to represent a typical paint film, and the initial aqueous-phase TMPD-MIB concentration was based on the mass composition in latex paint.[52] The bulk air dilution factor was set to 1.3 m^{-1} in consideration of the ubiquity of painted surfaces in indoor environments.[128] The process was simulated for a shorter period of 8 h to analyze short-term exposure to TMPD, one of the hydrolysis products of TMPD-MIB, during the phase in which the paint would be wet.

Scenario 3: Hydrolysis of Common PEs and PFRs

In this case study, the bulk gas-phase layer acted as an infinite reservoir of PEs and PFRs found in appreciable amounts in indoor air. PE and PFR concentrations were treated as constants at their reported airborne measurements from Bergh et al. (2011) listed in Table 4.11 (Supporting Information),[109] and the resulting uptake of airborne PEs and PFRs was the only source of parent esters in the aqueous film. The airborne measurements used in the model are sums of gas and particulate phases, but they are treated as gas-phase concentrations because they are known to be present predominantly in the gas phase.[54] Film thickness of 1 μm and bulk air dilution factor of 0.4 m^{-1} were used to consider an aqueous film trapped below the flooring. pH and ACH were at fixed values of 13 and 0.5 ACH, respectively, to target the maximum predictable gas-phase concentrations of the hydrolysis product species. The simulation time was extended to 300 h for all species.

4.3 Results and Discussion

Tables 4.2, 4.3, and 4.4 summarize the GAMMA-CIE predicted concentrations of gas-phase species in comparison to their respective field measurements in literature for scenarios 1 to 3, respectively. In-depth discussion on the simulation results for each scenario is elaborated below.

Table 4.2: Predicted and Measured Gas-Phase Concentrations (μg/m^3) of Species in Scenario 1: Hydrolysis of DEHA and DEHP

Name	GAMMA-CIE[a] (μg/m^3)	Reported Indoor Levels (μg/m^3)	Reference
Bis(2-ethylhexyl) adipate[b] (DEHA)	0.0016	0.005–0.015	Weschler and Nazaroff (2008)[54]
Bis(2-ethylhexyl) phthalate (DEHP)	0.095–20	<2.253	Fromme et al. (2004)[129]
Mono(2-ethylhexyl) adipate[b] (MEHA)	4.1×10^{-7}	*N/A*	*N/A*
Mono(2-ethylhexyl) phthalate (MEHP)	1.8×10^{-8}–3.8×10^{-6}	*N/A*	*N/A*
2-Ethylhexanol (2-EH)	4.7×10^{-6}–1.2×10^{-4}	0.3–1000+	Wakayama et al. (2019)[41]
Phthalic acid (PA)	*N/A*[c]	*N/A*	*N/A*
Adipic acid[b] (AA)	*N/A*[c]	*N/A*	*N/A*

[a]Steady-state concentrations. Simulation conditions were pH 13 and 0.5 ACH for low- and high-DEHP conditions.
[b]DEHA, MEHA, and AA are not affected by DEHP saturation condition, thus only having a single predicted value.
[c]Negligible concentrations of ~10^{-20} μg/m^3 were predicted for PA and AA.

Table 4.3: Predicted and Measured Gas-Phase Concentrations (μg/m^3) of Species in Scenario 2: Hydrolysis of TMPD-MIB

Name	GAMMA-CIE (μg/m^3)	Reported Indoor Levels (μg/m^3)	Reference
2,2,4-Trimethyl-1,3-pentanediol monoisobutyrate (TMPD-MIB)	810[a]	1680[b]	Norbäck et al. (1995)[130]
2,2,4-Trimethyl-1,3-pentanediol (TMPD)	240[c]	*N/A*	*N/A*
Isobutyric acid (IBA)	2.6×10^{-4}[d]	*N/A*	*N/A*

[a]Peak concentration during simulation time of 8 h. Simulation conditions were pH 10 and 0.5 ACH.
[b]Maximum exposure level measured during a 1 h house painting session.
[c]Peak concentration during simulation time of 8 h. Simulation conditions were pH 13 and 0.5 ACH.
[d]Steady state concentration after simulation time of 8 h. Simulation conditions were pH 10 and 0.5 ACH.

Table 4.4: Predicted and Measured Gas-Phase Concentrations (μg/m^3) of Species in Scenario 3: Hydrolysis of Common PEs and PFRs

Name	GAMMA-CIE (μg/m^3)	Reported Indoor Levels (μg/m^3)	Reference
Monoethyl phthalate (MEP)	3.9×10^{-6}	*N/A*	*N/A*
Monoisobutyl phthalate (MIBP)	8.7×10^{-8}	*N/A*	*N/A*
Monobutyl phthalate (MBP)	1.4×10^{-6}	*N/A*	*N/A*
Monobenzyl phthalate (MBzP)	5.1×10^{-10}	*N/A*	*N/A*
Bis(2-chloroethyl) phosphate (BCEP)	2.2×10^{-7}	*N/A*	*N/A*
Bis(1-chloro-2-propyl) phosphate (BCIPP)	2.1×10^{-9}	*N/A*	*N/A*
Ethanol (EtOH)	3.7×10^{-4}	49–2787[a]	Gallego et al. (2009)[131]
Isobutanol (*i*-BuOH)	3.2×10^{-6}	1–<5[b]	Brown et al. (1994)[132]
Butanol (BuOH)	6.6×10^{-5}	14–95[a]	Gallego et al. (2009)[131]
Benzyl alcohol (BnOH)	3.1×10^{-5}	864–5446[c]	Gerster et al. (2014)[133]
2-Chloroethanol (2-CE)	6.8×10^{-8}	*N/A*	*N/A*

1-Chloro-2-propanol (1C2P)	6.8×10^{-10}	*N/A*	*N/A*
Phthalic acid (PA)	*N/A*[d]	*N/A*	*N/A*

[a]During an odor episode in several locations of a single apartment dwelling.
[b]In established dwellings.
[c]During cleaning activities.
[d]Negligible concentrations of ~10^{-21} μg/m^3 were predicted for PA.

4.3.1 Scenario 1: Hydrolysis of DEHA and DEHP

Gas-phase parent ester DEHP equilibrated at 0.095 and 20 μg/m^3 at low- and high-DEHP conditions, respectively, as noted in Table 4.2. Reported mean concentrations of gas-phase DEHP ranged between 191 and 599 ng/m^3 with a maximum of 2253 ng/m^3,[129] implying overabundance of DEHP in the high-DEHP condition simulation and, on the contrary, underestimation of DEHP in low-DEHP condition simulation. Therefore, the predicted concentrations of the following hydrolysis products at low- and high-DEHP conditions should be interpreted as the lower and upper bounds in this scenario. The predicted gas-phase concentration of the other parent ester, DEHA, was 1.6 ng/m^3, which is close to the measured average range of 5 and 15 ng/m^3, indicating that the DEHA saturation assumption was appropriate.

As noted in Table 4.2, negligible amounts of gas-phase PA and AA were generated in the simulation at all pH and ACH values. The rate of interphase transport for PA and AA is significantly slower than other species because of their high effective Henry's law constant, which is pH dependent for organic acids. In such highly basic conditions where the acids are in their deprotonated form, the acids tend to remain in the aqueous phase.[134–136] The effective Henry's law constants for PA, AA, and IBA at pH 10 and 13 are greater than their intrinsic counterparts by several orders of magnitude, as shown in Table 4.13 (Supporting Information). While the slow interphase transport is responsible for the predicted negligible gas-phase concentrations of PA and AA, control simulations performed with lower arbitrary values of

Henry's law constant assigned to both species for faster mass transport suggest that the slow hydrolysis kinetics and overall low water solubilities of parent esters (DEHA and DEHP) would limit the gas-phase generation of PA and AA to low levels of ~10^{-5} μg/m^3.

Gas-phase 2-EH generation was simulated with varying pH and ACH to understand the effect of those parameters on the overall process, as illustrated in Figure 4.2. Increase in aqueous film pH by 1 (in the range 10-13) resulted in a proportional increase in 2-EH concentrations by a factor of approximately 10 for both low- and high-DEHP cases. It is apparent that the aqueous film pH, and consequently the indoor surface pH, is a key parameter in SE degradation by hydrolysis. Changes in ACH were most effective at low ventilation conditions, decreasing the predicted 2-EH concentrations by a factor of 3 when increasing from 0.5 to 1.5 ACH. Overall, the predicted levels of 2-EH were significantly lower than reported indoor values from the literature (Table 4.2). At pH 13, 0.5 ACH, and high-DEHP saturation condition, GAMMA-CIE predicted 1.2 × 10^{-4} μg/m^3 of gas-phase 2-EH, which is approximately 7 orders of magnitude lower than the upper bound of measured concentrations of ~1000 μg/m^3 in extreme SBS cases.[41]

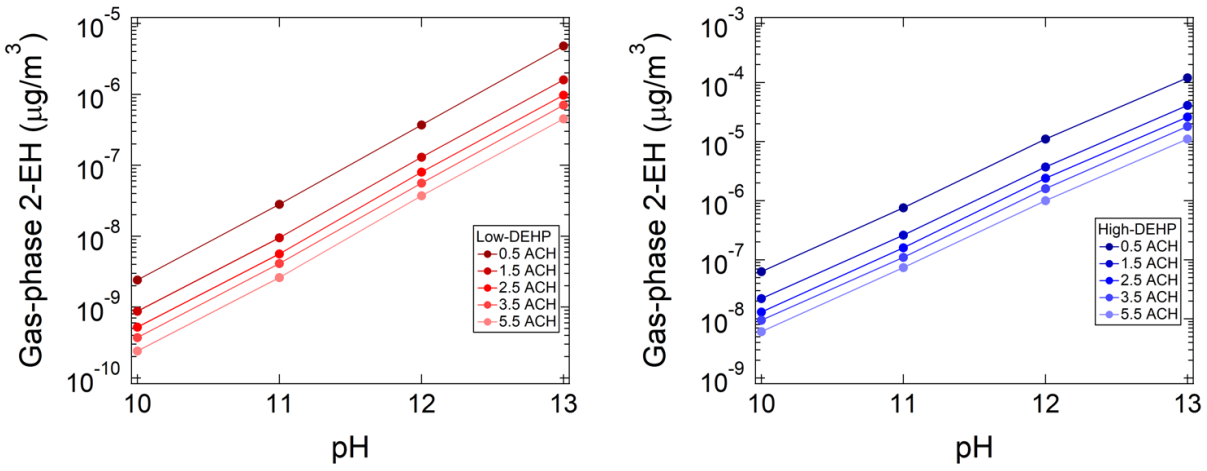

Figure 4.2: Predicted gas-phase 2-EH concentrations with varying aqueous film pH and ACH at low-DEHP (left) and high-DEHP (right) conditions.

Simulation results suggested that hydrolysis of DEHA and DEHP from PVC flooring would not produce gas-phase 2-EH at levels comparable to values measured during SBS incidents. Therefore, we hypothesized that an unknown, non-hydrolysis process (e.g., biotic degradation[137]) may be active in degrading DEHA and DEHP and their lower-order esters to produce 2-EH. To determine the magnitude of discrepancy between the hydrolysis kinetics and the mechanism necessary to produce gas-phase 2-EH concentrations observed in field studies, a hypothetical first-order aqueous degradation process was considered for DEHA, DEHP, MEHA, and MEHP under hydrolysis-ideal conditions of pH 13, 0.5 ACH, and high-DEHP saturation. The rate of this hypothetical process was adjusted by trial and error to produce steady-state gas-phase 2-EH concentration of 2 $\mu g/m^3$, emulating the observations of 1–4 $\mu g/m^3$ of gas-phase 2-EH during an incidence of SBS.[41] The hypothetical process was accelerated to 0.2 s^{-1} to produce gas-phase 2-EH concentration of 2 $\mu g/m^3$ as depicted by Figure 4.3 below. This rate is approximately 2 to 4 orders of magnitude faster than that of alkaline hydrolysis at pH 13. The difference in magnitude between the hypothetical process and alkaline hydrolysis could be even greater when considering 2-EH concentrations of ~1000 $\mu g/m^3$ was observed in certain episodes.

There are several possible explanations for the observed discrepancy. As noted above, biotic degradation by bacteria, yeast, and fungi could be a relevant process with a rate higher or comparable to that of abiotic hydrolysis at high relative humidity.[105,137] Another reason could be the acceleration of reaction kinetics in microfilms, where the partial solvation of the reactants leads to a lower activation barrier and higher reactivity, notably for reactions such as hydrolysis involving an attack at the carbonyl carbon.[69,138] Wei et al. (2020) suggests a hundredfold increase in the intrinsic reactivity from bulk-phase reaction to partially solvated reaction, which roughly corresponds to the magnitude of difference observed in our hypothetical rate constant.[69]

However, this effect has yet to be confirmed with further experimental data, specifically for the hydrolysis of SEs. Lastly, hydrolysis of acrylate and acetate copolymers in adhesives could be the dominant source instead, which is evident in emission studies but warrants further research on the reaction kinetics and adequate reaction systems for modeling purposes.[61,139,140]

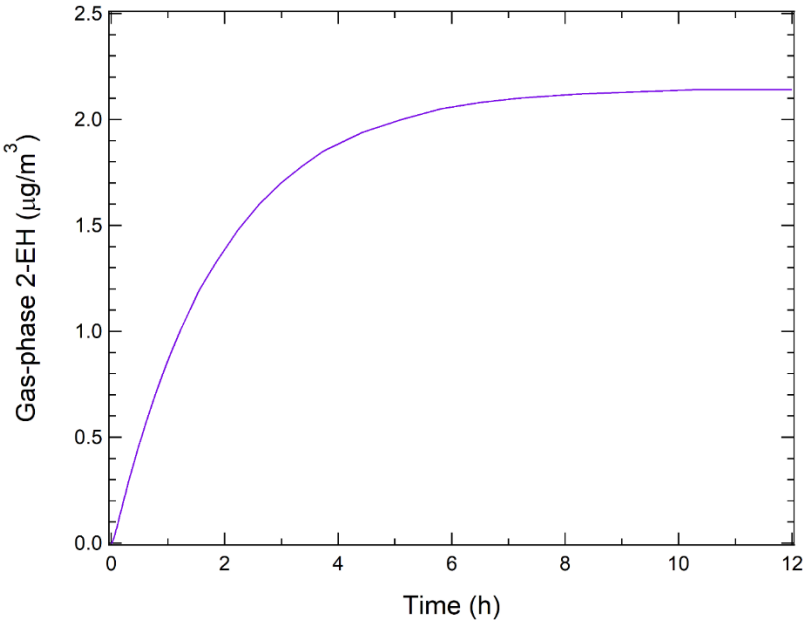

Figure 4.3: Predicted concentration profile of gas-phase 2-EH at aqueous film pH 13, 0.5 ACH, and high-DEHP condition, with the addition of a first-order hypothetical degradation process of 0.2 s^{-1} for aqueous-phase DEHA, DEHP, MEHA, and MEHP. See text for details.

4.3.2 Scenario 2: Hydrolysis of TMPD-MIB

Figure 4.4 below illustrates the concentration profile of gas-phase parent ester TMPD-MIB over simulation time of 8 h at pH 10 and 0.5 ACH with a peak concentration of 810 μg/m^3 at t = 0.6 h. Decreasing the film basicity to below pH 10 in GAMMA-CIE had a negligible increase on this predicted gas-phase peak concentration, most likely because the rate of interphase transport was already significantly faster than that of TMPD-MIB consumption by hydrolysis at pH 10. Field studies on SVOC emissions following latex paint application measured TMPD-MIB peak

concentrations of approximately 1~1.7 mg/m^3, comparable to the predicted peak considering that simulations were performed assuming a smaller TMPD-MIB content of 0.67% in paint than that of 1.35% in paint used by Sparks et al. (1999).[130,141] The trend is also similar between the concentration profile predicted by GAMMA-CIE in Figure 4.4 and those observed in experiments,[141,142] overall indicating good agreement on TMPD-MIB emission between model prediction and experimental measurements.

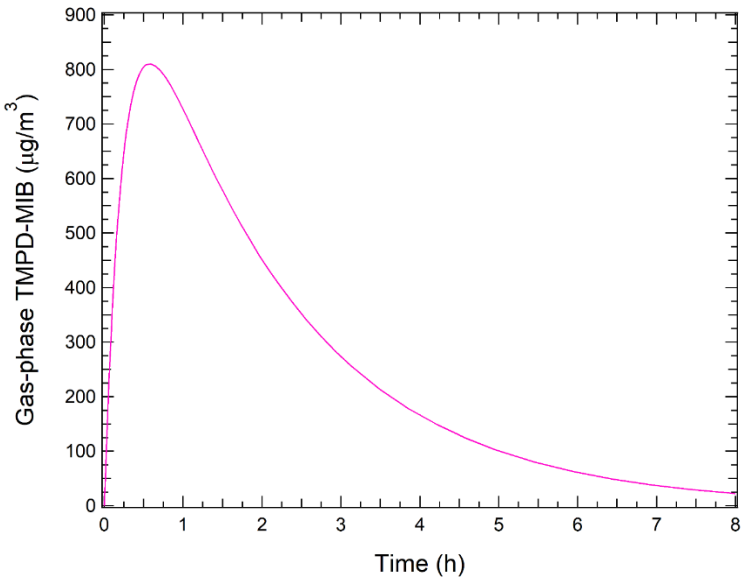

Figure 4.4: Predicted concentration profile of gas-phase TMPD-MIB at aqueous film pH 10 and 0.5 ACH with peak value of 810 μg/m^3.

The time evolution of gas-phase TMPD over simulation time of 8 h at varying film pH and low- and high-ACH conditions is shown in Figure 4.5. The predicted peak concentrations of TMPD at pH 13 were 240 μg/m^3 at t = 0.6 h for 0.5 ACH and 110 μg/m^3 at t = 0.3 h for 5.5 ACH. pH was the most influential factor in gas-phase evolution of TMPD, with near tenfold decrease in peak gas-phase concentrations per unit decrease in pH.

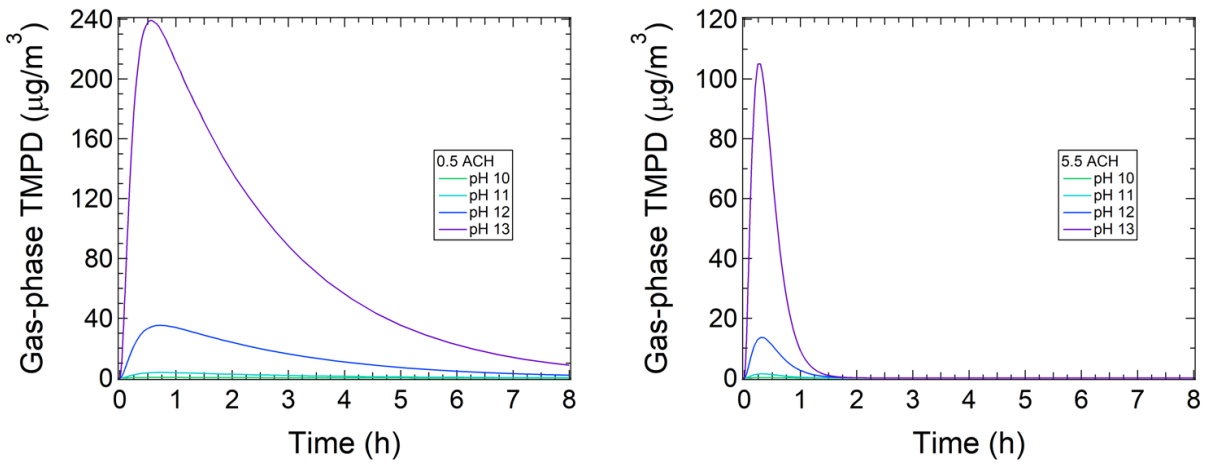

Figure 4.5: Predicted concentration profile of gas-phase TMPD with varying aqueous film pH at low-ACH (left) and high-ACH (right) conditions.

In contrast to TMPD-MIB and TMPD simulation results, GAMMA-CIE predicted much lower production of gas-phase IBA, rate-limited by the interphase mass transport from the high effective Henry's law constant. The predicted gas-phase concentration profile of IBA in Figure 4.6 below is distinctly different from those of TMPD-MIB and TMPD. Highest predicted concentration of gas-phase IBA was 2.6×10^{-4} μg/m^3 for 0.5 ACH and pH 10. As previously mentioned in the discussion of Scenario 1, higher pH conditions are associated with inhibition of interphase mass transport for acids such as IBA, resulting in an opposite trend compared to TMPD above. Similar to the gas-phase 2-EH concentrations in Scenario 1, increase in ventilation from 0.5 to 5.5 ACH resulted in a tenfold decrease in the predicted gas-phase IBA concentrations across all pH values. Accumulation of IBA in the aqueous phase was observed as shown in Figure 4.7 due to the slow partitioning process, with aqueous IBA concentration predicted to reach 0.018 M in the film at pH 13. Because IBA is a relatively weak acid, such concentrations are still not sufficient enough to significantly lower the pH of the film on its own. With the uptake of acidic gases indoors, however, it may be possible that this build-up of aqueous IBA

may partition into the gas phase as the film is acidified. Further discussion on indoor acids can be found in the Indoor Environment Implications section below.

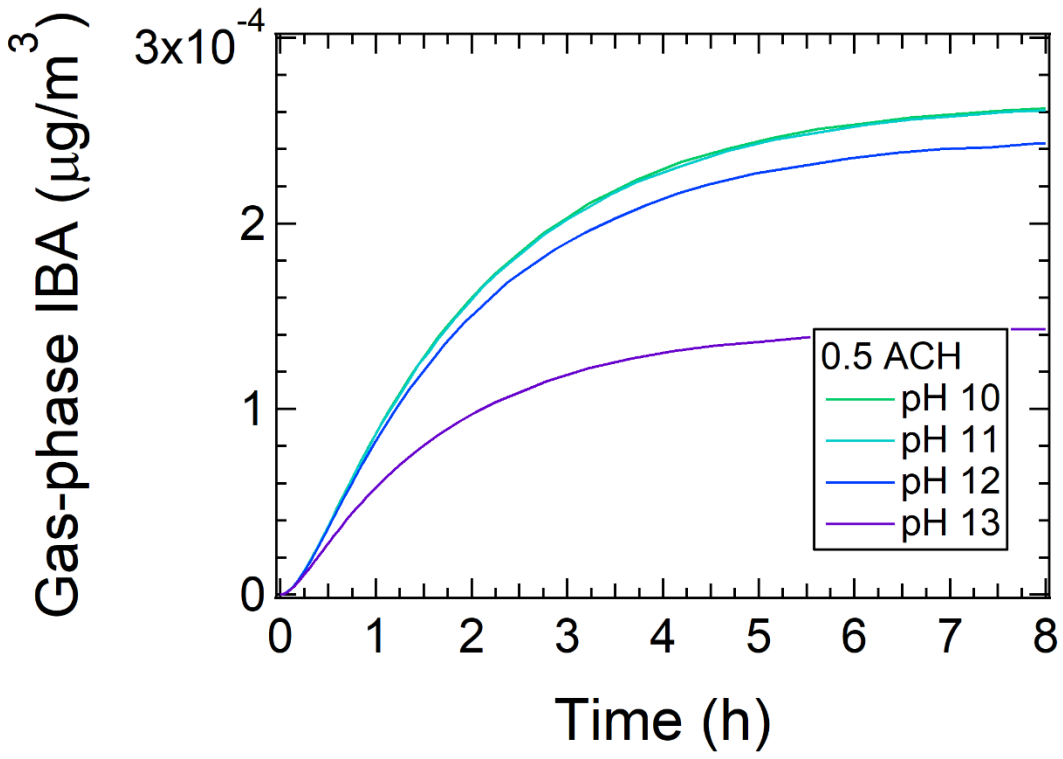

Figure 4.6: Predicted concentration profile of gas-phase IBA with varying aqueous film pH at low-ACH condition.

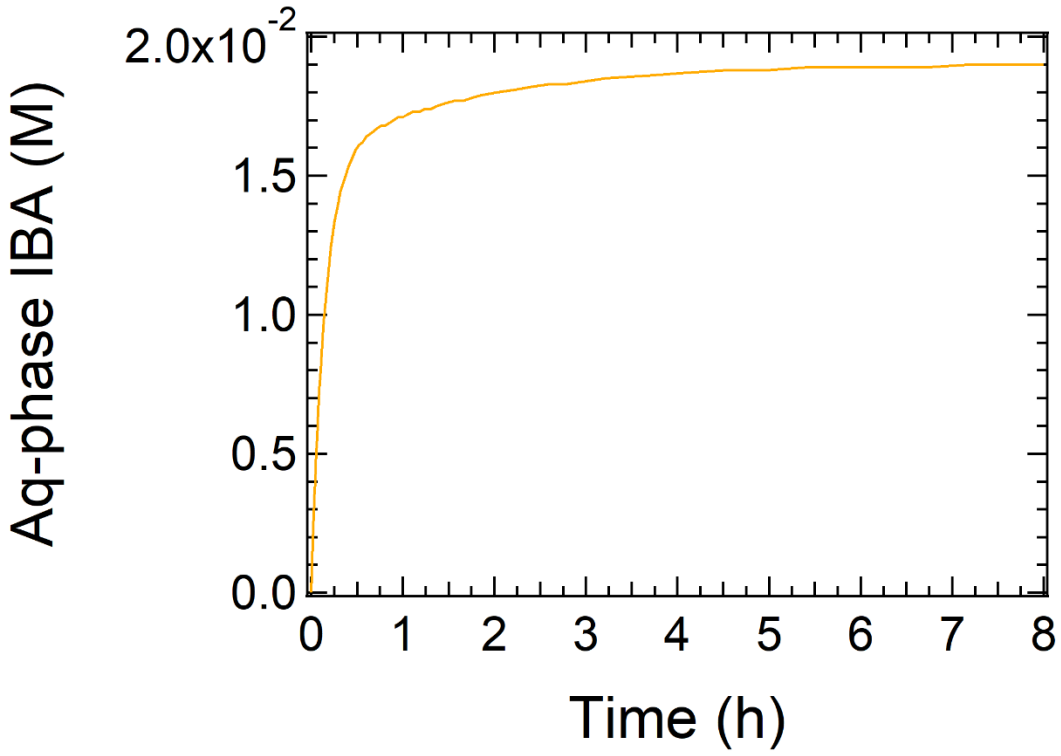

Figure 4.7: Predicted concentration profile of aqueous-phase IBA with at pH 13 and low-ACH condition.

Our predictions indicate that building occupants and interior painters may be exposed to high levels of irritants TMPD-MIB and its hydrolysis product TMPD during paintwork and shortly after its completion, especially in newly constructed buildings with high pH surfaces. Data on the indoor measurements and exposure limits of TMPD-MIB and TMPD are lacking, but both species are reported to cause irritation in the eyes, nose, skin, and respiratory tract.[143] Experimental data on the emissions of TMPD in paint applications would further validate the predicted results of this scenario.

4.3.3 Scenario 3: Hydrolysis of Common PEs and PFRs

The predicted gas-phase concentrations of SVOCs and VOCs under ideal hydrolytic degradation conditions are plotted in Figure 4.8 below. Among the lower-order esters, BCEP and BCIPP equilibrated more slowly than the other SVOCs primarily because they are the only lower-order esters stable to hydrolysis in the system. MEP and MBP were the most abundant species due to their high parent ester concentrations shown in Table 4.11 and relatively fast rate of production by hydrolysis. Even so, predicted secondary emissions of SVOCs from the airborne SE uptake and the ensuing hydrolysis were of negligible amounts, not exceeding 10^{-5} μg/m^3.

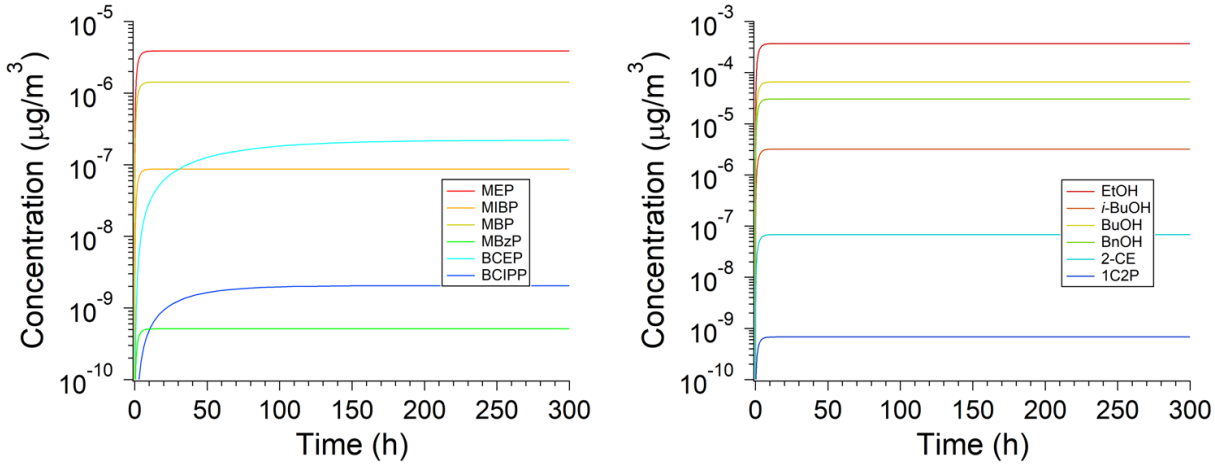

Figure 4.8: Predicted gas-phase concentration profile of SVOCs (left) and alcohols (right) at aqueous film pH 13 and 0.5 ACH.

Table 4.4 presents the predicted steady state concentrations in comparison to measured indoor concentrations of VOCs simulated in this study. It is apparent that the model predictions are several orders of magnitude smaller than the reported measurements for the alcohol species with available field data. This was expected since the reference values were collected during specific occasions (e.g., cleaning activities, odor episodes), likely affected by external (outdoor)

sources, primary emissions, and other secondary processes,[3,131,139,144] which are non-analogous to the simulation scenario of generalized airborne SE uptake by the aqueous film on an alkaline surface. Even so, the notable differences in the simulated concentrations and reported field concentrations suggest that hydrolysis from uptake of airborne SEs is not a significant contributor of indoor acids and alcohols in the proposed scenario. The uptake of airborne SE by aqueous films on indoor surfaces warrants further investigation, however, as the airborne concentrations of SEs may differ significantly depending on the presence of SE-rich objects at the location of interest. Additionally, it has been reported that substantial amounts of SEs can also be present in settled dust on indoor surfaces which have not been considered in this study,[54,109] so there may be greater amounts of parent SEs susceptible to degradation in this uptake process simulated in Scenario 3.

4.4 Indoor Environment Implications

This study employs a detailed multiphase chemistry model to quantitatively determine the development of gas-phase pollutants from indoor surface hydrolysis. We have used GAMMA-CIE in three indoor scenarios relevant to hydrolysis, but the applicability of the model can extend further to other indoor conditions, especially as information on indoor surface films becomes more available. In this following section, we discuss uncertainties and limitations in the model to be considered in extending the scope of the model.

The indoor film is likely comprised of various organic and inorganic species—namely aliphatic and aromatic hydrocarbons, carbohydrates, metals, sulfates, and nitrates—emitted from building occupants and different indoor activities.[38,145] Acknowledgement of such complex chemical composition introduces several possible factors which could be considered: indoor film

water content, aqueous-organic phase separation and phase equilibria, heterogeneous reaction, ionic strength, and so on.

For the alkaline hydrolysis of SEs, we have only considered specific base catalyzed hydrolysis because it is presumably the dominant mechanism in presence of high calcium hydroxide concentrations from fresh concrete. However, if other indoor bases, such as ammonia, nicotine, and inorganic and organic amines,[67] are transported into the aqueous film, then the organic esters may also degrade by general base catalyzed hydrolysis.[146–149] There are no studies on the general base catalyzed hydrolysis for SEs considered in our model, but this alternate degradation mechanism may be of importance in other indoor scenarios with high concentrations of indoor bases absorbed by the film.

Similar to the uptake of indoor bases mentioned above, uptake of acids may occur as there are several acids found indoors, such as carbon dioxide, nitric acid, sulfuric acid, and acetic acid.[67] In such instances, SEs may degrade by acid hydrolysis instead.[19,63] At the time of this study, experimental data on the kinetics of SE acid hydrolysis are unavailable, and the EPI Suite HYDROWIN is only able to estimate alkaline hydrolysis rate constants. Although acid hydrolysis is known to be generally slower than alkaline hydrolysis,[63] kinetic measurements on SE acid hydrolysis may open up the possibility of simulating common indoor scenarios which have not been explored yet.

4.5 Supporting Information

Table 4.5: List of Chemical Species

Name	Abbreviation	Phase
Hydroxyl radical	OH	gas
Hydroxide ion	OH^-	Aq
Bis(2-ethylhexyl) adipate	DEHA	gas, aq
Bis(2-ethylhexyl) phthalate	DEHP	gas, aq
Mono(2-ethylhexyl) adipate	MEHA	gas, aq
Mono(2-ethylhexyl) phthalate	MEHP	gas, aq
2-Ethylhexanol	2-EH	gas, aq
2,2,4-Trimethyl-1,3-pentanediol monoisobutyrate	TMPD-MIB	gas, aq
Isobutyric acid	IBA	gas, aq
2,2,4-Trimethyl-1,3-pentanediol	TMPD	gas, aq
Diethyl phthalate	DEP	gas, aq
Diisobutyl phthalate	DIBP	gas, aq
Dibutyl phthalate	DBP	gas, aq
Butyl benzyl phthalate	BBzP	gas, aq
Tris(2-chloroethyl) phosphate	TCEP	gas, aq
Tris(1-chloro-2-propyl) phosphate	TCIPP	gas, aq
Monoethyl phthalate	MEP	gas, aq
Monoisobutyl phthalate	MIBP	gas, aq
Monobutyl phthalate	MBP	gas, aq
Monobenzyl phthalate	MBzP	gas, aq
Bis(2-chloroethyl) phosphate	BCEP	gas, aq
Bis(1-chloro-2-propyl) phosphate	BCIPP	gas, aq
Phthalic acid	PA	gas, aq
Ethanol	EtOH	gas, aq
Isobutanol	*i*-BuOH	gas, aq
Butanol	BuOH	gas, aq
Benzyl alcohol	BnOH	gas, aq
2-chloroethanol	2-CE	gas, aq
1-chloro-2-propanol	1C2P	gas, aq

Table 4.6: List of Henry's Law Constants at 25 °C

Species	H (M/atm)	Reference
DEHA	2.30E+03	[150]
DEHP	22.9	[151]
MEHA	1E+05[a]	[117]
MEHP	5E+05[a]	[117]
2-EH	69.62	[152]
TMPD-MIB	1E+04[a]	[117]
IBA	1E+03	[135]
TMPD	1.4E+03	[135]
DEP	1.64E+03	[151]
DIBP	820	[151]
DBP	552	[151]
BBzP	1E+04	[135]
TCEP	3E+02	[135]
TCIPP	1.6E+02	[135]
MEP	2E+06[a]	[117]
MIBP	1E+06[a]	[117]
MBP	1E+06[a]	[117]
MBzP	1E+08[a]	[117]
BCEP	6E+06[a]	[117]
BCIPP	3E+06[a]	[117]
PA	5E+07	[135]

AA	2E+08	[135]
EtOH	2E+02	[135]
i-BuOH	1E+02	[135]
BuOH	1.2E+02	[135]
BnOH	2.9E+03	[135]
2-CE	9.6E+03	[135]
1C2P	5.7E+02	[135]

[a]Estimation from EPI Suite HENRYWIN

Table 4.7: Gas-Phase Oxidation Kinetics

Reaction	**kOH (cm^3 $molec^{-1}$ s^{-1})**	**T (°C)**	**Reference**
DEHA + OH → OXIDATION PRODUCTS	2.5E-11[a]	25	[117]
MEHA + OH → OXIDATION PRODUCTS	1.5E-11[a]	25	[117]
DEHP + OH → OXIDATION PRODUCTS	2.2E-11[a]	25	[117]
MEHP + OH → OXIDATION PRODUCTS	1.2E-11[a]	25	[117]
DEP + OH → OXIDATION PRODUCTS	3.5E-12[a]	25	[117]
MEP + OH → OXIDATION PRODUCTS	2.4E-12[a]	25	[117]
DBP + OH → OXIDATION PRODUCTS	9.3E-12[a]	25	[117]
MBP + OH → OXIDATION PRODUCTS	5.3E-12[a]	25	[117]
DIBP + OH → OXIDATION PRODUCTS	9.3E-12[a]	25	[117]
MIBP + OH → OXIDATION PRODUCTS	5.3E-12[a]	25	[117]
TCIPP + OH → OXIDATION PRODUCTS	4E-11[a]	25	[117]
TCEP + OH → OXIDATION PRODUCTS	2E-11[a]	25	[117]
BBzP + OH → OXIDATION PRODUCTS	1.1E-11[a]	25	[117]
MBzP + OH → OXIDATION PRODUCTS	7E-12[a]	25	[117]
TMPD-MIB + OH → OXIDATION	1.6E-11[a]	25	[117]
BCIPP + OH → OXIDATION PRODUCTS	3E-11[a]	25	[117]
BCEP + OH → OXIDATION PRODUCTS	1.5E-11[a]	25	[117]
IBA + OH → OXIDATION PRODUCTS	2E-12[a]	25	[117]
PA + OH → OXIDATION PRODUCTS	1E-12[a]	25	[117]
EtOH + OH → OXIDATION PRODUCTS	3.2E-12	25	[116]
BuOH + OH → OXIDATION PRODUCTS	8.5E-12	25	[116]

i-BuOH + OH → OXIDATION PRODUCTS	7E-12[a]	25	117
BnOH + OH → OXIDATION PRODUCTS	2.7E-11	25	116
2-EH + OH → OXIDATION PRODUCTS	1.13E-11	25	153
TMPD + OH → OXIDATION PRODUCTS	2E-11[a]	25	117
2-CE + OH → OXIDATION PRODUCTS	1.8E-12[a]	25	117
1C2P + OH → OXIDATION PRODUCTS	3.2E-12[a]	25	117

[a]Estimation from EPI Suite AOPWIN

Table 4.8: Aqueous-Phase Hydrolysis Kinetics

Reaction	**kOH^- (M^{-1} s^{-1})**	**T (°C)**	**Reference**
DEHA + OH^- → MEHA + 2-EH	4.8E-04	21	104
MEHA + OH^- → 2-EH + ADIPIC	3E-02[a]	25	117
DEHP + OH^- → MEHP + 2-EH	1.1E-04	30	62
MEHP + OH^- → 2-EH + PA	2E-02[a]	25	117
DEP + OH^- → MEP + EtOH	2.5E-02	30	62
MEP + OH^- → EtOH + PA	4E-02[a]	25	117
DBP + OH^- → MNBP + BuOH	1.0E-02	30	62
MBP + OH^- → BuOH + PA	3E-02[a]	25	117
DIBP + OH^- → MIBP + *i*-BuOH	1.4E-03	30	62
MIBP + OH^- → *i*-BuOH + PA	2E-02[a]	25	117
TCIPP + OH^- → BCIPP + 1C2P	7.2E-06	20	119
TCEP + OH^- → BCEP + 2-CE	9.7E-04	20	119
BBzP + OH^- → MBzP + BnOH	5.9E-02	21	104
MBzP + OH^- → BnOH + PA	1E-01[a]	25	117
TMPD-MIB + OH^- →TMPD + IBA	9.8E-03	20	104

[a]Estimation from EPI Suite HYDROWIN

Table 4.9: Initial Conditions, Hydrolysis of DEHA and DEHP

Species	**Concentration (M)**	**Notes**	**Reference**
DEHA (aq)	8.6E-09	DEHA water solubility. Held constant throughout simulation.	[123]
DEHP (aq) (low)	4.9E-09	DEHP water solubility. Held constant throughout simulation. For low-DEHP condition	[123]
DEHP (aq) (high)	1E-06	DEHP water solubility. Held constant throughout simulation. For high-DEHP condition	[123]

Table 4.10: Initial Conditions, Hydrolysis of TMPD-MIB

Species	**Concentration (M)**	**Notes**	**Reference**
TMPD-MIB (aq)	4E-02	Calculated on the basis of mass composition and bulk density of latex paint (0.67% mass)	[52]

Table 4.11: Initial Conditions, Hydrolysis of Common PEs and PFRs

Species	**Concentration (ng/m^3)**	**Notes**	**Reference**
DEP (g)	1598	Mean measurement at homes in Sweden. Held constant throughout simulation	[109]

DIBP (g)	310	Mean measurement at workplaces in Sweden. Held constant throughout simulation	[109]
DBP (g)	925	Mean measurement at homes in Sweden. Held constant throughout simulation	[109]
BBzP (g)	28	Mean measurement at homes in Sweden. Held constant throughout simulation	[109]
TCEP (g)	47	Mean measurement at day care centers in Sweden. Held constant throughout simulation	[109]
TCIPP (g)	110	Mean measurement at workplaces in Sweden. Held constant throughout simulation	[109]

Table 4.12: List of pKa

Species	**pKa1**	**pKa2**	**T (°C)**	**Reference**
IBA	4.84	*N/A*	20	[154]
PA	2.76	4.92	25	[155]
AA	4.44	5.44	25	[155]

Boundary Layer Characterization

In GAMMA-CIE, the boundary layer consists of 26 layers with varying thickness: 1.8E-1 cm for layers 1 (topmost) to 5; 1.8E-2 cm for layers 6 to 10; 1.8E-3 cm for layers 11 to 15; 1.8E-4 cm for layers 16 to 20; 1.8E-5 cm for layers 21 to 25; and 1E-5 cm for layer 26. Figure 4.9 below illustrates the evolution of 2-EH in Scenario 1 for different layers. The layers near the aqueous film are of thinner thickness to characterize the initial, rapid transport of gas species near the surface following their production in the aqueous film. As expected for species that are not highly reactive to atmospheric oxidation, the concentration differences among layers in the boundary layer are minimal, and the bulk air concentration is several orders of magnitude lower due to the greater dilution factor and loss by ventilation in this layer.

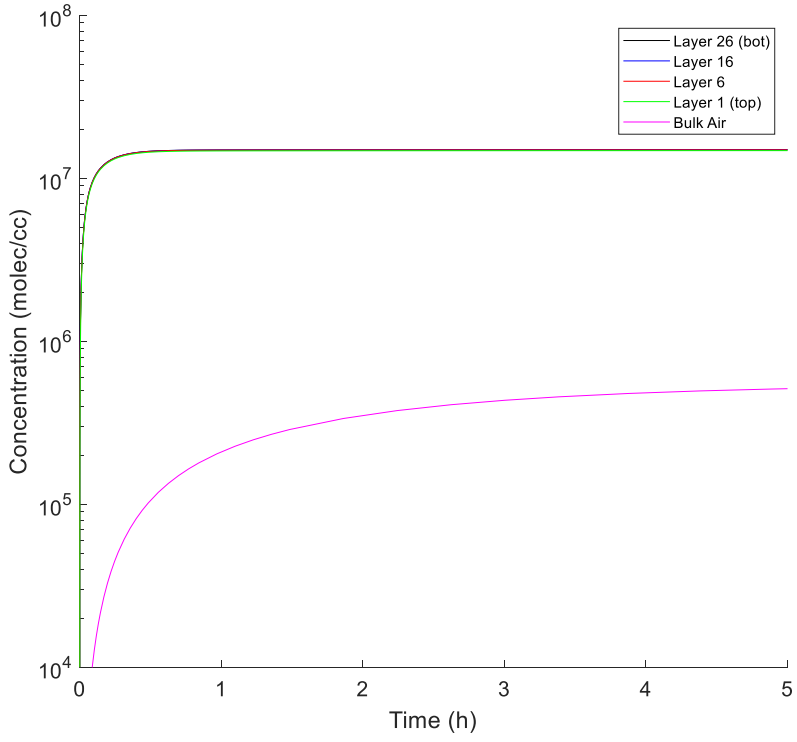

Figure 4.9: 2-EH concentration profile in various gas-phase layers for Scenario 1 at pH 13 and 0.5 ACH.

Gas-Phase Molecular Diffusion Coefficient Estimation

The gas-phase molecular diffusion coefficient estimation is as follows:[156]

$$D_{m,i} = 1.9(\mathrm{MW})^{-2/3} \quad (4.11)$$

where $D_{m,i}$ is the gas-phase molecular diffusion coefficient ($cm^2\ s^{-1}$) and MW is the molecular weight ($g\ mol^{-1}$).

Mass Transfer Coefficient Derivation

Closely following Schwartz (1986),[110] the mass transfer coefficient considers: (1) gas-phase diffusion of species *i* into the film and (2) interphase mass transport but has been modified to consider transport for a planar film instead of a spherical aerosol particle.

Gas-phase diffusion

We start with the gas-phase diffusion of species *i* in the bottommost layer (i.e., *n*th layer) of the boundary layer (BL) into the film in the absence of reactions, resulting in the following equation:

$$\frac{\partial C_g}{\partial t} - D_g \frac{\partial^2 C_g}{\partial y^2} = 0 \quad (4.12)$$

where C_g is the gas-phase concentration of species i, t is time, and y is distance normal to the film surface. We assume the following conditions at which the flux into the film is maximized: (1) steady-state conditions, (2) $C_g = 0$ at $y = 0$ (at the film surface), and (3) $C_g = C_{g,eq}$ at $y = \delta_n$, where δ_n is the thickness of the bottommost BL layer. Additionally, we also assume the bottommost layer in BL is quiescent (i.e., eddy diffusion is not considered), resulting in the equation below for the gas-phase concentration, C_g:

$$C_g = \frac{C_{g,eq}}{\delta_n} y \quad (4.13)$$

The maximum steady-state flux of species *i*, $F_{max,g}$, is:

$$F_{max,g} = -D_g \frac{dC_g}{dy} = -D_g \frac{C_{g,eq}}{\delta_n} \tag{4.14}$$

Using the expression above, we define the average molar uptake rate of species *i*, $R_{max,g}$, into the aqueous planar film and express it in partial pressure of species *i* at equilibrium, P_{eq}:

$$R_{max,g} = -\frac{A_{film}}{V_{film}} F = \frac{D_g C_{g,eq}}{\delta_{film}\delta_n} = \frac{D_g P_{eq}}{\delta_{film}\delta_n \mathrm{R}T} \tag{4.15}$$

where δ_{film} is the thickness of the aqueous film, R is the gas constant, and T is temperature. The time constant of film saturation of species *i* by gas-phase diffusion, τ_g, is in the order of $\delta_{film}\delta_n/D_g$ as shown below:

$$\tau_g = \frac{C_{aq,eq}}{R_{max,g}} = \frac{H^* RT \delta_{film}\delta_n}{D_g} \approx \frac{\delta_{film}\delta_n}{D_g} \tag{4.16}$$

Interphase mass transport

The interphase mass transport expression is on the basis of molecular collision of gas-phase species i on the aqueous-phase surface and is as follows:

$$\sigma_{coll} = \frac{P_{eq}\omega_i \alpha_i}{4\mathrm{R}T} \tag{4.17}$$

where ω_i is the thermal velocity of species *i* and α_i is the accommodation coefficient of species *i*. The partial pressure of species i should be its value at the interface ($y = 0$), but it is assumed here to be its value at equilibrium to determine the maximum average molar uptake rate, $R_{max,i}$, which is shown below:

$$R_{max,i} = -\frac{A_{film}}{V_{film}} \sigma_{coll} = \frac{P_{eq}\omega_i \alpha_i}{4\delta_{film}\mathrm{R}T} \tag{4.18}$$

The time constant of film saturation of species *i* by interphase mass transport, τ_i, is in the order of $4\delta_{film}/(\omega_i\alpha_i)$ as shown in the following equation:

$$\tau_i = \frac{C_{aq,eq}}{R_{max,i}} = \frac{4\delta_{film} H^* \mathrm{R}T}{\omega_i \alpha_i} \approx \frac{4\delta_{film}}{\omega_i \alpha_i} \tag{4.19}$$

Mass transfer coefficient

The mass transfer coefficient considers the time constants (i.e., resistances) of both gas-phase diffusion and interphase mass transport:

$$k_{mt} = (\tau_g + \tau_i)^{-1} \quad (4.20)$$

$$k_{mt} = \left(\frac{\delta_{film}\delta_n}{D_g} + \frac{4\delta_{film}}{\omega_i \alpha_i}\right)^{-1} \quad (4.21)$$

Effective Henry's Law Constant

The equations for the effective Henry's law constant are given in Tilgner et al. (2021):[136]

$$H_A{}^* = H_A\left(1 + \frac{K_{a1}}{[\mathrm{H}^+]}\right) \quad \text{for monoprotic acid} \quad (4.22)$$

$$H_A{}^* = H_A\left(1 + \frac{K_{a1}}{[\mathrm{H}^+]} + \frac{K_{a1}K_{a2}}{[\mathrm{H}^+]^2}\right) \quad \text{for diprotic acid} \quad (4.23)$$

where $H_A{}^*$ is the effective Henry's law constant, H_A is the Henry's law constant, $[H^+]$ is the hydrogen ion concentration, and Ka1 and Ka2 are the acid dissociation constants. Using the HA and pKa values in Tables 4.6 and 4.12, the effective Henry's law constant for IBA, PA, and AA are calculated below at pH 10 and 13.

Table 4.13: List of Effective Henry's Law Constant for Acids

Species	**H_A (M/atm)**	**$H_A{}^*$ at pH 10 (M/atm)**	**$H_A{}^*$ at pH 13 (M/atm)**	**T (°C)**
IBA	1E+03	1.4E+08	1.4E+11	20
PA	5E+07	1.0E+20	1.0E+26	25
AA	2E+08	2.6E+18	2.6E+24	25

Timescale of Loss by Ventilation vs. Atmospheric Oxidation by OH Radical

The following equations describe the timescales of two gas-phase processes, loss by ventilation and loss by atmospheric oxidation by OH radical:

$$\tau_{vent} = \frac{1}{ACH} \tag{4.24}$$

$$\tau_{ox} = \frac{1}{k_{ox} C_{\cdot OH}} \tag{4.25}$$

where τ_{vent} is the timescale of ventilation, ACH is the air changes per hour (converted to air changes per second), τ_{ox} is the timescale of atmospheric oxidation, k_{ox} is the second-order oxidation rate constant, and $C_{\cdot OH}$ is the OH radical concentration indoors.

At 0.5 ACH, the timescale associated with loss by ventilation is 7200 s.

$$\tau_{vent} = \frac{1}{0.5\ \mathrm{h^{-1}}} = 2\ \mathrm{h} = 7200\ \mathrm{s} \tag{4.26}$$

Assuming OH radical concentration of 4×10^5 molec cm^{-3} and k_{ox} of 4×10^{-11} cm^3 molec^{-1} s^{-1} for TCIPP (fastest gas-phase oxidation rate constant in GAMMA-CIE, found in Table 4.7), the timescale associated with loss by atmospheric oxidation is 62500 s, greater by a factor of 8.7 than that associated with ventilation.

$$\tau_{ox} = \frac{1}{k_{ox} C_{\cdot OH}} = \frac{1}{(4 \times 10^5)(4 \times 10^{-11})\ \mathrm{s^{-1}}} = 62500\ s$$

Scenario 1 Model Output

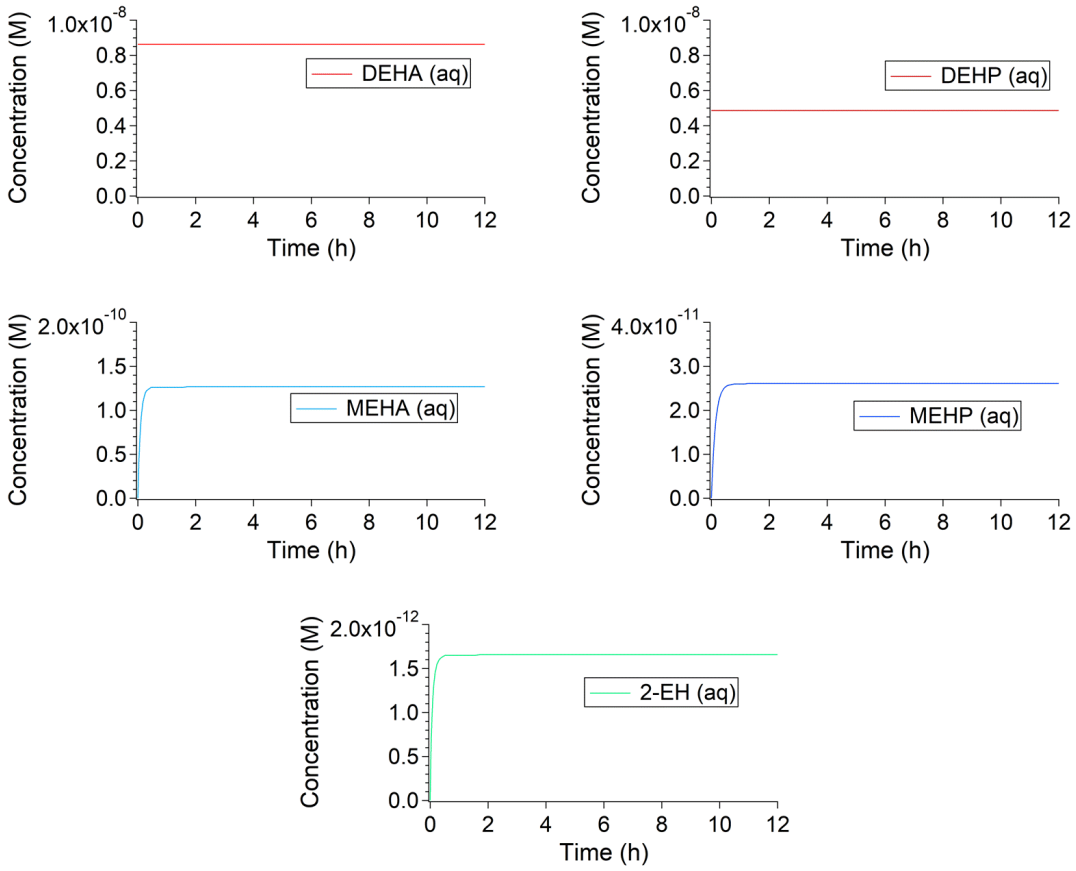

Figure 4.10: Predicted temporal evolution of aqueous-phase DEHA, DEHP, MEHA, MEHP, and 2-EH at pH 13 and 0.5 ACH in low-DEHP scenario.

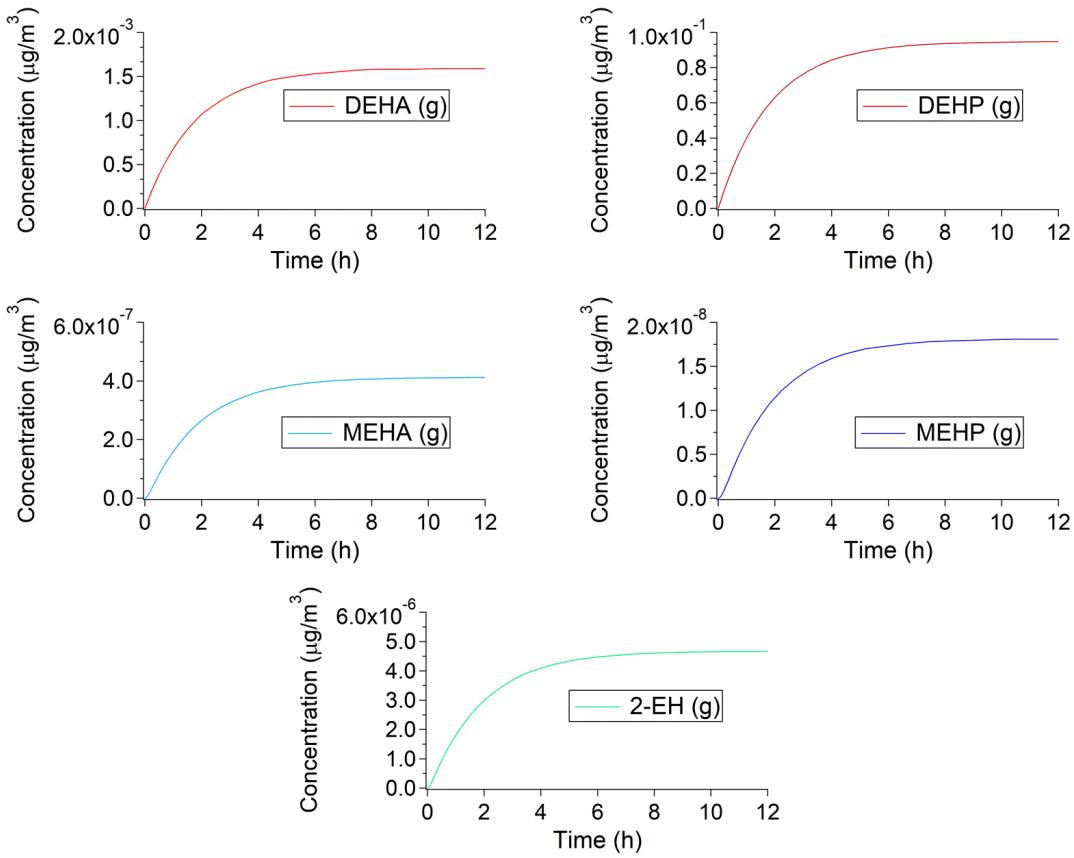

Figure 4.11: Predicted temporal evolution of gas-phase DEHA, DEHP, MEHA, MEHP, and 2-EH at pH 13 and 0.5 ACH in low-DEHP scenario.

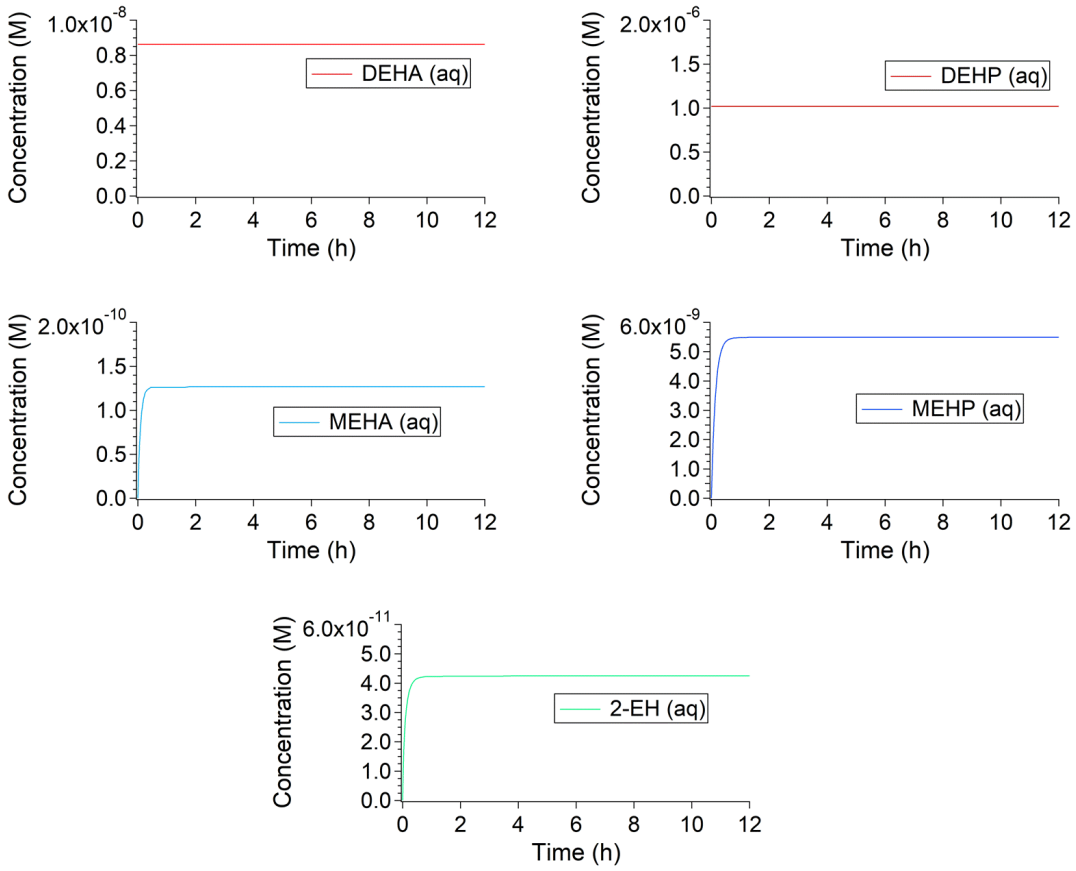

Figure 4.12: Predicted temporal evolution of aqueous-phase DEHA, DEHP, MEHA, MEHP, and 2-EH at pH 13 and 0.5 ACH in high-DEHP scenario.

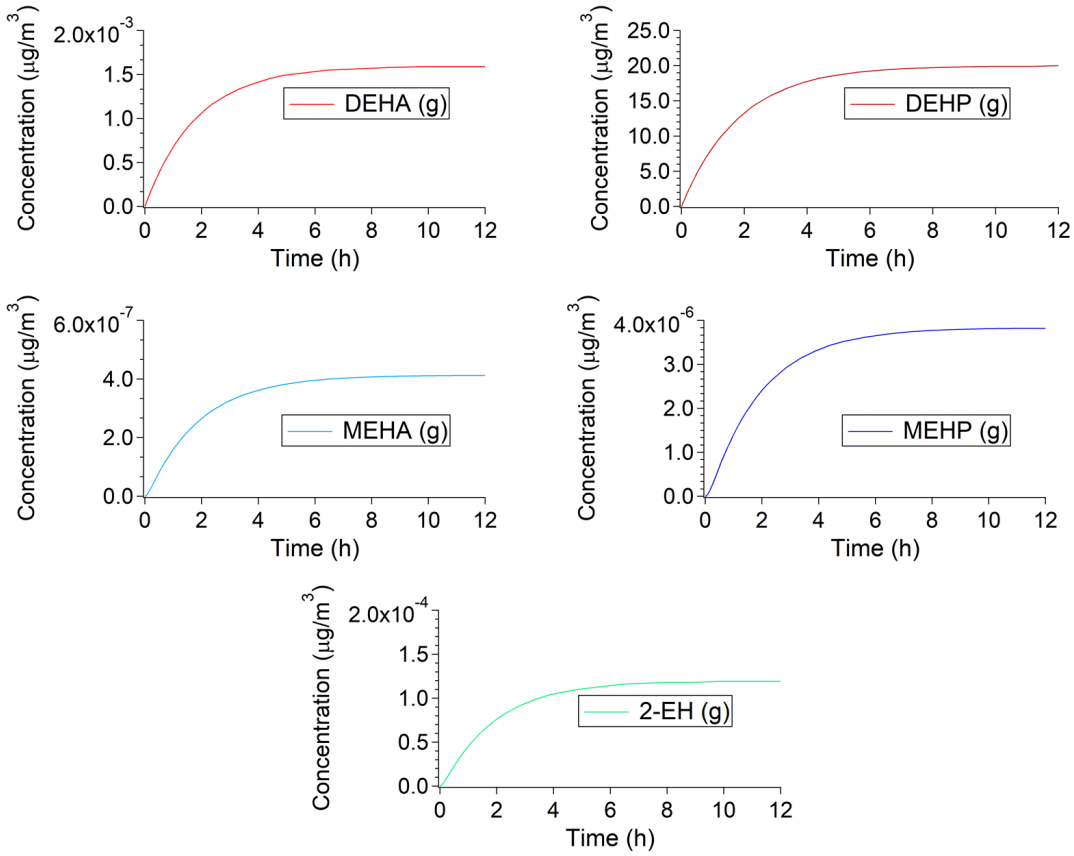

Figure 4.13: Predicted temporal evolution of gas-phase DEHA, DEHP, MEHA, MEHP, and 2-EH at pH 13 and 0.5 ACH in high-DEHP scenario.

Film Thickness Sensitivity Analysis

Film thickness was varied from 1 nm to 100 μm for the simulation of gas-phase 2-ethylhexanol (2-EH) generation in Scenario 1, pH 13, 0.5 ACH, high-DEHP condition to test the sensitivity of the system to film thickness. Figure 4.14 shows the 2-EH concentration profiles with varying thickness, with the predicted steady state concentrations are tabulated in Table 4.14 below.

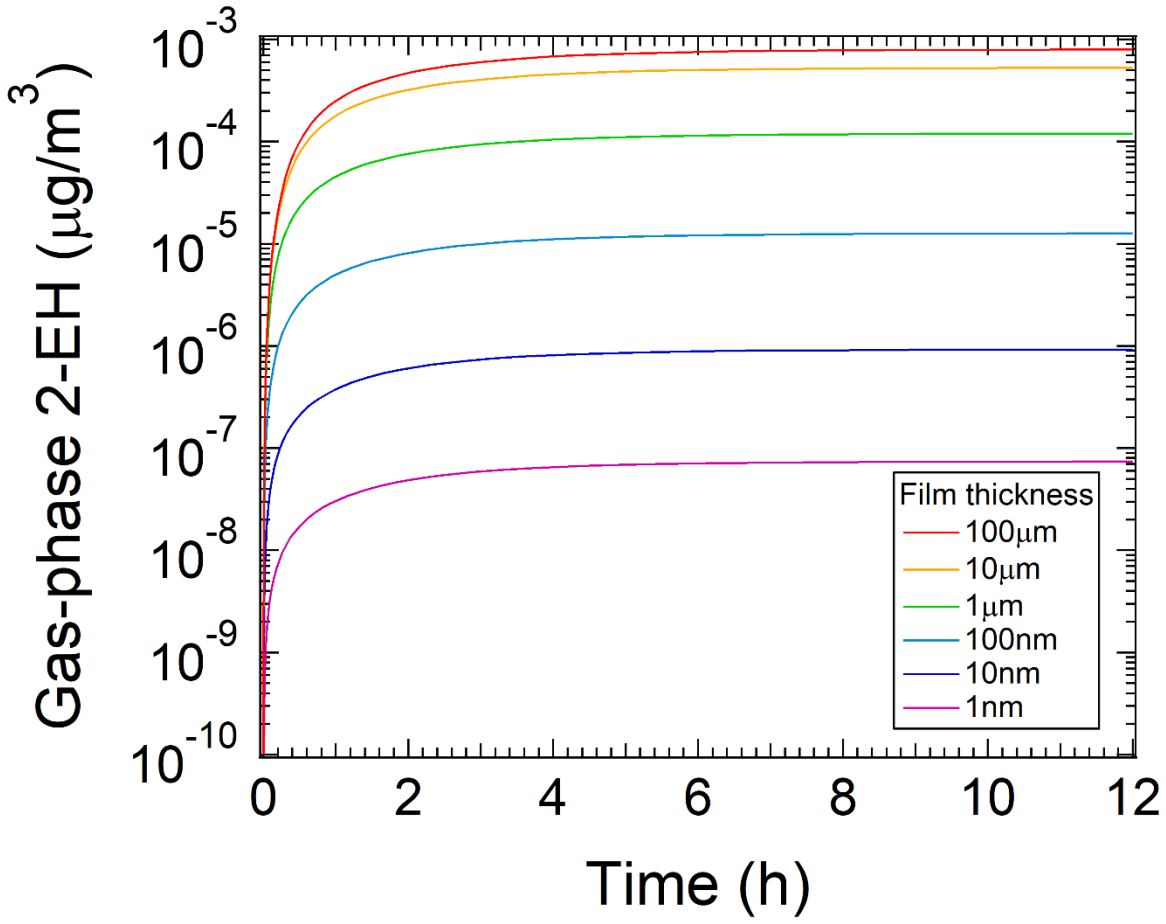

Figure 4.14: Scenario 1: sensitivity of temporal evolution of gas-phase 2-EH at pH 13 and 0.5 ACH in high-DEHP condition to aqueous film thickness.

Table 4.14: Scenario 1: Predicted Steady State 2-EH Concentrations at pH 13, 0.5 ACH, High-DEHP Condition, and Varying Aqueous Film Thickness

Aqueous Film Thickness	**2-EH Concentration (μg/m^3)**
100 μm	7.9E-04
10 μm	5.3E-04
1 μm	1.2E-04
100 nm	1.3E-05
10 nm	9.2E-07
1 nm	7.4E-08

Overall, the predicted steady state concentration decreased with decreasing film thickness. This was expected, with one of the key assumptions in Scenario 1 being that the parent reactant esters DEHA and DEHP would be in excess and remain at aqueous saturation limit throughout the simulation. Thus, thinner aqueous films would indicate lower amount of DEHA and DEHP available in the system. In the lower range of film thickness from 1 nm to 1 μm, a tenfold decrease in film thickness corresponded to approximately a proportional tenfold decrease in the predicted gas-phase 2-EH concentration at steady state. In the higher range from 1 μm to 100 μm, however, changes in film thickness were not as impactful in the evolution of gas-phase 2-EH, with only an eightfold increase in 2-EH concentration corresponding to a hundredfold increase in film thickness. A similar trend between film thickness and gas-phase evolution was observed in both Scenario 2 and 3 as shown in Tables 4.15 and 4.16 below.

Table 4.15: Scenario 2: Predicted Peak TMPD-MIB Concentrations at pH 10, 0.5 ACH, and Varying Aqueous Film Thickness

Aqueous Film Thickness	**TMPD-MIB Concentration ($\mu g/m^3$)**
100 µm	810
10 µm	726
1 µm	356
100 nm	61
10 nm	6.6
1 nm	0.67

Table 4.16: Scenario 3: Predicted Steady State EtOH Concentrations at pH 13, 0.5 ACH, and Varying Aqueous Film Thickness

Aqueous Film Thickness	**EtOH Concentration ($\mu g/m^3$)**
100 µm	9.3E-03
10 µm	4.8E-03
1 µm	3.7E-04
100 nm	9.8E-06
10 nm	5.0E-07
1 nm	3.3E-08

The simulation results suggest that film thickness can significantly affect the gas-phase evolution of hydrolysis products, especially in the 1 nm–1 µm range which is believed to be the likely scale for indoor film thickness.[39] In the model, film thickness restricts the overall load of synthetic esters (SEs) available for hydrolytic degradation and gas-phase partitioning in the

aqueous film, as the SEs are bound by their water solubilities. The predicted trend may not hold true in practice if SE concentrations can exceed water solubility limits in presence of other organics in the film. Further research is needed to fully understand the impact of film thickness on the emissions of hydrolysis products.

Chapter 5: Conclusion & Outlook

The work discussed in this dissertation provides insight into the role of alkaline hydrolysis and ventilation in indoor environments and their impact on the emissions and removal of VOCs in indoor air.

In chapter 2, the alkaline hydrolysis rate constants of four SVOCs commonly encountered indoors (TMPD-MIB, BP, DEHA, and BBzP) were experimentally determined in bulk aqueous solutions to evaluate their hydrolysis reactivity in indoor environments. The determined rate constants may be applicable to assessing the fate of the aforementioned SVOCs in bodies of water (e.g., rivers, lakes, seas) as they have been also detected in samples of aquatic environments and aquatic animals.[150,157–159] Comparison between experimental results and HYDROWIN (hydrolysis kinetics estimation tool) predicted values, shown in Table 5.1, demonstrate that HYDROWIN predictions may be useful in initially evaluating SVOCs which are highly susceptible to hydrolysis, but it is also likely that HYDROWIN may overpredict the rate constant by a factor of 20 for certain compounds. In regards to hydrolysis occurring in aqueous films on indoor surfaces, further research on the role of surfaces is warranted. Few studies have observed oxide (e.g., Al2O3, TiO2) and metal (e.g., Cu^{II}, Pb^{II}) surfaces catalyzing the hydrolysis of carboxylate and organophosphate esters,[160,161] but to the author's knowledge, indoor surfaces (e.g., concrete (CaCO3), glass (SiO2), carpet (nylon))[19] have not been investigated.

Table 5.1 Comparison Between Experimental Rate Constants and HYDROWIN Predicted Rate Constants

Ester	Experimental k (M^{-1} s^{-1})	Predicted k (M^{-1} s^{-1})
TMPD-MIB	9.8E-3	1.4E-2
BP	1.24E-4	5.1E-3
DEHA	4.8E-4	6.8E-2
BBZP	5.9E-	1.6E-1

In chapter 3, a wide array of ventilation measurement techniques and instrumentation is discussed, presenting their advantages and disadvantages and their applicability for different circumstances and conditions. Buildings with natural ventilation tended to be more poorly ventilated than those with mechanical ventilation in the Northeastern US, whereas the opposite was true for Southern California and Southeastern US where heat retention is not much of a design constraint. This study was motivated by the need to understand room-level ventilation for reducing COVID-19 transmission prior to vaccine availability, but this knowledge can be applied for general indoor air quality (IAQ) assessments as shown in chapter 4.

In chapter 4, the evolution of gas-phase VOCs from alkaline hydrolysis of various SVOCs in surface aqueous films was simulated using GAMMA-CIE, with its parameter values adjusted on the basis of experimental results in chapters 2 (hydrolysis kinetics) and 3 (air exchange rate). This work is arguably the first attempt in rigorously putting numbers to the concentrations of VOCs originating from indoor hydrolysis. Simulation results suggested that (1) hydrolysis of DEHA and DEHP in flooring likely does not contribute significantly to indoor 2-EH levels, (2) application of fresh latex paint on concrete may be a significant source of TMPD and TMPD-MIB, and (3) airborne SVOC uptake in surface aqueous films is not expected to produce significant amounts of VOCs. Experimental data on the emission profiles of VOCs in the proposed hydrolysis scenarios would be greatly beneficial in validating the model and its

simulated results, as TMPD-MIB is the only species of interest with available field measurements. Apart from the scenarios presented in this study, accounting for the uptake of settled dust, presence of microbes, other emission sources (e.g., cooking, cleaning), and the complex chemical composition of organic-aqueous mixed films would open up possibilities in investigating other (S)VOCs (e.g., SEs with heavier molecular weight, halogenated compounds) not discussed in this dissertation.[40,105,109,162]

In the current version of GAMMA-CIE, the rates of hydrolysis kinetics (i.e., pH), gas-phase diffusion, and removal by ventilation are all influential factors in the evolution of gas-phase VOCs, with the underlying assumption that the aqueous film is constantly saturated (for scenario 1) and well-mixed. A recent study by Henkel et al. (2022) suggests that diffusion of plasticizer esters in plastic may be the rate-limiting factor, in which case the constant saturation assumption may not hold true.[163] For scenarios where leaching from plastics is the major source of reactant SVOC, the addition of plastic-water migration mechanism may be valuable.

.

References

(1) US Environmental Protection Agency. *Report to Congress on Indoor Air Quality: Volume II*; Washington, DC, USA, 1989.

(2) Redlich, C. A.; Sparer, J.; Cullen, M. R. Sick-Building Syndrome. *Lancet* **1997**, *349* (9057), 1013–1016. https://doi.org/10.1016/S0140-6736(96)07220-0.

(3) Jones, A. P. Indoor Air Quality and Health. *Atmos. Environ.* **1999**, *33* (28), 4535–4564. https://doi.org/10.1016/S1352-2310(99)00272-1.

(4) Sundell, J. On the History of Indoor Air Quality and Health. *Indoor Air* **2004**, *14* (SUPPL. 7), 51–58. https://doi.org/10.1111/j.1600-0668.2004.00273.x.

(5) Li, Z.; Wen, Q.; Zhang, R. Sources, Health Effects and Control Strategies of Indoor Fine Particulate Matter (PM2.5): A Review. *Sci. Total Environ.* **2017**, *586*, 610–622. https://doi.org/10.1016/j.scitotenv.2017.02.029.

(6) Sen, D. Working with Asbestos and the Possible Health Risks. *Occup. Med. (Chic. Ill).* **2015**, *65* (1), 6–14. https://doi.org/10.1093/occmed/kqu175.

(7) Al-Zoughool, M.; Krewski, D. Health Effects of Radon: A Review of the Literature. *Int. J. Radiat. Biol.* **2009**, *85* (1), 57–69. https://doi.org/10.1080/09553000802635054.

(8) Jorens, P. G.; Schepens, P. J. C. Human Pentachlorophenol Poisoning. *Hum. Exp. Toxicol.* **1993**, *12* (6), 479–495. https://doi.org/10.1177/096032719301200605.

(9) Weschler, C. J. Changes in Indoor Pollutants since the 1950s. *Atmos. Environ.* **2009**, *43* (1), 153–169. https://doi.org/10.1016/j.atmosenv.2008.09.044.

(10) Ten Brinke, J. Development of New Volatile Organic Compound (VOC) Exposure

Metrics and Their Relationship to “Sick Building Syndrome” Symptoms. *Indoor Air* **1998**, *8* (3), 140–152. https://doi.org/10.1111/j.1600-0668.1998.t01-1-00002.x.

(11) Yu, C. W. F.; Kim, J. T. Building Pathology, Investigation of Sick Buildings - VOC Emissions. *Indoor Built Environ.* **2010**, *19* (1), 30–39. https://doi.org/10.1177/1420326X09358799.

(12) Kumar, P.; Kausar, M. A.; Singh, A. B.; Singh, R. Biological Contaminants in the Indoor Air Environment and Their Impacts on Human Health. *Air Qual. Atmos. Heal.* **2021**, *14* (11), 1723–1736. https://doi.org/10.1007/s11869-021-00978-z.

(13) Aydogdu, H.; Asan, A.; Otkun, M. T.; Ture, M. Monitoring of Fungi and Bacteria in the Indoor Air of Primary Schools in Edirne City, Turkey. *Indoor Built Environ.* **2005**, *14* (5), 411–425. https://doi.org/10.1177/1420326X05057539.

(14) Koskinen, O. M.; Husman, T. M.; Meklin, T. M.; Nevalainen, A. I. The Relationship between Moisture or Mould Observations in Houses and the State of Health of Their Occupants. *Eur. Respir. J.* **1999**, *14* (6), 1363–1367. https://doi.org/10.1183/09031936.99.14613639.

(15) Pastuszka, J. S.; Kyaw Tha Paw, U.; Lis, D. O.; Wlazlo, A.; Ulfig, K. Bacterial and Fungal Aerosol in Indoor Environment in Upper Silesia, Poland. *Atmos. Environ.* **2000**, *34* (22), 3833–3842. https://doi.org/10.1016/S1352-2310(99)00527-0.

(16) Morawska, L.; Tang, J. W.; Bahnfleth, W.; Bluyssen, P. M.; Boerstra, A.; Buonanno, G.; Cao, J.; Dancer, S.; Floto, A.; Franchimon, F.; et al. How Can Airborne Transmission of COVID-19 Indoors Be Minimised? *Environ. Int.* **2020**, *142* (May). https://doi.org/10.1016/j.envint.2020.105832.

(17) Chen, W.; Zhang, N.; Wei, J.; Yen, H. L.; Li, Y. Short-Range Airborne Route Dominates

Exposure of Respiratory Infection during Close Contact. *Build. Environ.* **2020**, *176* (January), 106859. https://doi.org/10.1016/j.buildenv.2020.106859.

(18) Weschler, C. J. Chemistry in Indoor Environments: 20 Years of Research. *Indoor Air* **2011**, *21* (3), 205–218. https://doi.org/10.1111/j.1600-0668.2011.00713.x.

(19) Ault, A. P.; Grassian, V. H.; Carslaw, N.; Collins, D. B.; Destaillats, H.; Donaldson, D. J.; Farmer, D. K.; Jimenez, J. L.; McNeill, V. F.; Morrison, G. C.; et al. Indoor Surface Chemistry: Developing a Molecular Picture of Reactions on Indoor Interfaces. *Chem* **2020**, 1–16. https://doi.org/10.1016/j.chempr.2020.08.023.

(20) Weschler, C. J.; Carslaw, N. Indoor Chemistry. *Environ. Sci. Technol.* **2018**, *52* (5), 2419–2428. https://doi.org/10.1021/acs.est.7b06387.

(21) Gligorovski, S.; Strekowski, R.; Barbati, S.; Vione, D. Environmental Implications of Hydroxyl Radicals (•OH). *Chem. Rev.* **2015**, *115* (24), 13051–13092. https://doi.org/10.1021/cr500310b.

(22) Carslaw, N. A New Detailed Chemical Model for Indoor Air Pollution. *Atmos. Environ.* **2007**, *41* (6), 1164–1179. https://doi.org/10.1016/j.atmosenv.2006.09.038.

(23) Nazaroff, W. W.; Cass, G. R. Mathematical Modeling of Indoor Aerosol Dynamics. *Environ. Sci. Technol.* **1989**, *23* (2), 157–166. https://doi.org/10.1021/es00179a003.

(24) Nazaroff, W. W.; Goldstein, A. H. Indoor Chemistry: Research Opportunities and Challenges. *Indoor Air* **2015**, *25* (4), 357–361. https://doi.org/10.1111/ina.12219.

(25) Forester, C. D.; Wells, J. R. Yields of Carbonyl Products from Gas-Phase Reactions of Fragrance Compounds with OH Radical and Ozone. *Environ. Sci. Technol.* **2009**, *43* (10), 3561–3568. https://doi.org/10.1021/es803465v.

(26) Forester, C. D.; Wells, J. R. Hydroxyl Radical Yields from Reactions of Terpene Mixtures

with Ozone. *Indoor Air* **2011**, *21* (5), 400–409. https://doi.org/10.1111/j.1600-0668.2011.00718.x.

(27) Waring, M. S.; Wells, J. R.; Siegel, J. A. Secondary Organic Aerosol Formation from Ozone Reactions with Single Terpenoids and Terpenoid Mixtures. *Atmos. Environ.* **2011**, *45* (25), 4235–4242. https://doi.org/10.1016/j.atmosenv.2011.05.001.

(28) Wolkoff, P. Indoor Air Chemistry: Terpene Reaction Products and Airway Effects. *Int. J. Hyg. Environ. Health* **2020**, *225* (September 2019), 0–7. https://doi.org/10.1016/j.ijheh.2019.113439.

(29) Waring, M. S.; Wells, J. R. Volatile Organic Compound Conversion by Ozone, Hydroxyl Radicals, and Nitrate Radicals in Residential Indoor Air: Magnitudes and Impacts of Oxidant Sources. *Atmos. Environ.* **2015**, *106* (3), 382–391. https://doi.org/10.1016/j.atmosenv.2014.06.062.

(30) Young, C. J.; Zhou, S.; Siegel, J. A.; Kahan, T. F. Illuminating the Dark Side of Indoor Oxidants. *Environ. Sci. Process. Impacts* **2019**, *21* (8), 1229–1239. https://doi.org/10.1039/c9em00111e.

(31) Reiss, R.; Ryan, P. B.; Tibbetts, S. J.; Koutrakis, P. Measurement of Organic Acids, Aldehydes, and Ketones in Residential Environments and Their Relation to Ozone. *J. Air Waste Manage. Assoc.* **1995**, *45* (10), 811–822. https://doi.org/10.1080/10473289.1995.10467411.

(32) Morrison, G. C.; Nazaroff, W. W. Ozone Interactions with Carpet: Secondary Emissions of Aldehydes. *Environ. Sci. Technol.* **2002**, *36* (10), 2185–2192. https://doi.org/10.1021/es0113089.

(33) Rim, D.; Gall, E. T.; Maddalena, R. L.; Nazaroff, W. W. Ozone Reaction with Interior

Building Materials: Influence of Diurnal Ozone Variation, Temperature and Humidity. *Atmos. Environ.* **2016**, *125*, 15–23. https://doi.org/10.1016/j.atmosenv.2015.10.093.

(34) Nazaroff, W. W.; Weschler, C. J. Indoor Ozone: Concentrations and Influencing Factors. *Indoor Air* **2022**, *32* (1), 1–21. https://doi.org/10.1111/ina.12942.

(35) Wisthaler, A.; Weschler, C. J. Reactions of Ozone with Human Skin Lipids: Sources of Carbonyls, Dicarbonyls, and Hydroxycarbonyls in Indoor Air. *Proc. Natl. Acad. Sci. U. S. A.* **2010**, *107* (15), 6568–6575. https://doi.org/10.1073/pnas.0904498106.

(36) Lakey, P. S. J.; Wisthaler, A.; Berkemeier, T.; Mikoviny, T.; Pöschl, U.; Shiraiwa, M. Chemical Kinetics of Multiphase Reactions between Ozone and Human Skin Lipids: Implications for Indoor Air Quality and Health Effects. *Indoor Air* **2017**, *27* (4), 816–828. https://doi.org/10.1111/ina.12360.

(37) Coffaro, B.; Weisel, C. P. Reactions and Products of Squalene and Ozone: A Review. *Environ. Sci. Technol.* **2022**, *56* (12), 7396–7411. https://doi.org/10.1021/acs.est.1c07611.

(38) Weschler, C. J.; Nazaroff, W. W. Growth of Organic Films on Indoor Surfaces. *Indoor Air* **2017**, *27* (6), 1101–1112. https://doi.org/10.1111/ina.12396.

(39) Duncan, S. M.; Sexton, K. G.; Turpin, B. J. Oxygenated VOCs, Aqueous Chemistry, and Potential Impacts on Residential Indoor Air Composition. *Indoor Air* **2018**, *28* (1), 198–212. https://doi.org/10.1111/ina.12422.

(40) Lim, C. Y.; Abbatt, J. P. Chemical Composition, Spatial Homogeneity, and Growth of Indoor Surface Films. *Environ. Sci. Technol.* **2020**, *54* (22), 14372–14379. https://doi.org/10.1021/acs.est.0c04163.

(41) Wakayama, T.; Ito, Y.; Sakai, K.; Miyake, M.; Shibata, E.; Ohno, H.; Kamijima, M. Comprehensive Review of 2-Ethyl-1-Hexanol as an Indoor Air Pollutant. *J. Occup.*

Health **2019**, *61* (1), 19–35. https://doi.org/10.1002/1348-9585.12017.

(42) Persily, A. Challenges in Developing Ventilation and Indoor Air Quality Standards: The Story of ASHRAE Standard 62. *Build. Environ.* **2015**, *91*, 61–69. https://doi.org/10.1016/j.buildenv.2015.02.026.

(43) Seppanen, O.; Fisk, W. J.; Lei, Q. H. Ventilation and Performance in Office Work. *Indoor Air* **2006**, *16* (1), 28–36. https://doi.org/10.1111/j.1600-0668.2005.00394.x.

(44) Hummelgaard, J.; Juhl, P.; Sæbjörnsson, K. O.; Clausen, G.; Toftum, J.; Langkilde, G. Indoor Air Quality and Occupant Satisfaction in Five Mechanically and Four Naturally Ventilated Open-Plan Office Buildings. *Build. Environ.* **2007**, *42* (12), 4051–4058. https://doi.org/10.1016/j.buildenv.2006.07.042.

(45) Fisk, W. J.; Mirer, A. G.; Mendell, M. J. Quantitative Relationship of Sick Building Syndrome Symptoms with Ventilation Rates. *Indoor Air* **2009**, *19* (2), 159–165. https://doi.org/10.1111/j.1600-0668.2008.00575.x.

(46) Bhagat, R. K.; Davies Wykes, M. S.; Dalziel, S. B.; Linden, P. F. Effects of Ventilation on the Indoor Spread of COVID-19. *J. Fluid Mech.* **2020**, *903*. https://doi.org/10.1017/jfm.2020.720.

(47) McLeod, R. S.; Hopfe, C. J.; Bodenschatz, E.; Moriske, H. J.; Pöschl, U.; Salthammer, T.; Curtius, J.; Helleis, F.; Niessner, J.; Herr, C.; et al. A Multi-Layered Strategy for COVID-19 Infection Prophylaxis in Schools: A Review of the Evidence for Masks, Distancing, and Ventilation. *Indoor Air* **2022**, *32* (10), 1–11. https://doi.org/10.1111/ina.13142.

(48) Khan, N.; Su, Y.; Riffat, S. B. A Review on Wind Driven Ventilation Techniques. *Energy Build.* **2008**, *40* (8), 1586–1604. https://doi.org/10.1016/j.enbuild.2008.02.015.

(49) World Health Organization. *WHO Guidelines for Indoor Air Quality: Selected Pollutants*;

2010.

(50) Turiel, I.; Hollowell, C. D.; Miksch, R. R.; Rudy, J. V.; Young, R. A.; Coye, M. J. The Effects of Reduced Ventilation on Indoor Air Quality in an Office Building. *Atmos. Environ.* **1983**, *17* (1), 51–64. https://doi.org/10.1016/0004-6981(83)90007-0.

(51) Godwin, A. D. Plasticizers. In *Applied Polymer Science: 21st Century*; Elsevier, 2000; pp 157–175. https://doi.org/10.1016/B978-0-08-043417-9.X5000-4.

(52) Lin, C. C.; Corsi, R. L. Texanol® Ester Alcohol Emissions from Latex Paints: Temporal Variations and Multi-Component Recoveries. *Atmos. Environ.* **2007**, *41* (15), 3225–3234. https://doi.org/10.1016/j.atmosenv.2006.07.057.

(53) Centers for Disease Control and Prevention. Parabens Factsheet https://www.cdc.gov/biomonitoring/Parabens_FactSheet.html (accessed Apr 2, 2021).

(54) Weschler, C. J.; Nazaroff, W. W. Semivolatile Organic Compounds in Indoor Environments. *Atmos. Environ.* **2008**, *42* (40), 9018–9040. https://doi.org/10.1016/j.atmosenv.2008.09.052.

(55) Till, D. E.; Reid, R. C.; Schwartz, P. S.; Sidman, K. R.; Valentine, J. R.; Whelan, R. H. Plasticizer Migration from Polyvinyl Chloride Film to Solvents and Foods. *Food Chem. Toxicol.* **1982**, *20* (1), 95–104. https://doi.org/10.1016/S0278-6915(82)80016-1.

(56) Takashima, K.; Riveros, J. M. Gas-Phase Pathways for Ester Hydrolysis. *J. Am. Chem. Soc.* **1978**, *100* (19), 6128–6132. https://doi.org/10.1021/ja00487a027.

(57) Schettler, T.; Skakkebæk, N. E.; De Kretser, D.; Leffers, H. Human Exposure to Phthalates via Consumer Products. *Int. J. Androl.* **2006**, *29* (1), 134–139. https://doi.org/10.1111/j.1365-2605.2005.00567.x.

(58) Reinmuth-Selzle, K.; Kampf, C. J.; Lucas, K.; Lang-Yona, N.; Fröhlich-Nowoisky, J.;

Shiraiwa, M.; Lakey, P. S. J.; Lai, S.; Liu, F.; Kunert, A. T.; et al. Air Pollution and Climate Change Effects on Allergies in the Anthropocene: Abundance, Interaction, and Modification of Allergens and Adjuvants. *Environ. Sci. Technol.* **2017**, *51* (8), 4119–4141. https://doi.org/10.1021/acs.est.6b04908.

(59) Brinke, J. Ten; Selvin, S.; Hodgson, A. T.; Fisk, W. J.; Mendell, M. J.; Koshland, C. P.; Daisey, J. M. Development of New Volatile Organic Compound (VOC) Exposure Metrics and Their Relationship to "Sick Building Syndrome" Symptoms. *Indoor Air* **1998**, *8* (3), 140–152. https://doi.org/10.1111/j.1600-0668.1998.t01-1-00002.x.

(60) Norback, D.; Wieslander, G.; Nordstrom, K.; Walinder, R. Asthma Symptoms in Relation to Measured Building Dampness in Upper Concrete Floor Construction, and 2-Ethyl-1-Hexanol in Indoor Air. *Int. J. Tuberc. Lung Dis.* **2000**, *4* (11), 1016–1025.

(61) Björk, F.; Eriksson, C. A.; Karlsson, S.; Khabbaz, F. Degradation of Components in Flooring Systems in Humid and Alkaline Environments. *Constr. Build. Mater.* **2003**, *17* (3), 213–221. https://doi.org/10.1016/S0950-0618(02)00036-3.

(62) Wolfe, N. L.; Steen, W. C.; Burns, L. A. Phthalate Ester Hydrolysis: Linear Free Energy Relationships. *Chemosphere* **1980**, *9* (7–8), 403–408. https://doi.org/10.1016/0045-6535(80)90023-5.

(63) Kirby, A. J. Hydrolysis and Formation of Esters of Organic Acids. In *Comprehensive Chemical Kinetics*; Bamford, C. H., Tipper, C. F. H., Eds.; Elsevier, 1972; Vol. 10, pp 57–207. https://doi.org/10.1016/S0069-8040(08)70344-3.

(64) Shija, R.; Bruce Sunderland, V.; McDonald, C. Alkaline Hydrolysis of Methyl, Ethyl and n-Propyl 4-Hydroxybenzoate Esters in the Liquid and Frozen States. *Int. J. Pharm.* **1992**, *80* (1–3), 203–211. https://doi.org/10.1016/0378-5173(92)90278-A.

(65) Yim, B.; Nagata, Y.; Maeda, Y. Sonolytic Degradation of Phthalic Acid Esters in Aqueous Solutions. Acceleration of Hydrolysis by Sonochemical Action. *J. Phys. Chem. A* **2002**, *106* (1), 104–107. https://doi.org/10.1021/jp011896c.

(66) Xu, Z.; Cheng, L.; Shi, J.; Lu, J.; Zhang, W.; Zhao, Y.; Li, F.; Chen, M. Kinetic Study of the Removal of Dimethyl Phthalate from an Aqueous Solution Using an Anion Exchange Resin. *Environ. Sci. Pollut. Res.* **2014**, *21* (10), 6571–6577. https://doi.org/10.1007/s11356-014-2556-x.

(67) Nazaroff, W. W.; Weschler, C. J. Indoor Acids and Bases. *Indoor Air* **2020**, No. March, 559–644. https://doi.org/10.1111/ina.12670.

(68) Björk, F.; Eriksson, C. A. Measurement of Alkalinity in Concrete by a Simple Procedure, to Investigate Transport of Alkaline Material from the Concrete Slab to a Self-Levelling Screed. *Constr. Build. Mater.* **2002**, *16* (8), 535–542. https://doi.org/10.1016/S0950-0618(02)00035-1.

(69) Wei, Z.; Li, Y.; Cooks, R. G.; Yan, X. Accelerated Reaction Kinetics in Microdroplets: Overview and Recent Developments. *Annu. Rev. Phys. Chem.* **2020**, *71*, 31–51. https://doi.org/10.1146/annurev-physchem-121319-110654.

(70) ASHRAE. *Standing Standard Project Committee 62.1, ANSI/ASHRAE Standard 62.1-2019, Ventilation for Acceptable Indoor Air Quality*; 2019.

(71) Corsi, R.; Miller, S. L.; VanRy, M. G.; Marr, L. C.; Cadet, L. R.; Pollock, N. R.; Michaels, D.; Jones, E. R.; Levinson, M.; Li, Y.; et al. Designing Infectious Disease Resilience into School Buildings through Improvements to Ventilation and Air Cleaning. *Lancet Covid-19 Comm. task force safe Work. safe Sch. safe Travel.* **2021**.

(72) Li, Y.; Leung, G. M.; Tang, J. W.; Yang, X.; Chao, C. Y. H.; Lin, J. Z.; Lu, J. W.;

Nielsen, P. V.; Niu, J.; Qian, H.; et al. Role of Ventilation in Airborne Transmission of Infectious Agents in the Built Environment - A Multidisciplinary Systematic Review. *Indoor Air* **2007**, *17* (1), 2–18. https://doi.org/10.1111/j.1600-0668.2006.00445.x.

(73) Miller, S. L.; Nazaroff, W. W.; Jimenez, J. L.; Boerstra, A.; Buonanno, G.; Dancer, S. J.; Kurnitski, J.; Marr, L. C.; Morawska, L.; Noakes, C. Transmission of SARS-CoV-2 by Inhalation of Respiratory Aerosol in the Skagit Valley Chorale Superspreading Event. *Indoor Air* **2021**, *31* (2), 314–323. https://doi.org/10.1111/ina.12751.

(74) Greenhalgh, T.; Jimenez, J. L.; Prather, K. A.; Tufekci, Z.; Fisman, D.; Schooley, R. Ten Scientific Reasons in Support of Airborne Transmission of SARS-CoV-2. *Lancet* **2021**, *397* (10285), 1603–1605. https://doi.org/10.1016/S0140-6736(21)00869-2.

(75) Fisk, W. J. The Ventilation Problem in Schools: Literature Review. *Indoor Air* **2017**, *27* (6), 1039–1051. https://doi.org/10.1111/ina.12403.

(76) Wargocki, P.; Porras-Salazar, J. A.; Contreras-Espinoza, S.; Bahnfleth, W. The Relationships between Classroom Air Quality and Children's Performance in School. *Build. Environ.* **2020**, *173* (December 2019). https://doi.org/10.1016/j.buildenv.2020.106749.

(77) Centers for Disease Control and Prevention. FLUVIEW: A Weekly Influenza Surveillance Report Prepared by the Influenza Division https://www.cdc.gov/flu/weekly/weeklyarchives2020-2021/ILI22.html.

(78) Gettings, J.; Czarnik, M.; Morris, E.; Haller, E.; Thompson-Paul, A. M.; Rasberry, C.; Lanzieri, T. M.; Smith-Grant, J.; Aholou, T. M.; Thomas, E.; et al. Mask Use and Ventilation Improvements to Reduce COVID-19 Incidence in Elementary Schools — Georgia, November 16–December 11, 2020. *MMWR. Morb. Mortal. Wkly. Rep.* **2021**, *70*

(21), 779–784. https://doi.org/10.15585/mmwr.mm7021e1.

(79) ASHRAE. *Core Recommendations for Reducing Airborne Infections Aerosol Exposure*; 2020.

(80) Jones, E.; Young, A.; Clevenger, K.; Salimifard, P.; Wu, E.; Lahaie Luna, M.; Lahvis, M.; Lang, J.; Bliss, M.; Azimi, P.; et al. *Schools for Health: Risk Reduction Strategies for Reopening Schools*; 2020.

(81) Levinson, M.; Geller, A. C.; Allen, J. G. Health Equity, Schooling Hesitancy, and the Social Determinants of Learning. *Lancet Reg. Heal. - Am.* **2021**, *2*, 100032. https://doi.org/10.1016/j.lana.2021.100032.

(82) U.S. Green Buildings Council. *New Construction V4 Minimum Indoor Air Quality Performance*.

(83) Turner, W. J. N.; Sherman, M. H.; Walker, L. S. Infiltration as Ventilation: Weather-Induced Dilution. *HVAC&R Res.* **2012**, *18* (6), 1122–1135. https://doi.org/https://doi.org/10.1080/10789669.2012.704836.

(84) Persily, A. K. Field Measurement of Ventilation Rates. *Indoor Air* **2016**, *26* (1), 97–111. https://doi.org/10.1111/ina.12193.

(85) Korsavi, S. S.; Montazami, A.; Mumovic, D. Ventilation Rates in Naturally Ventilated Primary Schools in the UK; Contextual, Occupant and Building-Related (COB) Factors. *Build. Environ.* **2020**, *181*, 107061. https://doi.org/10.1016/j.buildenv.2020.107061.

(86) ASHRAE. *Standard Project Committee 170, ANSI/ASHRAE Standard 111-2008 (RA 2017), Measurement, Testing, Adjusting, and Balancing of Building HVAC Systems*; 2017.

(87) Charlesworth, P. S. *Air Exchange Rate and Airtightness Measurement Techniques-an Applications Guide.*; 1988.

(88) Persily, A. *Tracer Gas Techniques for Studying Building Air Exchange*; 1988.

(89) NOAA Global Monitoring Laboratory. Trends in Atmospheric Carbon Dioxide.

(90) Tang, M.; Zhu, N.; Kinney, K.; Novoselac, A. Transport of Indoor Aerosols to Hidden Interior Spaces. *Aerosol Sci. Technol.* **2020**, *54* (1), 94–110. https://doi.org/10.1080/02786826.2019.1677854.

(91) Singer, B. C.; Delp, W. W. Response of Consumer and Research Grade Indoor Air Quality Monitors to Residential Sources of Fine Particles. *Indoor Air* **2018**, *28* (4), 624–639. https://doi.org/10.1111/ina.12463.

(92) Rudnick, S. N.; Milton, D. K. Risk of Indoor Airborne Infection Transmission Estimated from Carbon Dioxide Concentration. *Indoor Air* **2003**, *13* (3), 237–245. https://doi.org/10.1034/j.1600-0668.2003.00189.x.

(93) Batterman, S. Review and Extension of CO2-Based Methods to Determine Ventilation Rates with Application to School Classrooms. *Int. J. Environ. Res. Public Health* **2017**, *14* (2), 1–22. https://doi.org/10.3390/ijerph14020145.

(94) Peng, Z.; Jimenez, J. L. Exhaled CO 2 as a COVID-19 Infection Risk Proxy for Different Indoor Environments and Activities. *Environ. Sci. Technol. Lett.* **2021**, *8* (5), 392–397. https://doi.org/10.1021/acs.estlett.1c00183.

(95) Lednicky, J. A.; Lauzardo, M.; Fan, Z. H.; Jutla, A.; Tilly, T. B.; Gangwar, M.; Usmani, M.; Shankar, S. N.; Mohamed, K.; Eiguren-Fernandez, A.; et al. Viable SARS-CoV-2 in the Air of a Hospital Room with COVID-19 Patients. *Int. J. Infect. Dis.* **2020**, *100*, 476–482. https://doi.org/10.1016/j.ijid.2020.09.025.

(96) Bhangar, S.; Huffman, J. A.; Nazaroff, W. W. Size-resolved Fluorescent Biological Aerosol Particle Concentrations and Occupant Emissions in a University Classroom.

Indoor Air **2014**, *24* (6), 604–617. https://doi.org/10.1111/ina.12111.

(97) Howard-Reed, C.; Wallace, L. A.; Ott, W. R. The Effect of Opening Windows on Air Change Rates in Two Homes. *J. Air Waste Manag. Assoc.* **2002**, *52* (2), 147–159. https://doi.org/10.1080/10473289.2002.10470775.

(98) Sisson, P. Your Old Radiator Is a Pandemic-Fighting Weapon.

(99) Schaefer, T.; Kieslinger, B.; Fabian, C. M. Citizen-Based Air Quality Monitoring: The Impact on Individual Citizen Scientists and How to Leverage the Benefits to Affect Whole Regions. *Citiz. Sci. Theory Pract.* **2020**, *5* (1). https://doi.org/10.5334/cstp.245.

(100) Uhde, E.; Salthammer, T. Impact of Reaction Products from Building Materials and Furnishings on Indoor Air Quality-A Review of Recent Advances in Indoor Chemistry. *Atmos. Environ.* **2007**, *41* (15), 3111–3128. https://doi.org/10.1016/j.atmosenv.2006.05.082.

(101) Wolkoff, P. Impact of Air Velocity, Temperature, Humidity, and Air on Long-Term VOC Emissions from Building Products. *Atmos. Environ.* **1998**, *32* (14–15), 2659–2668. https://doi.org/10.1016/S1352-2310(97)00402-0.

(102) Cano, J. M.; Marín, M. L.; Sánchez, A.; Hernandis, V. Determination of Adipate Plasticizers in Poly(Vinyl Chloride) by Microwave-Assisted Extraction. *J. Chromatogr. A* **2002**, *963* (1–2), 401–409. https://doi.org/10.1016/S0021-9673(02)00642-8.

(103) Fromme, H.; Schütze, A.; Lahrz, T.; Kraft, M.; Fembacher, L.; Siewering, S.; Burkardt, R.; Dietrich, S.; Koch, H. M.; Völkel, W. Non-Phthalate Plasticizers in German Daycare Centers and Human Biomonitoring of DINCH Metabolites in Children Attending the Centers (LUPE 3). *Int. J. Hyg. Environ. Health* **2016**, *219* (1), 33–39. https://doi.org/10.1016/j.ijheh.2015.08.002.

(104) Maeng, D. Y.; McNeill, V. F. Kinetics of Alkaline Hydrolysis of Synthetic Organic Esters. *Int. J. Chem. Kinet.* **2022**, *54* (3), 218–222. https://doi.org/10.1002/kin.21552.

(105) Bope, A.; Haines, S. R.; Hegarty, B.; Weschler, C. J.; Peccia, J.; Dannemiller, K. C. Degradation of Phthalate Esters in Floor Dust at Elevated Relative Humidity. *Environ. Sci. Process. Impacts* **2019**, *21* (8), 1268–1279. https://doi.org/10.1039/c9em00050j.

(106) Wang, L.; Liao, C.; Liu, F.; Wu, Q.; Guo, Y.; Moon, H. B.; Nakata, H.; Kannan, K. Occurrence and Human Exposure of P-Hydroxybenzoic Acid Esters (Parabens), Bisphenol a Diglycidyl Ether (BADGE), and Their Hydrolysis Products in Indoor Dust from the United States and Three East Asian Countries. *Environ. Sci. Technol.* **2012**, *46* (21), 11584–11593. https://doi.org/10.1021/es303516u.

(107) McNeill, V. F.; Woo, J. L.; Kim, D. D.; Schwier, A. N.; Wannell, N. J.; Sumner, A. J.; Barakat, J. M. Aqueous-Phase Secondary Organic Aerosol and Organosulfate Formation in Atmospheric Aerosols: A Modeling Study. *Environ. Sci. Technol.* **2012**, *46* (15), 8075–8081. https://doi.org/10.1021/es3002986.

(108) Corsi, R. L.; Lin, C. C. Emissions of 2,2,4-Trimethyl-1,3-Pentanediol Monoisobutyrate (TMPD-MIB) from Latex Paint: A Critical Review. *Crit. Rev. Environ. Sci. Technol.* **2009**, *39* (12), 1052–1080. https://doi.org/10.1080/10643380801977925.

(109) Bergh, C.; Torgrip, R.; Emenius, G.; Östman, C. Organophosphate and Phthalate Esters in Air and Settled Dust - a Multi-Location Indoor Study. *Indoor Air* **2011**, *21* (1), 67–76. https://doi.org/10.1111/j.1600-0668.2010.00684.x.

(110) Schwartz, S. E. Mass-Transport Considerations Pertinent to Aqueous Phase Reactions of Gases in Liquid-Water Clouds. In *Chemistry of Multiphase Atmospheric Systems*; Jaeschke, W., Ed.; Springer Berlin Heidelberg: Berlin, Heidelberg, 1986; Vol. 41, pp 415–

471. https://doi.org/10.1007/978-3-642-70627-1_16.

(111) Shiraiwa, M.; Pfrang, C.; Pöschl, U. Kinetic Multi-Layer Model of Aerosol Surface and Bulk Chemistry (KM-SUB): The Influence of Interfacial Transport and Bulk Diffusion on the Oxidation of Oleic Acid by Ozone. *Atmos. Chem. Phys.* **2010**, *10* (8), 3673–3691. https://doi.org/10.5194/acp-10-3673-2010.

(112) Morrison, G.; Lakey, P. S. J.; Abbatt, J.; Shiraiwa, M. Indoor Boundary Layer Chemistry Modeling. *Indoor Air* **2019**, *29* (6), 956–967. https://doi.org/10.1111/ina.12601.

(113) Corner, J.; Pendlebury, E. D. The Coagulation and Deposition of a Stirred Aerosol. *Proc. Phys. Soc. Sect. B* **1951**, *64* (8), 645–654. https://doi.org/10.1088/0370-1301/64/8/304.

(114) Woo, J. L.; McNeill, V. F. SimpleGAMMA v1.0 - A Reduced Model of Secondary Organic Aerosol Formation in the Aqueous Aerosol Phase (AaSOA). *Geosci. Model Dev.* **2015**, *8* (6), 1821–1829. https://doi.org/10.5194/gmd-8-1821-2015.

(115) Staples, C. A.; Peterson, D. R.; Parkerton, T. F.; Adams, W. J. The Environmental Fate of Phthalate Esters: A Literature Review. **1997**, *35* (4), 667–749.

(116) Atkinson, R.; Baulch, D. L.; Cox, R. A.; Crowley, J. N.; Hampson, R. F.; Hynes, R. G.; Jenkin, M. E.; Rossi, M. J.; Troe, J. Evaluated Kinetic and Photochemical Data for Atmospheric Chemistry: Volume II – Gas Phase Reactions of Organic Species. *Atmos. Chem. Phys.* **2006**, *6* (11), 3625–4055. https://doi.org/10.5194/acp-6-3625-2006.

(117) US EPA. Estimation Programs Interface Suite™ for Microsoft® Windows, v 4.11. United States Environmental Protection Agency: Washington, DC, USA 2022.

(118) Weschler, C. J.; Shields, H. C. Production of the Hydroxyl Radical in Indoor Air. *Environ. Sci. Technol.* **1996**, *30* (11), 3250–3258. https://doi.org/10.1021/es960032f.

(119) Su, G.; Letcher, R. J.; Yu, H. Organophosphate Flame Retardants and Plasticizers in

Aqueous Solution: PH-Dependent Hydrolysis, Kinetics, and Pathways. *Environ. Sci. Technol.* **2016**, *50* (15), 8103–8111. https://doi.org/10.1021/acs.est.6b02187.

(120) Räsänen, V.; Penttala, V. The PH Measurement of Concrete and Smoothing Mortar Using a Concrete Powder Suspension. *Cem. Concr. Res.* **2004**, *34* (5), 813–820. https://doi.org/10.1016/j.cemconres.2003.09.017.

(121) McNeill, V. F.; Corsi, R.; Huffman, J. A.; King, C.; Klein, R.; Lamore, M.; Maeng, D. Y.; Miller, S. L.; Lee Ng, N.; Olsiewski, P.; et al. Room-Level Ventilation in Schools and Universities. *Atmos. Environ. X* **2022**, *13*, 100152. https://doi.org/10.1016/j.aeaoa.2022.100152.

(122) Daghigh, R.; Adam, N. M.; Sahari, B. B. Ventilation Parameters and Thermal Comfort of Naturally and Mechanically Ventilated Offices. *Indoor Built Environ.* **2009**, *18* (2), 113–122. https://doi.org/10.1177/1420326X09103013.

(123) Letinski, D. J.; Connelly, M. J.; Peterson, D. R.; Parkerton, T. F. Slow-Stir Water Solubility Measurements of Selected Alcohols and Diesters. *Chemosphere* **2002**, *48* (3), 257–265. https://doi.org/10.1016/S0045-6535(02)00086-3.

(124) Russell, D. J.; McDuffie, B. Chemodynamic Properties of Phthalate Esters: Partitioning and Soil Migration. *Chemosphere* **1986**, *15* (8), 1003–1021. https://doi.org/10.1016/0045-6535(86)90553-9.

(125) Lakey, P. S. J.; Eichler, C. M. A.; Wang, C.; Little, J. C.; Shiraiwa, M. Kinetic Multi-Layer Model of Film Formation, Growth, and Chemistry (KM-FILM): Boundary Layer Processes, Multi-Layer Adsorption, Bulk Diffusion, and Heterogeneous Reactions. *Indoor Air* **2021**, *31* (6), 2070–2083. https://doi.org/10.1111/ina.12854.

(126) Schwartz-Narbonne, H.; Donaldson, D. J. Water Uptake by Indoor Surface Films. *Sci.*

Rep. **2019**, *9* (1), 11089. https://doi.org/10.1038/s41598-019-47590-x.

(127) Sollinger, S.; Levsen, K.; Wünsch, G. Indoor Pollution by Organic Emissions from Textile Floor Coverings: Climate Test Chamber Studies under Static Conditions. *Atmos. Environ.* **1994**, *28* (14), 2369–2378. https://doi.org/10.1016/1352-2310(94)90491-X.

(128) Manuja, A.; Ritchie, J.; Buch, K.; Wu, Y.; Eichler, C. M. A.; Little, J. C.; Marr, L. C. Total Surface Area in Indoor Environments. *Environ. Sci. Process. Impacts* **2019**, *21* (8), 1384–1392. https://doi.org/10.1039/c9em00157c.

(129) Fromme, H.; Lahrz, T.; Piloty, M.; Gebhart, H.; Oddoy, A.; Rüden, H. Occurrence of Phthalates and Musk Fragrances in Indoor Air and Dust from Apartments and Kindergartens in Berlin (Germany). *Indoor Air* **2004**, *14* (3), 188–195. https://doi.org/10.1111/j.1600-0668.2004.00223.x.

(130) Norbäck, D.; Wieslander, G.; Edling, C. Occupational Exposure to Volatile Organic Compounds (VOCS), and Other Air Pollutants from the Indoor Application of Water-Based Paints. *Ann. Occup. Hyg.* **1995**, *39* (6), 783–794. https://doi.org/10.1093/annhyg/39.6.783.

(131) Gallego, E.; Roca, X.; Perales, J. F.; Guardino, X. Determining Indoor Air Quality and Identifying the Origin of Odour Episodes in Indoor Environments. *J. Environ. Sci.* **2009**, *21* (3), 333–339. https://doi.org/10.1016/S1001-0742(08)62273-1.

(132) Brown, S. K.; Sim, M. R.; Abramson, M. J.; Gray, C. N. Concentrations of Volatile Organic Compounds in Indoor Air – A Review. *Indoor Air* **1994**, *4* (2), 123–134. https://doi.org/10.1111/j.1600-0668.1994.t01-2-00007.x.

(133) Gerster, F. M.; Hopf, N. B.; Wild, P. P.; Vernez, D. Airborne Exposures to Monoethanolamine, Glycol Ethers, and Benzyl Alcohol during Professional Cleaning: A

Pilot Study. *Ann. Occup. Hyg.* **2014**, *58* (7), 846–859. https://doi.org/10.1093/annhyg/meu028.

(134) Sander, R. Modeling Atmospheric Chemistry: Interactions between Gas-Phase Species and Liquid Cloud/Aerosol Particles. *Surv. Geophys.* **1999**, *20* (1), 1–31. https://doi.org/10.1023/A:1006501706704.

(135) Sander, R. Compilation of Henry's Law Constants (Version 4.0) for Water as Solvent. *Atmos. Chem. Phys.* **2015**, *15* (8), 4399–4981. https://doi.org/10.5194/acp-15-4399-2015.

(136) Tilgner, A.; Schaefer, T.; Alexander, B.; Barth, M.; Collett, J. L.; Fahey, K. M.; Nenes, A.; Pye, H. O. T.; Herrmann, H.; McNeill, V. F. Acidity and the Multiphase Chemistry of Atmospheric Aqueous Particles and Clouds. *Atmos. Chem. Phys.* **2021**, *21* (17), 13483–13536. https://doi.org/10.5194/acp-21-13483-2021.

(137) Nalli, S.; Horn, O. J.; Grochowalski, A. R.; Cooper, D. G.; Nicell, J. A. Origin of 2-Ethylhexanol as a VOC. *Environ. Pollut.* **2006**, *140* (1), 181–185. https://doi.org/10.1016/j.envpol.2005.06.018.

(138) Banerjee, S.; Gnanamani, E.; Yan, X.; Zare, R. N. Can All Bulk-Phase Reactions Be Accelerated in Microdroplets? *Analyst* **2017**, *142* (9), 1399–1402. https://doi.org/10.1039/c6an02225a.

(139) Sjöberg, A.; Ramnäs, O. An Experimental Parametric Study of VOC from Flooring Systems Exposed to Alkaline Solutions. *Indoor Air* **2007**, *17* (6), 450–457. https://doi.org/10.1111/j.1600-0668.2007.00492.x.

(140) Chino, S.; Kato, S.; Seo, J.; Ataka, Y. Study on Emission of Decomposed Chemicals of Esters Contained in PVC Flooring and Adhesive. *Build. Environ.* **2009**, *44* (7), 1337–1342. https://doi.org/10.1016/j.buildenv.2008.07.003.

(141) Sparks, L. E.; Guo, Z.; Chang, J. C.; Tichenor, B. A. Volatile Organic Compound Emissions from Latex Paint - Part 2. Test House Studies and Indoor Air Quality (IAQ) Modeling. *Indoor Air* **1999**, *9* (1), 18–25. https://doi.org/10.1111/j.1600-0668.1999.t01-3-00004.x.

(142) Chang, J. C. S.; Tichenor, B. A.; Guo, Z.; Krebs, K. A. Substrate Effects on VOC Emissions from a Latex Paint. *Indoor Air* **1997**, *7* (4), 241–247. https://doi.org/10.1111/j.1600-0668.1997.00003.x.

(143) South Coast Air Quality Management District. *Final Program Environmental Impact Report for the 2012 Air Quality Management Plan*; 2012.

(144) Salthammer, T.; Fuhrmann, F.; Uhde, E. Flame Retardants in the Indoor Environment - Part II: Release of VOCs (Triethylphosphate and Halogenated Degradation Products) from Polyurethane. *Indoor Air* **2003**, *13* (1), 49–52. https://doi.org/10.1034/j.1600-0668.2003.01150.x.

(145) Lam, B.; Diamond, M. L.; Simpson, A. J.; Makar, P. A.; Truong, J.; Hernandez-Martinez, N. A. Chemical Composition of Surface Films on Glass Windows and Implications for Atmospheric Chemistry. *Atmos. Environ.* **2005**, *39* (35), 6578–6586. https://doi.org/10.1016/j.atmosenv.2005.07.057.

(146) Jencks, W. P.; Carriuolo, J. General Base Catalysis of Ester Hydrolysis. *J. Am. Chem. Soc.* **1961**, *83* (7), 1743–1750. https://doi.org/10.1021/ja01468a044.

(147) Fersht, A. R.; Kirby, A. J. The Hydrolysis of Aspirin. Intramolecular General Base Catalysis of Ester Hydrolysis. *J. Am. Chem. Soc.* **1967**, *89* (19), 4857–4863. https://doi.org/10.1021/ja00995a007.

(148) Stefanidis, D.; Jencks, W. P. General Base Catalysis of Ester Hydrolysis. *J. Am. Chem.*

Soc. **1993**, *115* (14), 6045–6050. https://doi.org/10.1021/ja00067a020.

(149) Ault, A. General Acid and General Base Catalysis. *J. Chem. Educ.* **2007**, *84* (1), 38–39. https://doi.org/10.1021/ed084p38.

(150) Felder, J. D.; Adams, W. J.; Saeger, V. W. Assessment of the Safety of Dioctyl Adipate in Freshwater Environments. *Environ. Toxicol. Chem.* **1986**, *5* (8), 777–784. https://doi.org/10.1002/etc.5620050809.

(151) Magdouli, S.; Daghrir, R.; Brar, S. K.; Drogui, P.; Tyagi, R. D. Di 2-Ethylhexylphtalate in the Aquatic and Terrestrial Environment: A Critical Review. *J. Environ. Manage.* **2013**, *127*, 36–49. https://doi.org/10.1016/j.jenvman.2013.04.013.

(152) Hiatt, M. H. Determination of Henry's Law Constants Using Internal Standards with Benchmark Values. *J. Chem. Eng. Data* **2013**, *58* (4), 902–908. https://doi.org/10.1021/je3010535.

(153) García, M. P. G. I.; Sanroma, A. M.; Porrero, M. P. M.; Valle, A. T.; Galán, B. C.; Muñoz, M. S. S. Reactivity of 2-Ethyl-1-Hexanol in the Atmosphere. *Phys. Chem. Chem. Phys.* **2010**, *12* (13), 3294–3300. https://doi.org/10.1039/b923899a.

(154) Kortüm, G.; Vogel, W.; Andrussow, K. *Dissociation Constants of Organic Acids in Aqueous Solution*; Butterworths: London, 1961.

(155) Serjeant, E. P.; Dempsey, B. *Ionisation Constants of Organic Acids in Aqueous Solution*; Pergamon Press, 1979.

(156) Lim, H. J.; Carlton, A. G.; Turpin, B. J. Isoprene Forms Secondary Organic Aerosol through Cloud Processing: Model Simulations. *Environ. Sci. Technol.* **2005**, *39* (12), 4441–4446. https://doi.org/10.1021/es048039h.

(157) Huff Chester, A.; Gordon, C.; Hartmann, H. A.; Bartell, S. E.; Ansah, E.; Yan, T.; Li, B.;

Dampha, N. K.; Edmiston, P. L.; Novak, P. J.; et al. Contaminants of Emerging Concern in the Lower Volta River, Ghana, West Africa: The Agriculture, Aquaculture, and Urban Development Nexus. *Environ. Toxicol. Chem.* **2022**, *41* (2), 369–381. https://doi.org/10.1002/etc.5279.

(158) Yamamoto, H.; Watanabe, M.; Katsuki, S.; Nakamura, Y.; Moriguchi, S.; Nakamura, Y.; Sekizawa, J. Preliminary Ecological Risk Assessment of Butylparaben and Benzylparaben -2. Fate and Partitioning in Aquatic Environments. *Environ. Sci.* **2007**, *14 Suppl* (2007), 97–105.

(159) Zhang, Y.; Jiao, Y.; Li, Z.; Tao, Y.; Yang, Y. Hazards of Phthalates (PAEs) Exposure: A Review of Aquatic Animal Toxicology Studies. *Sci. Total Environ.* **2021**, *771*, 145418. https://doi.org/10.1016/j.scitotenv.2021.145418.

(160) Torrents, A.; Stone, A. T. Oxide Surface-Catalyzed Hydrolysis of Carboxylate Esters and Phosphorothioate Esters. *Soil Sci. Soc. Am. J.* **1994**, *58* (3), 738–745. https://doi.org/10.2136/sssaj1994.03615995005800030014x.

(161) Smolen, J. M.; Stone, A. T. The Divalent Metal Ion-Catalyzed Hydrolysis of Phosphorothionate Ester Pesticides. *ACS Div. Environ. Chem. Prepr.* **1996**, *36* (2), 309–310.

(162) Vogel, T. M.; Criddle, C. S.; McCarty, P. L. ES&T Critical Reviews: Transformations of Halogenated Aliphatic Compounds. *Environ. Sci. Technol.* **1987**, *21* (8), 722–736.

(163) Henkel, C.; Hüffer, T.; Hofmann, T. Polyvinyl Chloride Microplastics Leach Phthalates into the Aquatic Environment over Decades. *Environ. Sci. Technol.* **2022**, *56* (20), 14507–14516. https://doi.org/10.1021/acs.est.2c05108.